Chem Soc Rev

REVIEW ARTICLE

View Article Online
View Journal | View Issue

Cite this: *Chem. Soc. Rev.*, 2025, **54**, 827

Black phosphorus-based nanoplatforms for cancer therapy: chemistry, design, biological and therapeutic behaviors

Ashkan Bigham, [ab] Manuel Serrano-Ruiz, [c] Maria Caporali,[c] Ines Fasolino,[a] Maurizio Peruzzini, [c] Luigi Ambrosio[a] and Maria Grazia Raucci *[a]

Cancer, a significant threat to human lives, has been the target of research for several decades. Although conventional therapies have drawbacks, such as side effects, low efficacy, and weak targeting, they have been applied extensively due to a lack of effective alternatives. The emergence of nanotechnology in medicine has opened up new possibilities and offered promising solutions for cancer therapy. In recent years, 2D nanomaterials have attracted enormous attention in nanomedicine due to their large surface-to-volume ratio, photo-responsivity, excellent electrical conductivity, *etc.* Among them, black phosphorus (BP) is a 2D nanomaterial consisting of multiple layers weakly bonded together through van der Waals forces. Its distinct structure makes BP suitable for biomedical applications, such as drug/gene carriers, PTT/PDT, and imaging agents. BP has demonstrated remarkable potential since its introduction in cancer therapy in 2015, particularly due to its selective anticancer activity even without the aid of near-infrared (NIR) or anticancer drugs. The present review makes efforts to cover and discuss studies published on the anticancer activity of BP. Based on the type of cancer, the subcategories are organized to shed light on the potential of BP nanosheets and BP quantum dots (BPQDs) against breast, brain, skin, prostate, and bone cancers, and a section is devoted to other cancer types. Since extensive attention has been paid to breast cancer cells and *in vivo* models, various subsections, including mono-, dual, and triple therapeutic approaches are established for this cancer type. Furthermore, the review outlines various synthesis approaches employed to produce BP nanomaterials, providing insights into key synthesis parameters. This review provides an up-to-date platform for the potential reader to understand what has been done about BP cancer therapy based on each disease, and the conclusions and outlook cover the directions in which this approach is going to proceed in the future.

Received 30th July 2024

DOI: 10.1039/d4cs00007b

rsc.li/chem-soc-rev

1. Introduction

Cancer is among the deadliest diseases in the world, and to date, resources of great value have been funded in this field.[1] Owing to various medical imaging techniques, including MRI, computed tomography, and ultrasound, the understanding and diagnosis of tumors have significantly improved. However, the diversity in cancer types, complexity, drug-resistance, *etc.*, pose significant challenges.[2,3] The available well-known clinical approaches include surgery, chemotherapy, and radiotherapy, but the first approach suffers from incomplete removal of cancer tissues, and the others have low efficiency and side effects in patients. There are new anticancer strategies, including hyperthermia through PTT and MHT using magnetic sensitive biomaterials, PDT/SDT, targeted/multi-drug delivery, and gene delivery, and some of them have successfully reached clinical settings but their availability is still in progress.[4–7]

In recent years, extensive research has been directed toward 2D materials for cancer therapy. These materials, specifically MXenes, have been applied in cancer diagnosis, combinational therapy, and regeneration stemming from their tunable layer-dependent bandgaps, high surface-to-volume ratios (suitable for drug delivery), strong absorption rates in the visible-NIR region, *etc.*[8] Moreover, these nanomaterials are known to degrade in the physiological medium and get eliminated from the body.[9] Black phosphorus (BP), a shiny star among the 2D materials family, is mono-elemental, and its attractive physico-chemical and biological properties have extended BP's applications from optical sensing to cancer therapy.[10] However, the

[a] *Institute of Polymers, Composites and Biomaterials, National Research Council of Italy (IPCB-CNR), Viale John Fitzgerald Kennedy 54, Mostra d'Oltremare Padiglione 20, 80125 Naples, Italy. E-mail: mariagrazia.raucci@cnr.it*
[b] *Department of Chemical, Materials and Production Engineering, University of Naples Federico II, Piazzale V. Tecchio 80, 80125 Naples, Italy*
[c] *Institute for Chemistry of OrganoMetallic Compounds, National Research Council of Italy (ICCOM-CNR), Via Madonna del Piano 10, 5019 Sesto Fiorentino, Italy*

application of BP in various fields is limited due to its rapid oxidation rate, which affects its photo-responsivity. However, this aspect has been exploited for cancer therapy and tissue regeneration applications.[11] BP undergoes oxidation when exposed to oxygen and water molecules, and clearly the optical properties weaken, but, for example, in bone tissue regeneration in which the biomaterial is supposed to form a bonding with the host bone and stimulate the regeneration rate, the BP's degradation accelerates these two demands through calcium phosphate formation and release of phosphate anions.[12,13] Furthermore, cancer cells have a higher metabolism rate than that of normal cells, leading to an acidic medium accelerating BP degradation. BP has been shown to degrade faster in cancer cells and generates ROS providing a cytotoxic environment for the cells, leading to apoptosis, whereas in the normal cells, no cytotoxicity was observed by the same concentration.[14,15] Therefore, BP is naturally endowed with therapeutic and regenerative potentials. Nonetheless, BP has a high surface area, making it an appropriate candidate for drug/gene delivery, and it is also a photo-responsive material capable of turning light into heat (PTT) and ROS (PDT).[16] It is important to bear in mind that the selective anticancer ability of BP without using any external stimuli was reported for the first time in 2019,[14] while the anticancer potential of BP through PTT was first published in

Ashkan Bigham

Ashkan Bigham is currently a PhD candidate in Materials Science & Engineering at the University of Naples Federico II and Research Associate at the Institute of Polymers, Composites, and Biomaterials (IPCB) of the National Research Council of Italy (CNR). He has worked on the development of various nanomaterials, nanocomposites, 3D scaffolds, and hydrogels for biomedical engineering for over 9 years. He has been in the world's top 2% scientists list released by Stanford University in 2024. His current scientific interests include the design of multifunctional therapeutic and regenerative platforms for cancer therapy and tissue regeneration.

Maurizio Peruzzini

Maurizio Peruzzini is currently the Emeritus Research Director at the National Research Council of Italy. He has received the "Nasini" (1993) and the "Cannizzaro" (2020) gold medal prizes (SCI), the French-Italian Prize 2011 by the Société Chimique de France and the Ziegler–Natta lectureship prize by the German Chemical Society (2020). MP has authored about 460 scientific articles and filed 6 patents. He has lectured in more than 80 Universities worldwide and has given invited talks in more than 100 Conferences. He has coordinated several EU and national projects. He is the recipient (PI) of the ERC ADVANCED GRANT for the project "Phosphorene functionalization" (PHOSFUN) and the ERC POC grant for the project "Exfoliated black phosphorus for biomedical applications" (PHOSMED).

Luigi Ambrosio

Luigi Ambrosio is the Emeritus Research Director at the Institute of Polymers, Composites & Biomaterials, National Research Council. He received his Doctoral Degree in Chemical Engineering, University of Naples "Federico II" in 1982. He is a Qualified Full Professor in Bioengineering and in Materials Science and Technology. He received the ESB "G. Winter Award" for his high worldwide contribution to Biomaterials Science. He is a Fellow of the American Institute for Medical and Biological Engineering, Fellow of Biomaterials Science and Engineering, Fellow of the European Alliance for Medical and Biomedical Engineering & Science, and Fellow and Member of the European Academy of Science. His publications include over 350 peer-reviewed journal articles.

Maria Grazia Raucci

Dr Maria Grazia Raucci is a Senior Research Scientist at IPCB-CNR, where she leads the Tissue Engineering & Cell Culture Laboratory. In addition to her PhD training and several years of collaboration with CNR, Dr Raucci has broadened her expertise through various international experiences. Her specialized skills include in vitro analysis, cell-material interactions, and the design and development of injectable scaffolds, ceramic materials, and hybrid materials via the sol–gel method. She is the Lead Investigator of scientific collaborations with various biomedical companies and is engaged in both national and international research partnerships.

2015.[17] BP was first adopted as an external stimuli-responsive agent, but gradually more research studies have been steered towards the natural anticancer potential of BP and combined it with other approaches to improve the therapeutic outcomes.

Since the first publication of BP in cancer therapy,[14,17] extensive research has been devoted to this biomaterial and notably the field is too large to cover every study, but the present review focuses on the BP's application in the form of either nanosheets or quantum dots in various cancer types (Scheme 1) and divides each one to give specific information on the advancement and achievements obtained for a specific disease. Here, in each section, an introduction is provided about the type of disease, and then step by step, the progress of BP toward that disease is discussed and covered. For instance, the majority of publications belonged to breast cancer therapy and BP has been recently shown to have promising results for other cancer types such as glioblastoma, prostate, bladder, and liver. Nonetheless, the chemistry and synthesis approaches used to yield BP nanomaterials are introduced and covered in detail to familiarize the potential reader with the effect of the synthesis technique and parameters on the final product's physicochemical properties. Some reviews have been published about the biomedical applications of BP and a few covered potential anticancer properties of BP,[18–25] but a comprehensive review, which in addition to the most recent advancement provides a complete platform spanning from chemistry to biology along with the potential for clinical translation is still missing. In this regard, *in vitro* and *in vivo* studies are comprehensively covered, more details about the physicochemical and biological properties are tabulated in each section, and the challenges and future trends of BP in cancer therapy are discussed.

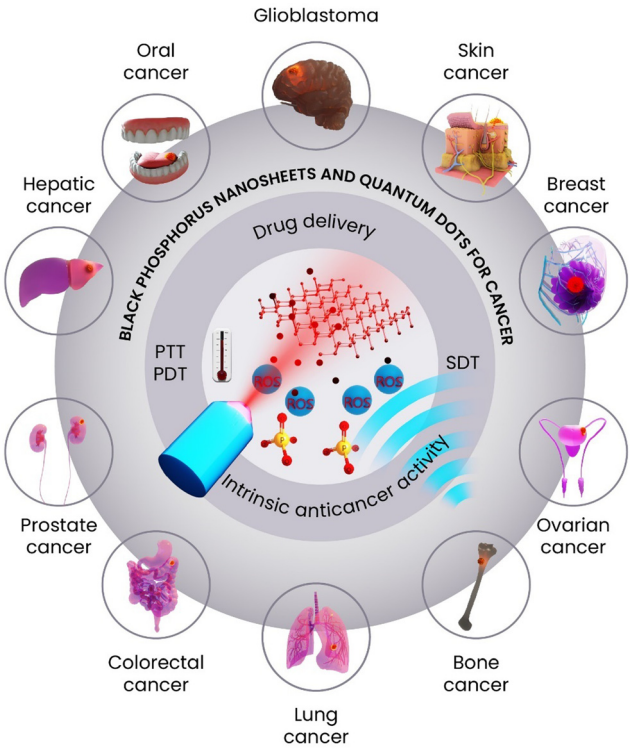

Scheme 1 BP nanosheets and quantum dots for cancer therapy.

2. Structural properties and synthesis routes of BP

Among the 2D nanomaterials, exfoliated BP is emerging as a highly promising candidate in many fields, spanning from nanoelectronics to catalysis, energy storage and biomedicine.[26–29] This wide application arises from its peculiar chemicophysical properties: BP is a natural semiconductor with a tunable band gap (from 0.3 eV in the bulk to 2.0 eV in the monolayer), a high carrier mobility, and similarly to graphite, it is a layered material, where the layers are kept together by van der Waals interactions, with an interlayer distance of 5.3 Å. While, graphenes are planar, constituted by C atoms with hybridization sp^2, BP is formed by P atoms having hybridization sp^3 that imparts a puckered structure, as shown in Scheme 2. As a result, it is possible to distinguish an armchair and a zig-zag structure in the x–y plane (see Scheme 2).

This structural in-plane anisotropy is also reflected in the chemicophysical properties of the material; BP shows a higher thermal conductivity at 300 K in the zig-zag (30 W m^{-1} K^{-1}) than in the armchair (13.7 W m^{-1} K^{-1}) direction, and the opposite trend is observed for the electrical conductivity. Additionally, combined ^{31}P solid-state NMR measurements and density functional theory calculations reveal the presence of two magnetically nonequivalent phosphorus nuclei within the network, distinguished by their different orientations of chemical shift tensors.[30]

From the corrugated structure, it derives a high surface-to-volume ratio that favors superficial interactions with metals, macromolecules, and biological molecules. Especially in the latter case, there is a flourishing work reported in the literature where BP rivals other 2D materials such as graphene oxides and transition metal dichalcogenides. In particular, phosphorus is a bone constituent, being ~1% of the total body weight (about 660 g on average), and participates in many physiological chemical reactions; this imparts to BP a superior biocompatibility in a physiological medium.[31] These exceptional properties have accelerated the widespread use of BP in various bioapplications including biosensing, medical imaging, pharmacological

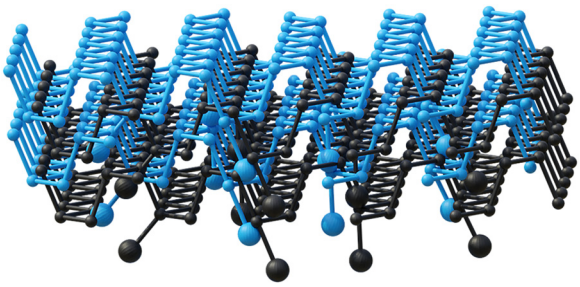

Scheme 2 Ball-stick model for four-layer BP, where black and blue balls represent P atoms.

treatments, and as a coating for scaffolds and prosthetic surfaces.[32]

As the interest in nanobiomedicine is constantly increasing, the application of BP-based nanomaterials is growing exponentially and a synthetic route that delivers BP on a large scale is highly desirable. To meet this goal, the first step to face is the production of bulk BP, which is not trivial. Bulk BP is solid under ambient conditions characterized by an orthorhombic crystal structure, and the elemental cell is composed of eight atoms, each of which covalently connected to three neighboring atoms with remaining lone electron pairs on each P atom, which is responsible for the high reactivity of BP, *in primis* towards oxygen and water.[33]

Various techniques have been developed to produce BP crystals with high quality and uniformity. Since the pioneering work by P. Bridgeman in 1914 who fabricated BP microcrystals using white phosphorus as a P-source under high-pressure conditions (1.2 GPa) and heating at T = 200 °C, alternative routes have been set up to avoid such dangerous and energy-consuming reaction conditions.[34] In 1955, the first low-pressure synthesis of BP was reported, where white phosphorus was combined with equal amounts of mercury, and the two reagents were sealed inside a vacuumed quartz ampoule and heated at a temperature ranging from 280 °C to 380 °C for a week.[35] Improvements were made by growing crystals of BP from white phosphorus dissolved in molten bismuth, which provided needle-shaped crystals easier to purify with respect to the method with mercury. Although this route is not easy to handle and involves toxic compounds, it is the method of choice for the synthesis of BP for decades, until 2007 when T. Nilges reported a chemical vapor transport route to grow large BP crystals from red P heated at T = 650 °C for three days inside a vacuumed ampule in the presence of AuSn alloy and SnI_4 as mineralization agents.[36] A remarkable improvement in this procedure, which still nowadays represents the state of the art, was achieved in 2014. This route uses only Sn and SnI_4 as mineralization agents, which are added to red P, and the sealed ampule is heated at T = 650 °C for three days, finally obtaining centimeter-scale bulk BP crystals, with the advantage of avoiding the use of noble metal Au and drastically reducing the amount of by-products.[37,38] This is considered the most successful method for the growth of high-quality bulk BP crystals, which is mandatory to obtain afterward high-quality 2D BP nanosheets.

Alternative routes that are less time-consuming and do not require special equipment are based on the solvothermal (ST) protocol and ball milling, respectively; however, they have the drawback of producing amorphous materials or microcrystals of lower quality. In the ST treatment, red phosphorus is suspended in ethylenediamine at 200 °C, and the vessel is closed under argon and heated up for 10 h. By this protocol, gram-scale BP nanocrystals can be synthesized.[39] The production of bulk BP by ball milling involves the mechanochemical conversion of the red allotrope by using a high-energy planetary ball mill, which has the advantage of reaching a high yield (~90%) of BP.[40]

There are a wide variety of methods for the preparation of exfoliated BP that can be summed up in the so-called top-down strategy, which includes mechanical exfoliation, ball milling, liquid exfoliation and electrochemical exfoliation, and bottom-up methods, such as physical epitaxial growth, ST synthesis, and pulsed laser deposition, as shown in Scheme 3. Additionally, Table 1 summarizes the current preparation methods of phosphorene, highlighting the pros and cons for each route.

As mentioned above, bulk BP is a layered solid similar to graphite, and with the layers kept together by weak van der Waals interaction,[37] the first strategy exploited for the fabrication of BPNSs was the mechanical exfoliation which dates back to 2014 when phosphorene was prepared for the first time autonomously by Y. Zhang and P. D. Ye groups using the scotch tape method.[41,52] Mechanical exfoliation enables the isolation of ultra-thin flakes, typically ranging in size from 4 to 6 nm, with larger lateral dimensions than those of the other top-down methods. This technique also maintains the crystallinity of the original material, making it highly suitable for electronic-grade applications. From the morphological point of view, the drawbacks are the irregular size of the flakes and uncontrollable layer number, and additionally, only a very tiny amount of the material can be produced, and thus, this technique is limited mainly to laboratory research. A different approach is the liquid-phase exfoliation (LPE) carried out by the action of ultrasounds on a suspension of bulk BP in a suitable solvent. The most common solvents used are *N*-methyl-2-pyrrolidone (NMP),[42] ionic liquids,[43] dimethyl sulfoxide (DMSO),[44] isopropanol and ethanol deoxygenated water,[53–55] anhydrous acetone and *N,N*-dimethylformamide (DMF).[56,57] In 2014, J. Brent *et al.* were the first to carry out the LPE of BP; they used NMP as a solvent and could achieve the preparation of thin BP flakes with a lateral dimension around 100 nm. In general, the selected solvent should have a similar surface energy to BP for successful and efficient exfoliation. Additionally, the LPE process not only exerts the separation of flakes, but also causes their fragmentation, and thus, flakes having different sizes and thicknesses are produced.[43] Increasing the sonication time yields thinner flakes, but at the same time, their fragmentation occurs, yielding flakes with reduced average dimensions. A comparative study of BP exfoliation in a wide variety of organic solvents was conducted by M. C. Hersam *et al.*, using a probe-sonication apparatus. It was found that polar aprotic solvents with high dielectric constants are best suited for LPE.[58] As confirmed by extensive characterization, BP flakes obtained by LPE in organic solvents are structurally preserved and morphologically similar to mechanically exfoliated ones. Additionally, once applied in the construction of field effect transistors, they showed an ambipolar behavior with current on/off ratios up to 10^4 and mobilities ~50 $cm^2\ V^{-1}\ s^{-1}$, which are lower but still comparable to BP flakes obtained by the scotch-tape method.[55] Further studies demonstrated that DMSO is also highly effective for LPE, showing similar performances to DMF. A detailed study on the use of DMSO in the production of BPNSs was carried out by M. Serrano-Ruiz *et al.* The study specifically, evaluated the effect of a tiny amount of deoxygenated

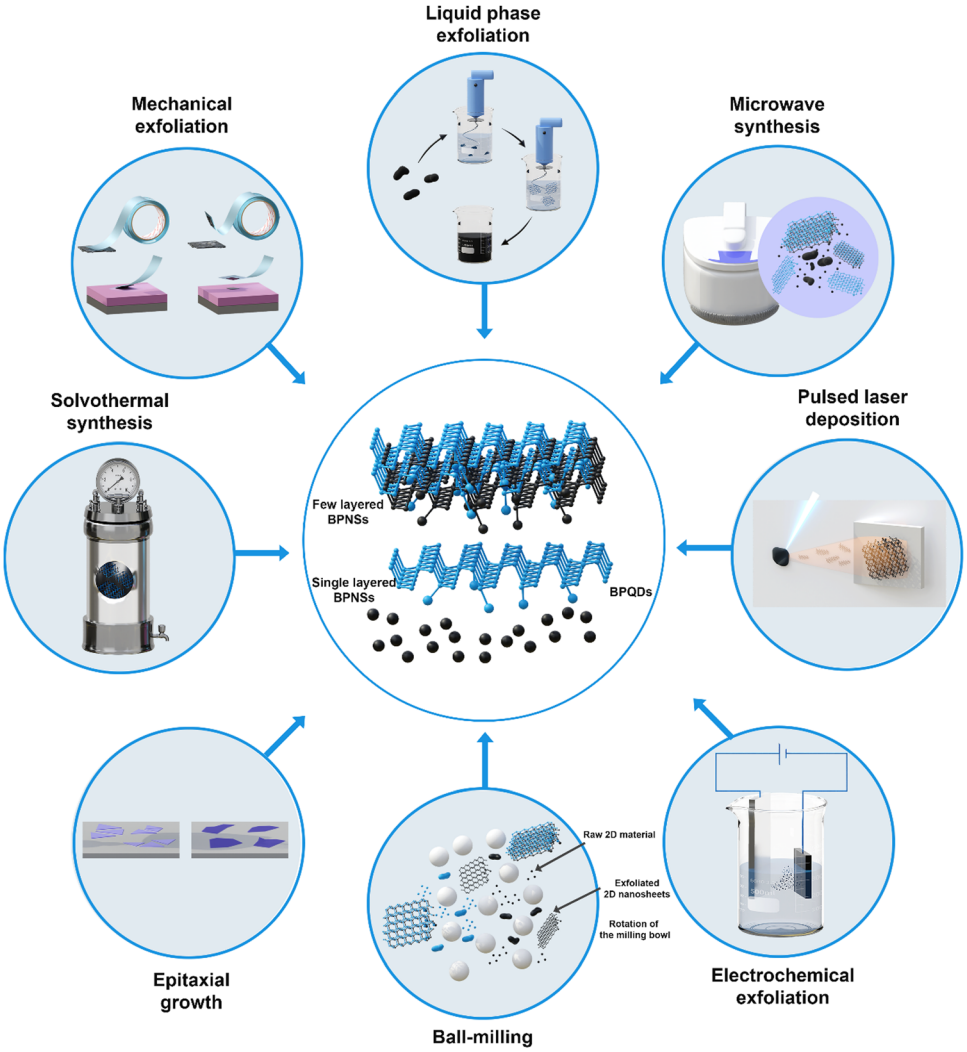

Scheme 3 Different routes for the conversion of bulk BP into few-layer BPNSs and BPQDs.

water on the efficiency of the LPE process and the quality of the final exfoliated material.[44] Surprisingly, it was observed that water has a non-innocent behavior and the specific P/H_2O molar ratio influences the morphology and size distribution of BP flakes. M.C. Hersam and colleagues demonstrated that BP can be successfully exfoliated in water with the addition of a stabilizing surfactant such as sodium dodecyl sulfate.[55] By this method, a homogenous distribution of thin flakes was obtained. Overall, we can state that LPE can be successfully applied for the large-scale production of BPNSs, but the BPNSs often contain defects due to several hours of ultrasonication and may be contaminated by the solvent or the surfactant molecules, which remain adsorbed on the surface, and still the yield and size control need to be further improved.

Bat-Erdene *et al.* demonstrated that the microwave-assisted LPE process can be very efficient and completed in 11 min, while ultrasonication protocols usually take several hours or even days. The as-prepared BP shows lateral dimensions from hundreds of nanometers to ~4 μm and thickness in the range of 4–11 layers.[59] An alternative to LPE carried out by sonication, though much less common, is electrochemical exfoliation.[60] In the latter process, bulk BP is used as a working electrode immersed in a suitable aqueous electrolyte, and in conjunction with an applied positive voltage, it drives the structural expansion and exfoliation of the individual layers of bulk BP.[45] The electrolyte can be a tetraalkylammonium salt that is first intercalated between the layers of BP favoring the separation among layers and then the anodic potential is applied to separate them. Using electrochemical delamination, X. Feng and co-workers showed that high-quality defect-free BPNSs can be fabricated with a domain size up to 119 μm and a thickness of around 3.6 nm.[61] M. Pumera and colleagues reported a related electrochemical method based on the concept of bipolar electrochemistry. In this approach, two platinum foils are used as electrodes, and when a voltage is applied, the BP crystals become polarized at their opposite extremities. This creates a potential difference across each crystal, leading to their fragmentation into smaller flakes.[62] A great advantage of electrochemical exfoliation is that the yield can reach more than 80%, which is higher than that of other methods,

Table 1 Summary of the different methods used for the synthesis of exfoliated BP

Methods	Type	Raw material	Advantages/applications	Disadvantages	Ref.
Mechanical Exfoliation	Top-down	Bulk BP	High hole carrier mobility (286 $cm^2 V^{-1} s^{-1}$) low cost, very thin flakes 4–6 nm, FET optoelectronics	Very low yield, surface oxidation, uncontrolled size	41 and 42
Liquid phase exfoliation	Top-down	Bulk BP	Low-cost, easy to scale-up, photocatalysts, electrocatalysts, therapeutic agents	Bring in extrinsic chemical residuals, uncontrolled size	43 and 44
Electrochemical exfoliation	Top-down	Bulk BP	High yield (~80%), ion batteries	Low hole carrier mobility (100 $cm^2 V^{-1} s^{-1}$)	45 and 46
Ball-milling	Top-down	Bulk P	High yield, ion batteries	Amorphous	40
Microwave	Top-down	Bulk BP	BPQDs High purity Fast procedure High crystallinity	Low yield	47
Solvothermal synthesis	Bottom-up	White P	Rapid, scalable, cost effective	Poor crystalline quality	48
Epitaxial growth	Bottom-up	White P	BP film, BPQDs High purity High crystallinity optoelectronics	Fabricated on a support	49 and 50
Pulsed laser deposition	Bottom-up	BP crystal	Centimeter-scale BP film, thin (2–8 nm) High controllability, high production rate, high quality	Fabricated on a support	51

as shown in Table 1. By choosing the suitable electrolyte and voltage, the initial drawback connected to a wide variety of sizes and thicknesses could be solved and high-quality uniform BP flakes were prepared by Li *et al.*[46]

Meanwhile, most 2D materials including graphenes and transition metal dichalcogenides have been successfully grown by chemical vapor deposition, and similar synthetic protocols were unsuccessful with BP. Thus, among the bottom-up methods for producing exfoliated BP, we can mention the ST route, which uses white phosphorus as a P-source and by warming for several hours in ethylenediamine, amorphous BP nanosheets are obtained.[48] Another route is based on the molecular beam epitaxial growth of BPQDs on a Si substrate and also uses white phosphorus as the precursor.[49] Lately, J. Hao *et al.* successfully produced a few-layer BP film on the centimeter scale through pulsed laser deposition on mica as the support.[51] Under these conditions, the formation of BP clusters within the confined region near the target substrate is favored using thermal heaters, resulting in the large-scale growth of BP films. Using a single BP crystal as a precursor and by heating at 150 °C, precise control over the film thickness was achieved by adjusting the laser pulses during deposition, resulting in a unidirectional, homogeneous BP thin film. Notably, the centimeter-scale BP film demonstrated highly uniform electrical performance when used in field-effect transistors. In general, with the bottom-up strategy, it is difficult to achieve large-scale production of BP and it is also challenging to redisperse the material in a solvent afterward, since it is directly fabricated on support, thus it is mainly directed to applications in electronics.

BP nanomaterials for biomedical applications are usually obtained by LPE since this route yields phosphorene with small thicknesses reaching the monolayer limit, and by centrifugation at different speeds, particles with different sizes can be separated. In this regard, P. K. Chu *et al.* have shown that BPNSs with a large lateral size (394 ± 75 nm) are more efficient in PTT for cancer cell ablation. This suggests that according to the type of application (PTT, bio-imaging, and drug delivery), the size and morphology of BPNSs should be finely tuned to reach the highest performance.[63]

A functional decoration of the nanosheets' surface is usually performed as well to meet the biological need for low toxicity, dispersibility, and long circulation time. Next to 2D nanosheets, zero-dimensional (0D) BPQDs have also gained great interest since 2015 when they were first prepared by Zhang *et al.* by using an LPE strategy and NMP as the solvent.[64] Despite being composed of stacked monolayers, BPQDs lack bidimensionality, having a size typically in the range of 3–8 nm and variable thickness in the range of 1–3 nm.[65] Compared to BPNSs, BPQDs are endowed with a higher specific surface area and more surface-active sites, which also indicates more favorable surface modification and functionalization. BPQDs are usually prepared by LPE, *via* a combination of probe sonication and ice-bath sonication. The preferential formation of quantum dots over nanosheets is governed by the specific conditions under which the exfoliation process is carried out. Other LPE protocols have been reported using different solvents, such as

N-vinyl-pyrrolidone, isopropyl alcohol, and DMF.[65] Next to ultrasonic exfoliation, various methods such as electrochemical exfoliation, microwave, ST treatment, pulsed laser ablation, and epitaxial growth have been applied for the preparation of BPQDs. For instance, the ST route exploits the combined effect of high temperature and solvent stabilization, and in comparison to LPE, has the advantage of affording a homogeneous distribution of BPQDs in larger-scale production.[66] It was shown that BPQDs have excellent water dispersibility, high stability (in buffer solutions), and high quantum yields, and above all, they can absorb light in the NIR region, thus they can significantly kill tumor cells under NIR irradiation Owing to these properties, BPQDs are highly promising candidates in the biomedical field, especially for fluorescence imaging, PTT, and PDT.[17,67]

Given the extensive investigation of LPE in few-layer BP production, our special focus here is on researching this approach across several solvents, as well as analyzing the ultimate yield in large-scale BP synthesis. LPE in solvents, particularly ionic liquids, or with surfactants or chemical compounds has emerged as a feasible method for large-scale manufacturing. This is accomplished using various techniques including ultrasound (US), high-shear mixer (HSM), high-pressure homogenization (HPH), electrochemistry (EC), microwave (MW), ST, and pulsed-laser (PL), as shown in Table 2. Despite the significant benefits revealed by LPE in terms of processability, scalability, and stability, it is worth noting that many exfoliation processes frequently fail to report the exfoliation yield (EY), which is an important component in scaling. Some processes have shown a very high EY in our examination of LPE methodologies for few-layer BP production, suggesting strong exfoliation efficiency. Interestingly, ultrasound-assisted LPE in DMSO[44] produces flakes with dimensions between 4 and 30 nm for flake thickness (FT) and 100 and 500 nm for lateral size (LS), with an EY of 92%. Similarly, EC-assisted LPE in DMF and acetonitrile has an EY around 100%,[68] yielding flakes with LS and FT diameters of 500–1500 nm and 4–6 nm, respectively. Furthermore, LPE PL-assisted in isopropyl alcohol (IPA)[69] produces a noteworthy EY of 93.7%. In contrast, our analysis finds a range of techniques with lower EYs, indicating various levels of exfoliation efficiency. Notable among them are techniques with EY values ranging from 60 to 90%, such as EC-assisted LPE in water (>80%),[45] DMSO (>80%),[46] and propylene carbonate (78%);[61] as well as HSM-assisted[70] and US-assisted LPE methods.[71] These findings highlight the wide range of LPE approaches, underlining the need for method selection adapted to individual production goals.

The exploration of LPE techniques reveals a diverse range of procedures, each presenting distinct advantages and limitations. Within this spectrum, procedures yielding EY ranging from 30% to 60% offer valuable insights into the nuanced dynamics of exfoliation. Notable among them is US-assisted LPE in NMP, which has an EY of 45%.[73] Similarly, US-assisted LPE with Li_2SiF_6 in solvents such as MeOH, IPA, EtOH, and acetone[71] give EYs ranging from 40% to 47%, demonstrating the approach's adaptability across multiple solvent matrices. Furthermore, HSM-assisted LPE in solvents such as DMF, NMP, and diethylene glycol dimethyl ether (Diglyme) shows promising efficiency, boosting EYs from 36% to 47%.[70] This underscores its versatility across diverse solvent environments. Likewise, MW-assisted LPE in Cyclohexylpyrrolidone (CHP), NMP, and DMF shows EYs ranging from 30% to 40% within an hour, indicating its potential for scalable production.[96] Finally, US-assisted LPE in ionic liquids, especially with 1-hydroxyethyl-3-methylimidazolium trifluoromethanesulfonate ([HOEMIM][TfOTfms]), reaches an EY of 32%, showing reasonable efficiency in this solvent category. These findings shed light on the diverse environment of LPE techniques, emphasizing the need for carefully selecting solvents to obtain maximum exfoliation performance.[43]

The processes with the lowest EY in the range of 0–30% include various approaches, each demonstrating the difficulties associated with attaining efficient exfoliation. Notable among these are US-assisted LPE methods in IPA, MeOH, EtOH, and THF, with reported EYs ranging from 0% to 24%.[76,79,98] Similarly, HSM-assisted LPE in NMP achieves an EY of 25%,[90] whereas MW-assisted LPE in ionic liquids, specifically employing 1-butyl-3-methylimidazolium tetrafluoroborate ([BMIM][BF4]) and 1-hexyl-3-methylimidazolium tetrafluoroborate ([HMIM][BF_4]), achieves EYs in the 20–25% range.[96] The efficacy of US-assisted LPE methods in ionic liquids, notably with 1-butyl-3-methylimidazolium trifluoromethanesulfonate ([BMIM][Tfms]) and 1-ethyl-3-methylimidazolium bis[(trifluoromethyl)sulfonyl]imide [EMIM][Tf_2N][43] which achieved EYs of 7% and 3%, respectively, provides useful scientific insights. These findings add to our understanding of the complex relationship between solvent characteristics and exfoliation efficiency. Ionic liquids have unique physicochemical properties that impact the exfoliation process, including low volatility, strong ionic conductivity, and variable polarity.

It is crucial to underscore the significance of EY alongside morphological characterization in the studies reported in the literature, as detailed in Table 2. Only a subset of methodologies provide comprehensive data on EY along with detailed morphological characteristics of over 90% of the exfoliated material. For instance, among these, only two procedures, namely US-assisted LPE in DMSO[44] and PL-assisted LPE,[69] achieve an EY exceeding 90% while elucidating the characteristics of the exfoliated material. Electrochemical exfoliation in DMSO, propylene carbonate, and water produces notable results for operations with EY levels ranging from 60 to 90%.[46] These techniques measure FT from 1.3 to 10 nm and LS from 2 to 30 μm.[45] Similarly, techniques with EY values ranging from 30 to 60%, such as US-assisted LPE in NMP[73] show differences in NSs and QDs, with FT averaging 1.3 to 5.4 nm and LS averaging 2 to 2500 nm. In addition, processes with EY ranging from 0 to 30% show various morphologies such as NSs and QDs. Notably, HSM-assisted LPE in NMP[76] and MW-assisted LPE in ionic liquids ([BMIM][BF4] and [HMIM][BF4])[96] have FT between 0.6 and 5.3 nm and LS between 1.8 and 2500 nm. Furthermore, US-assisted LPE in ionic liquids ([BMIM]-[Tfms])[43] exhibits unique properties, with FT ranging from

Table 2 Different approaches adopted to yield BP nanomaterials along with their key factors

Solvent	Parameters	Thickness range (nm)	Lateral size range (nm)	Yield (%)	Ref.
Liquid exfoliation					
DMF	200 W, — kHz, 4 h, RT	3.1–4.3	50–100	16	
DMSO		—	—	24	
NMP		—	—	14	
Water	360 W, 20–25 kHz, 21 h, <15 °C	4.02 ± 3.05	312 ± 13	—	72
	380 W, 20–25 kHz, 0,5 h, RT	4–12	—	—	
	380 W, 20–25 kHz, 0,5 h, RT	3–7	—	—	
DMF	130 W, 40 kHz, 15 h, RT	6–12	~190	—	57
DMF	360 W, 20–25 kHz, 21 h, <15 °C	4.49 ± 3.26	289 ± 9	—	72
DMSO	700 W, 37 kHz, 120 h, ~30 °C	4–30	100–500	92	44
NMP	350 W, 40 kHz, 6 min, 30 °C	2.5 ± 1.2	434 ± 135	45	73
	350 W, 40 kHz, 18 min, 30 °C	1.7 ± 0.6	2.6 ± 1.0	45	
NMP	200 W, — kHz, 15 h, <20 °C	~0.6–2.3	2.7 ± 0.7	—	74
NMP	300 W, — kHz, 72 h, ~10 °C	2.4–2.8	~1.5–4.5	—	
NMP	30 W, 20 kHz, 1 h, RT	~5–300	~100–280	—	58
NMP	1200 W, 19–25 kHz, 3 h, <5 °C; 300 W, 10 h	1.5 ± 0.6	2.6 ± 1.8	—	17
NMP	600 W, — kHz, 6 h, —°C	2.8 ± 1.1	6.00 ± 0.97	—	75
NMP	400 W, 20 kHz, 8 h, ~20 °C	3–8	600–1000	—	76
CHP	750 W, power 60%, 20 kHz, 5 h, RT	5 – 25	~100–3000	—	77
CHP	200 W, 45 kHz, 6 h, RT	6–20	50–300	—	78
N,*N*′-dimethylpropylene urea	400 W, 40 kHz, 3 h, RT	2 – 15	500–2500	16	79
Li_2SiF_6					
Methanol	300 W, 40 kHz, 5 h, RT	—	—	40.1	71
IPA		6–20	500–5000	42	
Ethanol		—	—	45	
Acetone		—	—	47.3	
DMF		—	—	65.1	
1,2-Dichlorobenzene (DCB)		—	—	67.2	
CHP		—	—	70	
N-Vinylpyrrolidone (NVP)		—	—	72.3	
DMSO		—	—	75	
Water/Surfactant					
Triton X-100	820 W, power 30%, 37 kHz, 48 h, RT	<20	100–200	—	80
SDS	70 W, 20 kHz, 1 h, <20 °C	2–8	25–300	—	55
		—	—	—	
CTAB	— W, — kHz, 4 h, <20 °C	3–10	800–3000	—	81–83
Tetrabutylammonium hydroxide		>20	500–1500	—	
Zonyl 7950	820 W, power 30%, 37 kHz, 36 h, RT	17 ± 2	324 ± 30	—	84
Solvent/NaOH					
NMP/NaOH saturated solution	— W, power 80%, 40 kHz, 4 h, RT	5.3 ± 2.0	~670	—	85
NMP/NaOH saturated solution	150 W, 40 kHz, 1 h, RT/CO_2, 15 MPa, 3 h, 40 °C	3–20	~4500	—	86
NMP/NaOH saturated solution	solvothermal, 140 °C, 6 h	—	2.1 ± 0.9	—	87
Solvents mixture					
IPA/H_2O (3 : 7 v/v)	120 W, 35 kHz, 6 h, RT	1–4	~118	—	88
EtOH/H_2O (1 : 1 v/v)	100 W, 20 kHz, 20 min, — °C	1.1–2.5	756 ± 25	—	89
High-shear mixer					
DMF	Milling/16 000 rpm, 6 h	—	~110	36	70
NMP		—	~130	47	
Acetonitrile		—	~150	66	
Diglyme		—	~100	33	
NMP	160 W, 40 kHz, 2.5 h, RT/5000 rpm, 3 h (× 2)	0.6–3	50–250	25	90
Ultrahigh pressure homogenization					
NMP	150 MPa, 50 mL min^{-1}, 8 °C (10 times)	1–1.5	~50 × 200	—	91

Table 2 (*continued*)

Solvent	Parameters	Thickness range (nm)	Lateral size range (nm)	Yield (%)	Ref.
Electrochemical					
PC	As cathode, [TBA]PF_6, +30 V, 12 h	2–7	∼200 × 1000	—	92
PC	As cathode, [TBA]HSO_4, −8 V, 15 min	1.3–9.5	2000–21 000	78	61
Ethyl carbonate/dimethyl carbonate	BP foamed Ni (cathode), $NaClO_4$, 50 mA g^{-1}	1 – 2	∼2000 × 3000	—	93
DMSO	As cathode, [TBA]BF_4, −5 V, 10 min	∼4	∼10 000	>80	46
	As cathode, [CTA]Cl, 50 °C, −30 V, 30 min	—	∼11 400	—	94
		5–9	∼500/∼10 700	37	
		1–5	∼270	—	
Acetonitrile	As cathode, [TBA]PF_6, RT, −3.8 V, 3 h	∼4	∼500	∼100	68
DMF	As cathode, [TBA]PF_6, RT, −3.8 V, 5 h	∼6	∼1500	∼100	
H_2O	As anode, Na_2SO_4, RT, +7 V, ∼1 mA, 1.5 h	1.4–10	500–30 000	>80	45
Microwave					
NMP	600 W, 50 °C, <12 min/220 W, 70 °C, 3 min	6.5 ± 2.6	100–4000	—	59
NMP	600 W, 50 °C, 10 min	—	∼400	—	95
NMP	600 W, 120 °C, 30 min	3.59 ± 1.12	2.59 ± 0.59	—	
Ethanol	— W, 70 °C, 11 min/— W, 80 °C, 30 min	2.19 ± 1.33	2.4 ± 0.85	—	47
CHP/NMP/DMF	140 W, 140 °C/120 °C/95 °C, 60 min	∼2.5–5.4	∼2000–7100	30–40	96
[BMIM][BF_4]/[HMIM][BF_4]	30 W, 165 °C, 30 min	∼2.7–5.3	∼1800–6800	20–25	
Solvothermal					
Acetonitrile	200 °C, 24 h/360 W, — kHz, 1 h	1.9–2.1	10 000–15 000	—	97
Benzonitrile	500 °C, 40 kHz, 1.5h/150 °C, 6 h		1.6–3.2		
Ionic Liquids					
[BMIM][Tfms]	100 W, 40 kHz, 24 h, <30 °C	8.5–12.8	450–550	7.3	43
[HOEMIM][Tfms]	100 W, 40 kHz, 24 h, <30 °C	3.6–8.9	400–550	31.6	43
[EMIM][Tf2N]	100 W, 40 kHz, 24 h, <30 °C	—	—	3.3	43
Pulsed Laser					
IPA	Nd:YAG Q-switched pulsed laser	2.5–5	<20	93.7	68
	λ = 1064 nm, 650 mJ, 8 mm, 8 ns per pulse, 2,4 ms	5–8	>5000		

8.5 to 12.8 nm and LS ranging from 450 to 550 nm. Furthermore, it is critical to identify the optimum methods for producing NSs and QDs. The EC-assisted LPE technique using propylene carbonate, DMSO, and water[45,46,61] is preferred for creating big flakes with low thickness and high EY. In contrast, for QDs, the US-assisted LPE approach in NMP[17,73,74,76,99] or MW-assisted LPE in NMP[95] and EtOH[47] are favored. Furthermore, QDs have been effectively produced by US-assisted LPE in DMSO[63] and ST-assisted LPE in NMP/NaOH.[87] These findings highlight the versatility and adaptability of LPE techniques, which are designed to obtain certain morphological properties for a wide range of nanotechnology applications.

Within the field of LPE, the final flakes usually display a range of sizes, indicating the inherent variability present in the process. The exfoliation techniques used (*e.g.*, US, HSM, HPH, EC, MW, ST, and PL) and the specifics of each technique's exfoliation parameters (*e.g.*, solvent selection, power intensity, duration, and temperature) have a significant influence on this diversity.[43,73] For instance, prolonged sonication in solvents with high boiling points such as DMSO[44,57] and DMF[72] yields high-quality crystalline flakes, characterized by an FT spanning from 4 to 30 nm and an LS ranging from 100 to 600 nm. Conversely, extended sonication in NMP promotes the production of very small flakes, often referred to as QDs, with elevated EYs.[73,74,76] Significantly, QDs have been obtained with lower processing times employing MW-assisted LPE methods in NMP[95] and EtOH.[47] Additionally, another efficient technique for generating consistent flake sizes is the use of centrifugation for separation, which is a frequently used technology in the field of LPE. By applying centrifugal forces to the exfoliated material, flakes of different sizes may be successfully separated depending on their sedimentation rates, resulting in the separation of fractions with desirable properties. This approach is critical for controlling the size distribution and characteristics of exfoliated materials, allowing for more exact control and application-specific modification.[69,71,84,85] The selection of an exfoliation technique may, in theory, be tailored to the material properties needed for a particular application. For example, it is recommended to use EC-assisted LPE methods in PC,[61] DMSO,[46] DMF[68] and H_2O[45] to prepare big flakes (between 2 and 30 μm) with high EYs. However, US-assisted LPE procedures in NMP[17,73,75,76] or MW-assisted LPE techniques in a variety of solvents, such as DMF, ionic liquids ([BMIM][BF_4] and [HMIM][BF_4]), and cyclohexylpyrrolidone, are suggested for the preparation of QDs with higher EYs.[95,96] Furthermore, the production of BP with high EYs and particular FT between 2 and 20 nm and LS between 50 and 700 nm may be achieved by US-assisted LPE procedures in DMSO/DMF,[44,57] NMP,[58,77] H_2O/Zonyl 7950[84] and 1-hydroxyethyl-3-methylimidazolium trifluoromethanesulfonate ([HOEMIM][Tfms]) ionic liquids[43] and other solutions that show promise. These findings underscore the importance of tailoring LPE techniques to achieve desired material characteristics, thereby enhancing their applicability across a wide range of technological contexts.

3. Stability of BP nanomaterials for biological applications

The rapid degradation rate of BP nanomaterials negatively affects their functionality for various applications.[100] In the case of biomedical applications, the degradation of BP is considered a double-edged sword; on the one hand, the selective anticancer activity and bioactivity of BP arise from this feature, and on the other hand, BP nanomaterials are required to perform for longer periods like drug delivery applications. Moreover, the photocatalytic activities of BP such as PTT, PDT, and SDT weaken as the oxidation increases, which affects its functionality.[26,68,72,101] Therefore, different strategies have been considered to decrease the oxidation rate which will be discussed in this section.

Phosphorus is physiologically regarded as benign, existing in the cells, and participating in every physiological reaction.[11] One of the earliest approaches for BP protection was to encapsulate it into polymeric carriers. This protocol is an effective strategy, but the synthesis conditions are important. For instance, using water as a solvent and also exposure of BP to oxygen deteriorate the chemical stability. In this regard, the encapsulation of BP into PLGA through a simple emulsion method is one of the most effective ways. The synthesis process is non-destructive since the polymer and BP were combined in acetone and upon addition of the mixture to water, precipitation occurs and the BP is perfectly isolated in the interior part of PLGA from the external environment. The *in vitro* and *in vivo* experiments revealed excellent biocompatibility along with a high photothermal conversion rate and tumor-targeting ability.[102] Another popular polymer coating is PEG, which not only acts as a protective layer against oxidation but also can prolong the circulation time of a nanomaterial in the bloodstream.[103,104] BP nanosheets were functionalized with PEG-NH_2 groups *via* electrostatic interactions to adjust the chemical stability and biocompatibility.[105] Somewhere else, BP nanosheets were coated with a combination of folic acid and PEG-NH_2 groups; the lateral size and thickness were found to be approximately 100 and 3 nm, respectively for the surface-coated nanomaterials and the surface functional groups improved the loading efficacy of DOX on the nanomaterials and also the chemical stability.[106] Cyanine 7 and cyanine 7-NH_2-coated PEG-BP nanomaterials were synthesized for NIR imaging and cancer therapy. Upon intravenous injection of the nanomaterials, they could exhibit a long-enough circulation time followed by satisfactory tumor accumulation.[107] Polyethyleneimine is a cationic polymer that has been applied on BP nanomaterials to protect them against oxidation. This polymer does not affect the photothermal conversion rate of BP, but due to the high density of amine groups, it endows BP nanomaterials with the ability to carry genes. This coating has been applied on BP for the first time by Wang *et al.*[108] to carry small interfering RNA and knock down the surviving expression and yield the synergistic PTT and gene delivery. Polydopamine is a biocompatible polymer that has been widely applied as a surface coating to functionalize nanoparticles.[109] This polymer is

yielded through self-polymerization of dopamine under an alkaline condition. It is known that polydopamine is a multifunctional polymer that besides its high biocompatibility can protect BP from oxidation and also reinforce the photothermal conversion rate of BP nanomaterials.[110,111] It has been indicated that the polydopamine-coated BP nanocomposite could increase the solution temperature by 3.1 °C upon exposure to an 808 nm laser (1 W cm^{-2}, 10 min). PEG-folic acid was coupled to the BP-polydopamine nanocomposite *via* the Michael additive reaction to enhance the circulation time in the bloodstream and tumor-targeting ability.[112] Forming a hydrophobic interaction between BP nanomaterials and polymers is another technique to improve the chemical stability of BP. Silk fibroin is a protein that is extracted from silk with high biocompatibility and extended use in various biomedical applications.[113] An interesting method was devised by Huang *et al.*[114] to passivate the surface of BP with silk fibroin and the polymer was added during the exfoliation process of BP. It turned out that a strong bond was formed between each compound *via* hydrophobic interactions and the polymer coating had hydrophilic ends which prevented the aggregation of BP nanosheets in water. The nanocomposite was exposed to air and water for two weeks and the solution was very steady. After 20 days, the color of the solution started to change as a sign of BP degradation, whereas the color of pristine BP in water changed quickly and faded away due to the fast oxidation and degradation rate. The silk fibroin-coated BP was tested in terms of photothermal conversion after 14 days of exposure to air and water. The PTT ability of the nanocomposite was unchanged while pristine BP under the same condition showed nearly zero absorption over time.[114] Another approach is to load BP nanomaterials in different types of hydrogels. Although this strategy can decrease the oxidation rate of BP since these hydrogels encompass water, it oxidizes the loaded BP. A hydrogel platform composed of 2D BP nanosheets and agarose was developed for anticancer drug delivery. Upon applying NIR irradiation to the hydrogel, the encapsulated BP turns light into heat and increases the hydrogel's temperature. Then, reversible hydrolysis and softening of hydrogels occur, leading to the controlled release of loaded drug molecules. A further increase in the temperature causes a biosafe degradation of the hydrogel into oligomers, which can be excreted through urine.[115] In our study, we adopted an innovative synthesis strategy to develop a multifunctional platform of BP for cancer therapy and tissue regeneration. In this regard, we took advantage of the evaporation-induced self-assembly sol–gel technique followed by applying a two-step microwave irradiation to synthesize bioactive glass-BPQD nanocomposites. In the presence of Pluronic F127 as the surfactant, the hydrophobic BPQDs with a size of 4 nm were encapsulated in the inner side of liquid crystals. The light absorption of pristine BPQDs and the nanocomposite was tested over time through UV spectroscopy, and it was found that the bioactive glass-F127 coating could significantly decrease the oxidation rate of BPQDs.[11] Coordination chemistry provides an opportunity for the passivation of BP nanomaterials since the lone pair electrons of phosphorus react with oxygen. Through the coordination of electropositive metals such as titanium, platinum, and lanthanide, it is possible to protect BP from oxidation and degradation.[116] To passivate and functionalize BP nanomaterials with various structures including BPQDs, BP nanosheets, and BP microflakes, a surface modification strategy was adopted; lanthanide sulfonate complexes were used accordingly and the lone-pair electrons of phosphorus were occupied with the complex endowing the BP nanomaterials with excellent air and water stability. Besides the original photothermal conversion of BP, the gadolinium-modified BP nanostructures showed great potential in magnetic resonance imaging due to high R1 relativities and other lanthanide-coordinated structures indicated fluorescence in visible and NIR regions.[117] Table 3 indicates some of the biomaterials applied on the BP nanomaterials to improve the chemical stability and functionality.

4. Intrinsic anticancer activities of BP nanomaterials

Compared to the wide variety of 2D materials, BP nanosheets are endowed with inherent anticancer activities which induce antitumoral effects without being triggered by any external or internal stimulus. This superiority comes from the BP nanosheets' unique physicochemical properties. Thus far, some studies have taken advantage of the intrinsic anticancer activities of BP nanomaterials and proposed some mechanisms of action.[13–15,129] Generally, it undergoes degradation when exposed to oxygen, water, and oxidative stress. The bio-products resulting from the degradation are phosphate anions which are known as biocompatible species with physiological buffering capability. However, elevation in the phosphate anions' concentration in a cell increases ATP hydrolysis, leading to programmed cell death. Indeed, it is well reported that phosphate anions play a crucial role in regulating ATP hydrolysis and triggering apoptosis in cancer cells through various interconnected mechanisms that disrupt cellular energy balance, metabolism, and key signaling pathways. ATP hydrolysis, a vital process for cellular energy release, breaks down ATP into ADP or AMP, releasing phosphate anions. Cancer cells, which often exhibit altered metabolism, such as increased glycolysis, ATP production, and consumption, are already disrupted, making them particularly sensitive to changes in phosphate levels. When phosphate accumulates, it accelerates ATP hydrolysis,[130] rapidly depleting the cell's energy reserves. This accumulation of inorganic phosphate can also impair mitochondrial function, further reducing ATP production. Excess phosphate destabilizes the mitochondrial membrane potential, initiating a cascade of harmful events. One event may be mitochondrial dysfunction where the loss of membrane potential triggers the release of pro-apoptotic factors such as cytochrome *c*, which activates caspases and activates the apoptosis process. One more event involves oxidative stress. The increased ATP hydrolysis elevates ROS production, further damaging mitochondria and driving the cell toward apoptosis. As ATP levels drop due to rapid hydrolysis, the AMP-to-ATP ratio rises,

Table 3 Some surface modifications applied to BP to improve its chemical stability and functionality

Surface coating composition	Impacts	Applications	Ref.
PEG	–Making the BP nanomaterials hydrophilic –Improving the circulation of BP in the bloodstream –Improvement in the dispersibility –Active targeted therapy	Cancer therapy and imaging	106, 118 and 119
Polyethyleneimine	–Turning the surface of charge of BP towards positive making it a suitable carrier of genes	Cancer therapy	108 and 120
Polydopamine	–Reinforcing the photothermal conversion of BP nanomaterials –Improving the biocompatibility –Capable of being coupled with other polymers or functional molecules	Cancer therapy and imaging	112, 121 and 122
PLGA	–More effective protection of BP from oxidation than polydopamine and PEG –Capable of being functionalized with aptamers	Cancer therapy and tissue regeneration	123–126
Pluronic F127	–Capable of being combined with the sol–gel method to yield BP-based hybrids *in situ* –Benign synthesis medium that does not induce oxidation to BP –Controlled release of BP –Thermosensitive hydrogel and drug delivery	Cancer therapy and tissue regeneration	11 and 127
Silk fibroin	–It can be used as an exfoliating and stabilizing agent –High dispersibility –Long-term stability	Wound healing	114
Hyaluronic acid	–Drug release triggered by pH/NIR stimuli	Cancer therapy	128
Lanthanide sulfonate complexes	–Prevention of BP oxidation with excellent stability in air and water –Additional functionality like magnetic resonance imaging, fluorescence imaging, *etc.* based on the type of element	Cancer therapy and imaging	117

activating AMP-activated protein kinase (AMPK), which serves as an energy sensor. Prolonged energy depletion keeps AMPK active, which can eventually push damaged cancer cells into apoptosis, especially if mitochondrial dysfunction prevents the cell from restoring adequate energy levels. Cancer cells have a higher metabolism rate and the concentration of oxidative stress species is higher than that in normal cells generating a faster degradation rate of BP. This different degradation pattern of BP in cancer cells leads to its selective anticancer potential. In 2019, Zhou *et al.* revealed the selective anticancer potential of BP against various cancer cell lines including breast cancer cells (MCF-7). The anticancer activity of BP was compared simultaneously to well-known DOX against the cancer cell lines; the degradation of BP was found to elevate the levels of phosphate anions in the intracellular environment and exhibited strong antiproliferation effects against the cancer cells while leaving no negative impact on the normal cells (Scheme 4). The efficacy was superior to the applied DOX, which is an added value to take into consideration. Raman scattering mapping was adopted to track the degradation of BP throughout both healthy and cancer cells; BP has three distinct Raman peaks by which the average of signal intensities was determined up to 48 h. Raman spectra related to BP (4 μg mL^{-1})-treated MCF-7, A549, and healthy bone mesenchymal stem cells were recorded after different time intervals including 6, 12, 24, and 48 h. Moreover, the phosphate anion concentration was measured during this assay, which together with Raman images showed that the BP internalization and release of phosphate anions in cancer cells were higher than those of healthy ones. The cellular response of BP (0.125–16 μg mL^{-1}) to three cancer cell lines and two healthy ones was assessed *in vitro*. It was found that the IC_{50} value of BP for the cancer cells was less than 2 μg mL^{-1}, whereas no negative effect was observed for the healthy cells even at higher concentrations. Furthermore, although the IC_{50} of DOX was lower than that of BP and eradicated the cancer cells at lower concentrations, it strongly affected the healthy cells at the same concentration and killed them, which is considered as the main side-effect of this chemotherapeutic drug. Through fluorescence-activated cell sorting, the cell cycle analysis on the BP-treated cells was performed at 24 h and 48 h with different BP concentrations. The MCF-7 cells treated with BP showed a significant rise in G2/M phase arrest, where the time and the concentration exert an additional effect. In contrast, the healthy cells' cycle remained unchanged (G0/G1). Noteworthy, cyclin B1 is known to directly relate to G2/M transition and through immunoblotting against cyclin B1. BP increases the expression of it in the cancer cells while it was negligible in the healthy cells. Followed by desirable *in vitro* studies, BP was *in vivo* intratumorally injected through the mice xenografted with HeLa cells along with phosphate buffer saline (PBS) and DOX as the negative and positive control, respectively. The tumor volume and body weight changes were carefully tracked and it was found that the anticancer activity of BP was similar to that of DOX. The histological and dissected tumors treated after 18 days with different samples revealed shrinkage and necrosis for the ones treated with the drug and BP.[14]

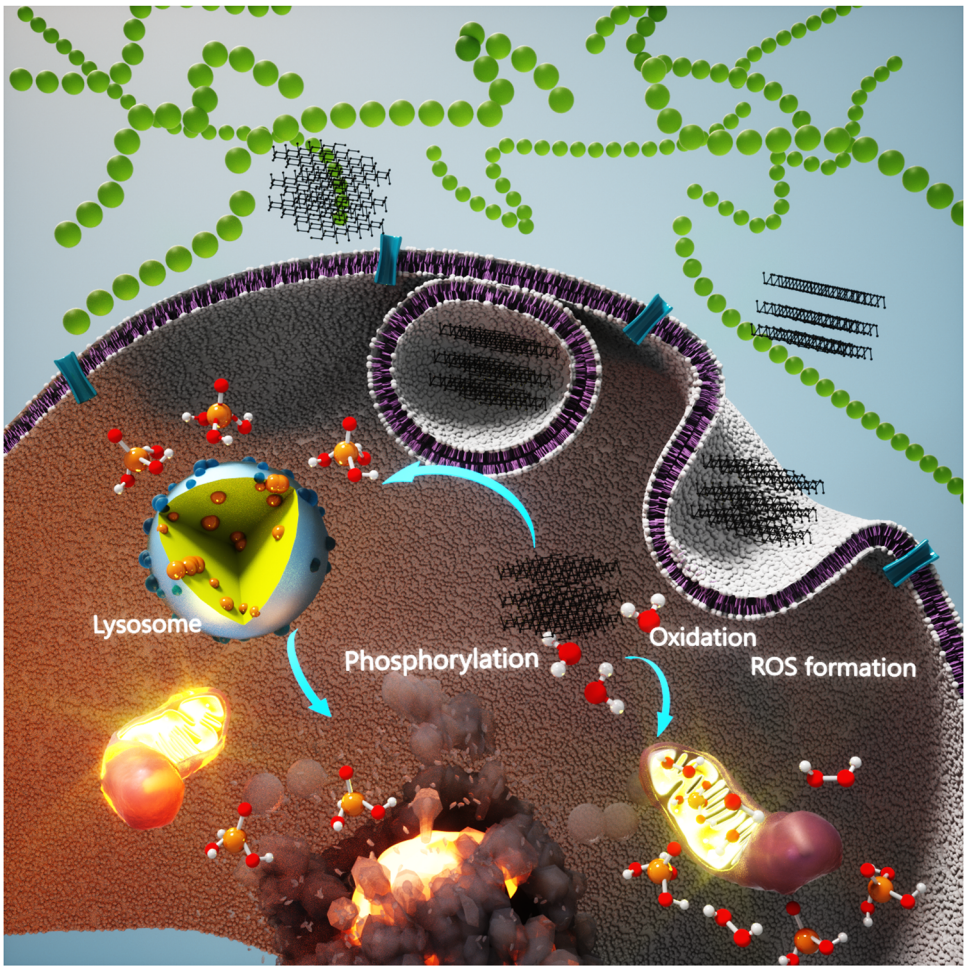

Scheme 4 Selective anticancer activity of BP. Schematic of how BP materials induce anticancer activity intrinsically.

In 2020, an update to the previous proposed mechanism of action was published. The authors have systematically revealed that the lipid peroxidase level goes up due to phosphate anions release and causes a decrease in superoxide dismutase activity when BP nanomaterials are exposed to cancer cells, leading to higher ROS generation in these cells (Fig. 1(A)). However, they suggested certain dosage range of applied BP called the selective killing range, beyond which BP nanomaterials can induce cytotoxicity on the healthy cells, leading to DNA damage and pathological abnormalities in the organs. Two cell lines—HeLa and A549 cancer cells and D551 and Hek293 normal cells—were comprehensively assessed (Fig. 1(B–G)). The cell cycle arrest of these cells was evaluated, and it was found that BP could extend the G2/M phase of cancer cells in a concentration-dependent manner, whereas no significant effect was observed in the healthy cells. It is known that the G2/M phase is closely related to DNA damage and apoptosis, and hence, the level of DNA damage in this study was also analyzed; poly(ADP-ribose) polymerase and γ-H2AX were used as the markers of cellular apoptosis and DNA breaks, respectively. In the case of cancer cells (HeLa and A594), significant activation of apoptosis and DNA damage was detected in the domains of II + III and III + IV, in turn, while lower damage to the healthy cells' DNA was observed, which was not high enough to induce irreversible damage followed by apoptosis to these cells. The anticancer efficacy was tested *in vivo* in the HeLa and A549 xenograft tumor models. The immunohistochemistry analysis indicated that the BP-induced ROS caused high expression of cleaved caspase 3, while the proliferation marker of K_i-67 decreased as the result of apoptosis increase and inhibition of the tumor growth.[15] A study has reported the surface modification of BP nanosheets through a combination of polymers and peptides to not only stabilize the nanosheets against oxidation but also induce therapeutic effects through the released peptides against breast cancer. The polymers were poly-L-lysine and PEG, which first conjugated on the peptides and then the combination was anchored to the surface of BP. The anticancer potential of the nanosheets and the surface-modified ones was assessed *in vitro* against MCF-7, MDA-MB-231, and human mammary luminal epithelial cell line. The applied concentrations were 0.8, 4, and 20 μg mL^{-1} for 72 h and the MTT results of bare BP showed antiproliferative effects against the cancer cells when the concentration increased to 4 μg mL^{-1} and specifically, this concentration was more toxic towards the

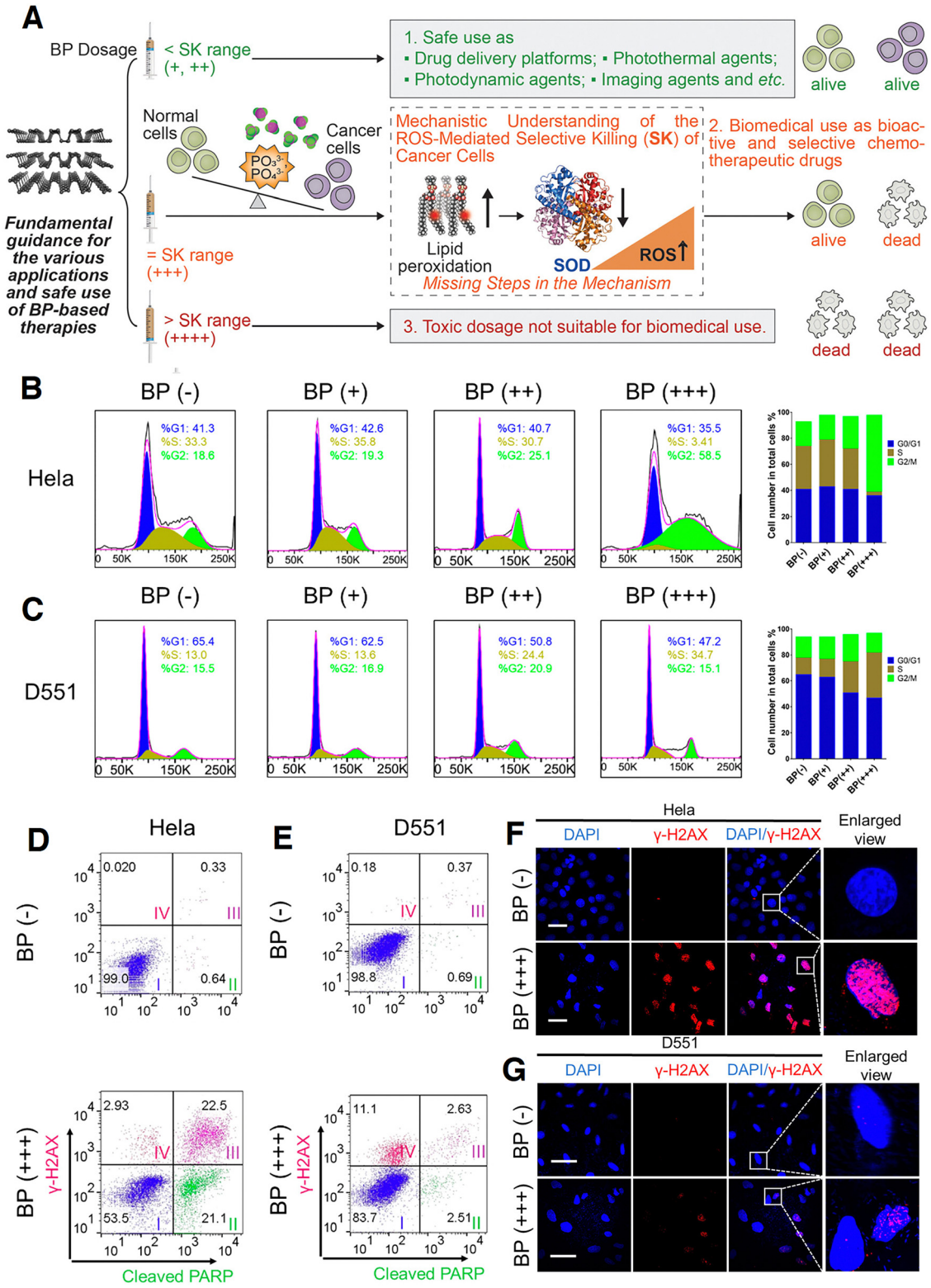

Fig. 1 ROS-mediated selective anticancer activity of BP nanosheets. (A) Mechanistic understanding of how BP nanosheets induce selective anticancer activity; Three dosages of BP including low (+, 100 μg mL^{-1}), middle (++, 200 μg mL^{-1}), and high (+++, 400 μg mL^{-1}) were applied. The degradation of BP is synchronized with the increase in the phosphate anions and lipid peroxidation, followed by a decrease in the superoxide dismutase, all of which lead to higher ROS generation and selective anticancer activity of BP. (B) and (C) Cell cycle distribution of two cancer cell lines treated with different concentrations of BP and the control (BP (−)). (D) and (E) DNA damage and apoptosis markers detected by dual staining. (F) and (G) Confocal microscopic images of the cancer cells treated with BP nanosheets (scale bars, 50 μm) related to the unrepaired DNA damage in cancer cells compared to the normal ones. DAPI was used for nuclei staining (blue), and the red color is related to the γH2AX foci per nucleus stained using an anti-γH2AX antibody. Reprinted from[15] with permission from the American Chemical Society.

MDA-MB-231 cells rather than MCF-7. However, the highest concentration (20 μg mL^{-1}) affected the healthy cells negatively. The modification of BP nanosheets with PEG-peptides was synchronized with neutralizing the anticancer effect of bare BP, but attaching the poly-L-lysine-peptide combination showed a different behavior; the cytotoxicity against normal cells was reduced, while the same effect against the cancer cells was reinforced. A comparison between the bare BP nanosheets and the surface-modified ones shows that the anticancer efficacies of both was almost equal at 20 μg mL^{-1}, but the former inhibited the growth of healthy cells besides cancer cells.[131]

Cells are actively divided through two main phases—interphase (G1, S, and G2) and mitosis (Scheme 5). The former is known as the longest cell cycle in which the cell grows followed by copying DNA to prepare itself for mitosis. During the interphase period, the cells grow, internal organelles are cloned, and then, through the synthesis phase, a DNA copy will be synthesized. At the final stage of interphase, the cells continue to grow and reorganize the contents getting ready for division. When it comes to mitosis, the previously copied DNA and cytoplasm are divided, resulting in two new identical daughter cells.[132] The mitosis has four phases—prophase, metaphase, anaphase, and telophase. Over half period of mitosis is occupied by the first phase through which the membrane of the nucleus breaks down forming small vesicles and the centrosome is duplicated moving to the opposite end of the cell. Microtubule production is organized by centrosomes, leading to the formation of spindle fibers and then mitotic spindle constitution. From prophase to metaphase, the cell can undergo multipolar spindles due to various defects in the integrity of the mitotic spindle pole, which causes cell death in the progeny mainly because of the large mis-integration in chromosomes. In this way, the daughter cells with far fewer chromosomes are less likely to survive[133] (Scheme 5). The most recent update to the anticancer mechanism of action of BP nanomaterials is published by Shao *et al.*,[129] shedding light on the molecular interaction of BP with cancer cells. In this study, it has been revealed that BP directly affected the cell's centrosome machinery (Scheme 6). Different from the previous studies which reported that BP induces only apoptosis (G2/M arrest) due to degradation and ROS generation, Shao *et al.* provided a new mechanism of action and indicated that the cohesion of pericentriolar material

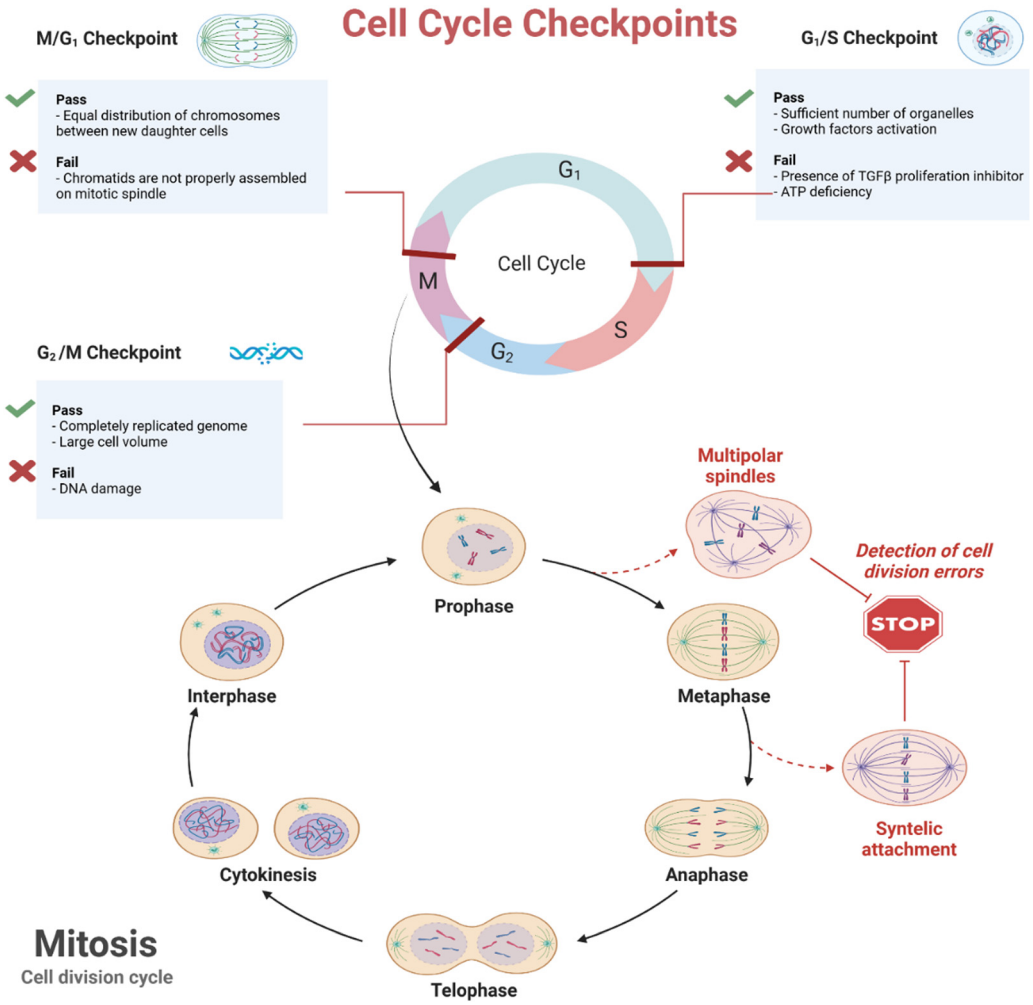

Scheme 5 Eukaryote cell cycles and mechanism of formation with possible failures. Created with BioRender.com.

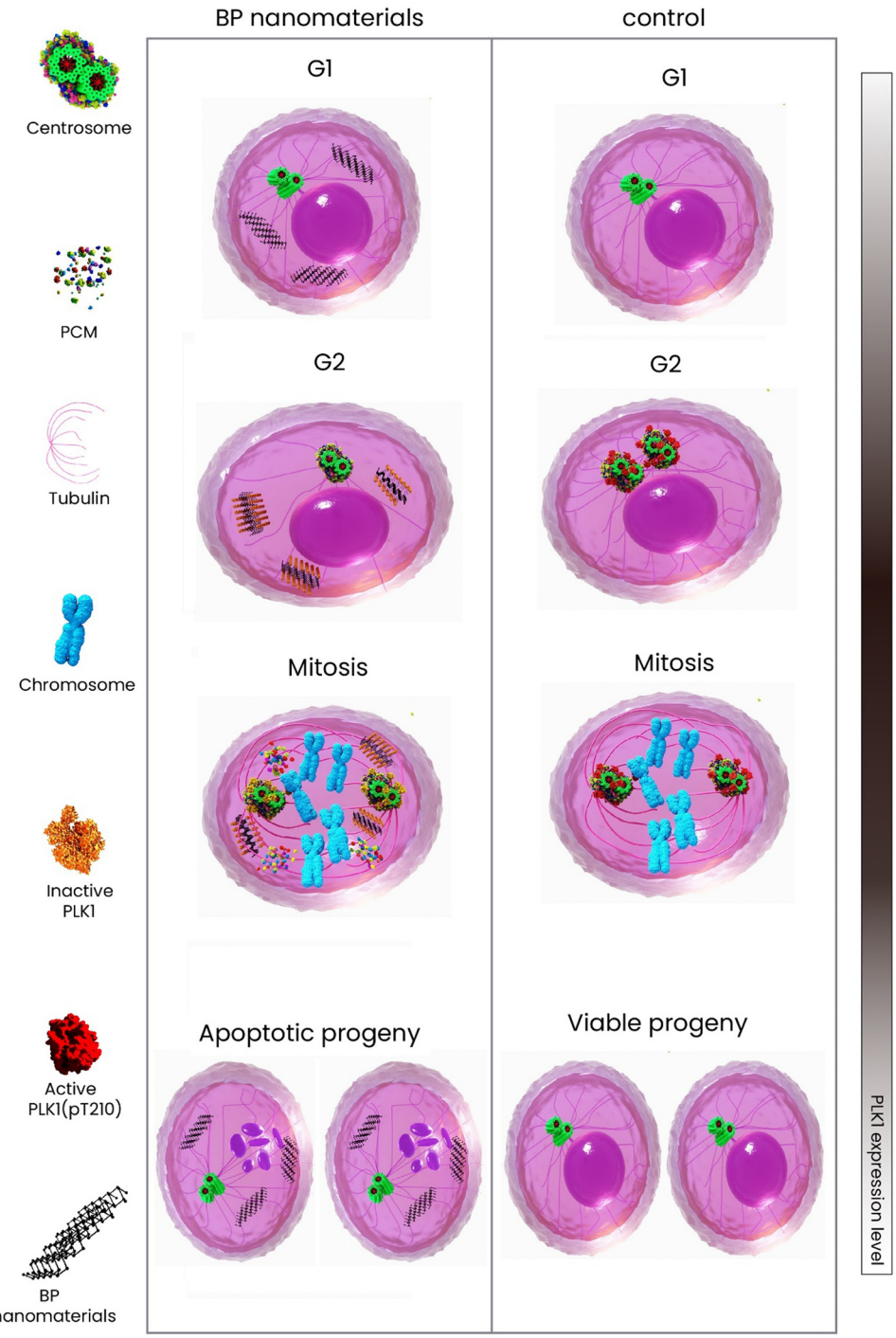

Scheme 6 Schematic of the molecular anticancer activity of BP.

was attenuated due to destabilization made by BP on the mitotic centrosomes, leading to the fragmentation of centrosome through the mitosis. The cancer cells treated with BP were found with multipolar spindles and mitotic delay followed by apoptosis. In detail, the centrosome kinase polo-like kinase 1 was observed being deactivated when treated with BP, which compromised the integrity of centrosomes; the kinase was attached to BP's surface and its aggregation was increased and this impeded the mobility of kinase followed by being recruited by centrosomes for activation. In this work, *in vitro* and *in vivo* studies were comprehensively conducted and proved this mechanism of action (Fig. 2).

5. Breast cancer

Breast cancer is at the top of the cancer list of women as the most common and primary cause of mortality. The statistics

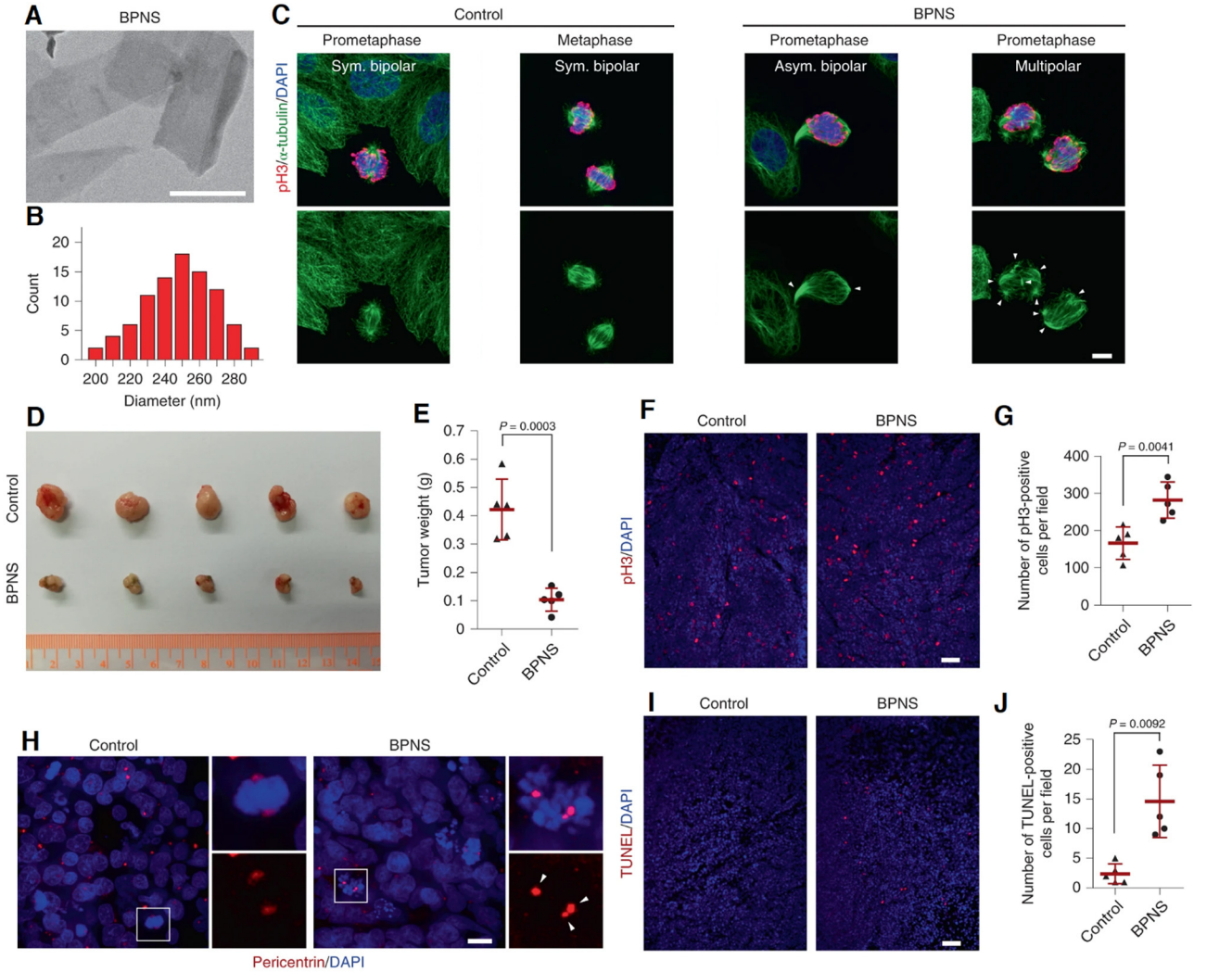

Fig. 2 Mitotic centrosome destabilization effect of BP against cancer cells. (A)and (B) Morphology and size distribution of BP nanosheets through TEM. (C) Double immunostaining of HeLa cells to take images of each mitosis phase from the control and the cells treated with BP nanosheets (4 μg mL^{-1}); the white arrows indicate the multipolar spindles. (D)and (E) Tumor xenografts were developed on the right flank of BALB/c nude mice and once reached the size of 50 mm^3, BP (25 μg) was intratumorally injected four times every 2 days. The images were taken from the dissected tumors plus tumor weights treated with BP at the end of the study, which can be compared with the control. Images from the tumor section, which were stained for (F) pH3, (H) pericentrin, and (I) Tunel. (G) and (J) Quantitative results related to pH3 and Tunel-related positive cells, respectively. Reprinted from[129] with permission from Nature.

tell us that about 60% of total deaths take place in developing countries and the survival rate differs worldwide—5 years for less than 40% of patients in developing countries while about 80% for their counterpart.[134] Apart from early diagnosis and screening through mammography which significantly declined the mortality rate, various treatments are being applied. Some preventive treatments are hormone therapy through applying antiestrogens to the individuals with the potential for developing breast cancer and also surgery to remove the tissue and prevent cancer progression.[135] Once a patient is diagnosed with breast cancer, other approaches including radiotherapy, chemotherapy, and targeted therapy are applied, but in the case of distant tumors and metastasis, the focus is on the survival rate and improving the quality of life.[136–138] Both the devastating side effects and undesirable outcomes of the mentioned approaches were the driving force behind searching for newer ones with fewer disadvantages and more efficacy. The breast is mainly formed by tissues called adipose, and the female's breast normally has more glandular tissues than a man and there are about 12 to 20 lobes which are divided into smaller ones.[139] Based on the size and type of tumor and also the penetration of cancerous cells into the tissue, the breast cancer stages vary spanning from stage 0 attributed to non-invasive to stage IV as the metastatic breast cancer (Scheme 7). Through stage 0, the healthy and cancer cells are on the boundaries from which the tumor starts to grow, but still there is no sign of invasion.[140] Stage I has two subcategories I(A) and I(B), and at this stage, microscopic invasion is possible; the first subcategory relates to the tumors with a maximum size of 2 cm but none of the lymph nodes are involved, but the latter

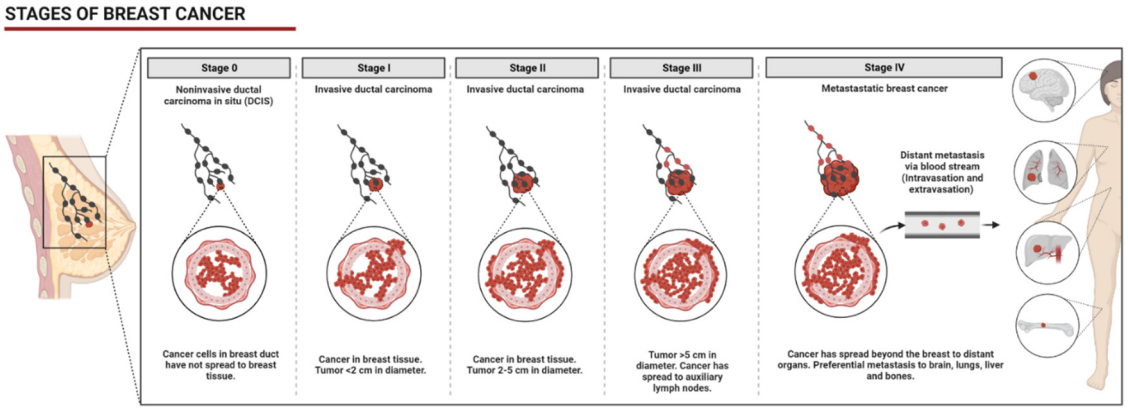

Scheme 7 Schematic of the different stages of breast cancer. Created with BioRender.com.

subcategory describes a situation in which tumors larger than 2 cm are found in the lymph nodes.[141] Similar to the first stage, the second stage is divided into two—II(A) and II(B). The former is ascribed to the tumors located in the sentinel and/or axillary lymph nodes but not in the breast and the size can be varied from below to more than 2 cm but not beyond 5 cm. However, the tumors in the case of the latter one can be larger than 5 cm.[142] There are three subcategories for stage III in which III(A) describes that still no tumor is in the breast but they can be found in 4–9 lymph nodes; the second one (III(B)) means the tumors despite their size have caused swelling and may have spread to about 9 lymph nodes and this stage is also known as inflammatory breast cancer. III(C) is a situation of spreading the tumors to more than 10 axillary lymph nodes.[143] The final stage is the advanced stage showing the spread of tumor to other organs (Scheme 7).[144]

Among different types of cancers, BP nanosheets and BPQDs have been competitively more adopted for the studies related to breast cancer imaging and sensing compared with other cancer types. BP intrinsically and selectively showed anticancer activity and also it is responsive to light and induces heat and ROS both of which induce apoptosis.[145] Through this section, the potential of BP either alone or in combination with chemotherapeutic drugs and external stimuli is covered in detail. The sub-sections are divided based on the therapeutic potential of BP; in this way, the BP-loaded carriers with a single therapeutic technique including PTT, PDT, SDT, and chemotherapy are discussed in the single therapy section, and in the case of dual and triple therapeutic approaches, the same way is followed. Table 4 provides information about the BP-based materials for breast cancer therapy.

5.1. Stimuli-responsive and cargo delivery

BP nanomaterials are appropriate for photonic-based applications and they are responsive to visible and NIR and turn light into heat (PTT) and ROS (PDT).[32] PTT is a minimally invasive type of cancer therapy that can effectively kill cancer cells due to heat generation. Once a light-responsive agent has reached a cancer cell and got stimulated, the agent releases heat locally, leading to cancer cell death. The efficacy of this approach depends on various parameters—type of light-responsive agent, laser power and density, and time of irradiation, all of which can be manipulated to obtain desirable results.[174,175] A study took advantage of the PTT potential of BP against breast cancer. The applied BP in this study is in the form of quantum dots, which were obtained through LPE from bulk BP followed by encapsulation into PLGA (lactic (50): glycolic (50)). The BPQDs were dispersed into an organic solvent in which PLGA had already been dissolved and upon addition of the PLGA-BPQDs to deionized water, the BPQD-encapsulated PLGA nanoparticles were formed. The hydrophobic nature of PLGA could successfully isolate the interior BPQDs from oxygen and water preserving their optical properties as intact as possible. The anticancer potential of PLGA-BPQDs against three cell lines was assessed *in vitro*—human skin fibroblast, breast cancer cells (MCF-7), and melanoma cells (B16)—with and without stimulation by NIR. The nanoparticles, in various concentrations (2–100 μg mL^{-1}), were exposed to each cell line for 48 h. Without applying any light irradiation, there was no significant change in the cell viability of samples even at the highest concentration. The light irradiation caused the cell viability of cancer cells to fall about 20% for the lowest concentration (2 μg mL^{-1}) followed by a 50% decrease when the concentration was increased to 5 μg mL^{-1}; 10 and 20 μg mL^{-1} exhibited nearly a complete eradication of cancer cells and fluorescence images were also in agreement with the results—the stained cells in green and red were live and dead, respectively. The *in vivo* PTT studies on the MCF-7 breast tumors were performed once the tumors reached the volume of 200 mm^3, and PLGA, BPQDs alone, and PLGA-BPQDs were injected *via* the tail vein. After 24 h post-injection, the mice were anesthetized and NIR was irradiated to the tumors and the PTT efficiency was recorded through infrared imaging. The biodistribution study revealed that in 24 h the nanoparticle concentration reached their highest point in the tumor, and hence, the best time point to apply the NIR was 24 h post-injection. The highlight of PTT *in vivo* study was the superior efficacy of PLGA-BPQDs compared to bare BPQDs; applying 10 min irradiation was enough for the combination to increase the temperature of the tumor up to 60 °C while the bare BPQDs just could raise the

Table 4 Physicochemical and biological properties of BP-based materials in breast cancer therapy

Nanovehicle	Particle size (nm) Zeta potential (mV) Photothermal conversion (%)	Type of therapy	*In vitro* and *in vivo* models	Cargo	Remarks	Ref.
BP nanosheets	297.6 ± 7.01 nm 27.5 ± 0.26 mV —	Selective anti-cancer activity	*In vitro*: MCF-7, HeLa, A549, QSG-7701, hMSCs *In vivo*: HeLa xenografts	—	–BP, for the first time was found to induce anticancer activity selectively with a strong efficacy similar to DOX –BP prohibited the cancer cells' growth while leaving no negative effects on the healthy cells –Phosphorylation and ROS generation as the result of degradation in the cancer cells were proposed as the mechanism of action	14
Polymer-peptide-modified BP	200 nm Bare BP: 0 mV —	Selective anti-cancer activity	*In vitro*: MCF-7, MDA-MB-231, and human mammary luminal epithelial cell line *In vivo*: —	—	–BP was surface-modified with a combination of two different polymers and peptides against breast cancer cells –Bare BP could induce an anticancer effect at 4 μg mL^{-1} with no effect on the healthy cells whereas increasing up to 20 μg mL^{-1} showed cytotoxic effects on the normal cells –The surface modification composed of poly-L-lysine-peptides could induce the same anticancer effect as the bare BP at 20 μg mL^{-1} without inhibiting the growth of normal cells	131
PLGA-BPQDs	127.6 ± 43.8 nm — —	PTT	*In vitro*: human skin fibroblast, MCF-7, B16 *In vivo*: MCF-7 breast cancer tumors	—	–BPQDs were encapsulated into PLGA for breast cancer therapy –The PLGA-BPQDs showed anticancer activity *in vitro* when the NIR was applied –The polymer successfully stabilized the BPQDs and improved the physicochemical and biological properties *in vivo*	102
BP with different particle sizes	394 ± 75 nm (Large BP) 118 ± 22 nm (Medium BP) 4.5 ± 0.6 nm (Small BP)	PTT	*In vitro*: LO2 and MCF-7 *In vivo*: —	—	–BP nanomaterials with different sizes were developed through liquid exfoliation –Ultrasound time and centrifugal speed were the parameters by which those sizes were obtained –All the samples showed no cytotoxicity towards healthy cells –The PTT potential *in vitro* against MCF-7 revealed stronger PPT potency of the larger particles	146
Nile Blue@BP	35 nm — —	PTT and imaging	*In vitro*: LO_2 and MCF-7 *In vivo*: MCF-7 breast tumors	—	–Nile Blue was covalently anchored onto BP nanosheets to improve the stability and endow fluorescence imaging –The biocompatibility of nanoparticles was shown through *in vitro* cell viability –The modified nanoparticles could effectively mark the tumor cells *in vivo* with red fluorescence and ablate the tumor upon exposure to NIR	147
BP-dextran/poly(ethyleneimine)-folic acid/cyanine7	30.2 nm −24.5 mV 41%	PTT and imaging	*In vitro*: 3T3 and 4T1 *In vivo*: 4T1 breast tumors	—	–BP nanomaterials were functionalized for targeted breast cancer therapy and imaging –The nanoparticles were found to produce photoacoustic and NIR images –The nanoparticles successfully reached the tumor site due to the conjugation of folic acid and under NIR ablated the tumor cells *in vivo*	148

Table 4 (*continued*)

Nanovehicle	Particle size (nm) Zeta potential (mV) Photothermal conversion (%)	Type of therapy	*In vitro* and *in vivo* models	Cargo	Remarks	Ref.
Indocyanine green@BP nanosheets-PEG	240 ± 28 nm −16.2 mV —	PTT and imaging	*In vitro*: RPE, MCF-7, and 4T1 *In vivo*: 4T1 breast tumors	Indocyanine green	–Indocyanine green was loaded on the BP nanosheets followed by being modified with PEG for breast tumor-targeting and fluorescence imaging –*In vitro* cytotoxicity evaluation exhibited the biocompatibility nature of nanoparticles without irradiation –Compared to free indocyanine green, the nanoparticles could passively accumulate in the tumor's site through enhanced permeation and retention and eradicate the cancerous cells under NIR	149
BP nanosheets@streptavidin@CD146	158 ± 25 nm ∼−15 mV —	Mild PTT	*In vitro*: MDA-MB-231 *In vivo*: —	—	–BP nanoparticles were surface-modified with Streptavidin and CD146 to reverse the epithelial–mesenchymal transition followed by stopping the invasiveness of breast cancer -The applied imaging techniques and immunoblotting revealed that the nanoparticles plus mild hyperthermia successfully turned mesenchymal-type breast cancer cells into an epithelial phenotype	150
BP-gelatin composite scaffold	—	PTT and regeneration	*In vitro*: MDA-MB-231 *In vivo*: MDA-MB-231-seeded on the scaffolds	—	-A composite scaffold comprised of gelatin and BP nanosheets was fabricated *via* the freeze-drying technique -The scaffold had an interconnected porosity and BP nanoparticles were homogenously distributed through the structure -The BP addition improved the compressive strength of the scaffold and endowed it with PTT potential and PTT efficacy depended on the BP content -The composite scaffold was found to eradicate the breast cancer cells followed by stimulating adipose regeneration	151
Platelet membrane-BPQDs	140 nm −30.5 ± 2.5 mV —	Drug delivery	*In vitro*: MCF-7 *In vivo*: MCF-7-induced tumors	Hederagenin	-A new formulation was developed for breast targeted cancer therapy -The chemotherapeutic drug molecules were loaded onto the BPQDs followed by being encapsulated in a platelet membrane -The drug-loaded BPQDs were camouflaged with the platelet membrane and successfully accumulated in the tumor and inhibited the growth rate *in vivo*	152
Poly-lysine-BP nanosheets	128.38 ± 3.98 nm 25.56 ± 3.55 mV —	Gene delivery	*In vitro*: MCF-7 and MDA-MB-231 *In vivo*: MDA-MB-231-induced tumors	Cas13a/crRNA	-A gene carrier composed of poly-lysine-coated BP nanosheets to inhibit Mcl-1 at the transcriptional level was designed for breast cancer therapy -The carrier reached inside the cancer cells through endocytosis and successfully knocked down Mcl-1 at the transcriptional level and inhibited the cell activity -The complex had a tumor suppression efficacy of 65.16% after intratumoral injection	153
BP nanosheets	—	PDT	*In vitro*: MDA-MB-231 *In vivo*: MDA-MB-231 tumor-bearing mice	—	-The first study on the usage of BP nanosheets as a photosensitizer for PDT breast cancer therapy -The *in vitro* and *in vivo* studies showed the anticancer activity of BP nanosheets followed by degrading to biocompatible phosphorus oxide	154

Table 4 (*continued*)

Nanovehicle	Particle size (nm) Zeta potential (mV) Photothermal conversion (%)	Type of therapy	*In vitro* and *in vivo* models	Cargo	Remarks	Ref.
BP nanosheets-C_{60}	— —	PDT	*In vitro*: 4T1, MCF-7, Huh-7, U937, and RAW 264.7 *In vivo*: 4T1 tumor-bearing mice	—	-C_{60} was grafted covalently on the BP to improve the physiological stability and ROS generation of nanosheets -Through the *in vitro* studies, the hybrid had an inhibition rate of 90% against breast cancer cells in the exposure of NIR -The hybrid was injected into the tumor-bearing mice through intravenous and intratumoral ways and achieved 65.6 and 88.2% inhibition rate, respectively	155
BP nanosheets-C_{60}	— —	SDT	*In vitro*: 4T1 *In vivo*: 4T1 tumor-bearing mice	—	-The role of covalent functionalization of C_{60} and benzoic acid to BP nanosheets on the SDT potency against breast cancer was assessed *in vitro* and *in vivo* -It was found that the samples with covalent functionalization had stronger SDT potential generating more ROS and inducing a significant decrease in the cancer cells' viability and tumor growth rate	156
BP nanosheets-poly-L-lysine-hyaluronic acid	— −29.4 ± 1.4 mV —	Chemotherapy and PTT	*In vitro*: MCF-7 and MDA-MB-231 *In vivo*: MDA-MB-231 tumor-bearing mice	DOX	-A novel synthesis technique for the preparation of BP nanosheets was proposed -Red phosphorus was catalytically converted into BP nanosheets with the aid of iodine, gold, and tin -The BP was surface-modified with poly-L-lysine and hyaluronic acid for simultaneous chemo-thermo breast cancer therapy -Concurrent effects of DOX release and PTT caused an effective tumor growth suppression	157
Poly-(2-ethyl-2-oxazoline) modified BP nanosheets	248.6 ± 22.0 nm −4.9 ± 0.5 mV —	Chemotherapy and PTT	*In vitro*: MCF-7 *In vivo*: MCF-7 tumor-bearing mice	DOX and Bortezomib	-A pH- and light-responsive carrier with two chemotherapeutic drugs was prepared through a layer-by-layer strategy -The carrier could reverse the surface charge from negative to positive which facilitated the cell's internalization -The therapeutic outcomes were reinforced under NIR irradiation culminating in the release of two drugs plus PTT	110
Poly-L-lysine-coated BP nanosheets	187 ± 1.097 nm −14.8 ± 0.153 mV	Chemotherapy and PTT	*In vitro*: 4T1 *In vivo*: 4T1 tumor-bearing mice	DOX	-A carrier based on BP nanosheets responsive to glutathione and light was synthesized -The DOX was loaded on the nanosheets through electrostatic interactions followed by coating of the polymer onto the drug-loaded nanosheets -The polymer not only stabilized the carrier physiologically but also prevented early undesired liberation of DOX -The carrier showed potent anticancer outcomes without side effects of DOX	158
BPQDs-encapsulated PLGA	130 nm — —	Chemotherapy and PTT	*In vitro*: 4T1-LG12 *In vivo*: 4T1-LG12 tumor-bearing mice	Docetaxel	-BPQDs and docetaxel were together encapsulated inside of PLGA -The nanomaterials have shown desirable anticancer effects on both primary tumors and lung metastatic ones -The PTT was found to accelerate the release rate of drug molecules and the synergistic chemo- and thermo-therapy ablated the tumors *in vivo*	125

Table 4 (*continued*)

Nanovehicle	Particle size (nm) Zeta potential (mV) Photothermal conversion (%)	Type of therapy	*In vitro* and *in vivo* models	Cargo	Remarks	Ref.
BPQDs-cysteine-based poly-(disulfide amide)	155 nm ~ -40 mV 39.90%	Chemotherapy and PTT	*In vitro*: 4T1, HepG2, H1650, and NIH-3T3 *In vivo*: 4T1-tumor-bearing mice	Paclitaxel	-A redox-responsive agent comprised of BPQDs and a polymer with a disulfide bond was synthesized for combined PTT and chemotherapy -The polymer could easily respond to glutathione and release BPQDs and the loaded drug *in vitro* and *in vivo*	159
Biomimetic BPQDs	100 nm -13 mV 28.4%	PTT and immunotherapy	*In vitro*: 4T1 *In vivo*: 4T1-tumor-bearing mice	PD-1 antibody	-BPQDs were encapsulated in erythrocyte membranes for simultaneous PTT and immunotherapy -The PTT induced release of tumor neoantigens besides directly killing the cancer cells through hyperthermia -Combination of PTT and release of PD-1 delayed the growth rate of tumors *in vivo*	160
Surface-modified BP nanosheets	250 nm 35.5 mV 28.41%	PTT and immunotherapy	*In vitro*: 4T1 *In vivo*: 4T1-tumor-bearing mice	CpG	-BP nanosheets were modified with bPEI-PEG followed by grafting of CpG -PTT parameters were manipulated in order to optimize the activation of necroptosis -The increase in the tumor's local temperature together with the immune adjuvant resulted in high-performance cancer photo-immunotherapy	161
PEG-BP nanosheets	100 nm -8.34 mV 36%	PTT and immunotherapy	*In vitro*: L929, 4T1, and B16 *In vivo*: B16-tumor-bearing mice	Imiquimod	-PEG-BP with different concentrations (5–100 μg mL^{-1}) were exposed to the cell lines and did not show a significant cytotoxicity after 24 h -In the presence of imiquimod, the PTT induced a strong immune response *in vivo* and the combined therapy was stronger than monotherapy	162
Biomimetic BPQDs	30 nm -24.1 ± 3.1 mV —	PTT and immunotherapy	*In vitro*: 4T1 *In vivo*: 4T1-tumor-bearing mice	PD-1 antibody	-Cancer cell membrane-coated BPQDs were designed for targeted PTT and immunotherapy -The nanoparticles were found to directly kill the cancer cells and elicited dendritic cell maturation -The mentioned outcomes were further reinforced with the PD-1 antibody and inhibited the tumor recurrence and metastasis	163
Biomimetic BP-Au	350 nm -30 ± 1.7 mV —	PTT and immunotherapy	*In vitro*: 4T1 *In vivo*: 4T1-tumor-bearing mice	CpG	-CpG was loaded on BP-Au and together co-encapsulated into in cancer cell membrane to eliminate primary and metastatic breast tumors -Thanks to the surface coating, the carrier reached tumor cells selectively and the combined PTT and immune adjuvant release led to the generation of tumor-associated agents followed by tumor-specific immunity	164
BPQDs-doped multifunctional hydrogel	—	PTT and immunotherapy	*In vitro*: MDA-MB-231 *In vivo*: MDA-MB-231-tumor-bearing mice	Zoledronate	-A hydrogel composed of poly(N-isopropyl acrylamide) and BPQDs was designed for breast PTT and immunotherapy -Upon NIR irradiation, the BPQDs elevated the local temperature which not only caused the loaded drug to release faster from the temperature-sensitive polymer but also induced hyperthermia -The Gamma-delta (γδ) T cells were observed to show strong anticancer activity against breast and bladder tumors stemming from improved secretion of perforin and granzyme B	165

Table 4 (*continued*)

Nanovehicle	Particle size (nm) Zeta potential (mV) Photothermal conversion (%)	Type of therapy	*In vitro* and *in vivo* models	Cargo	Remarks	Ref.
BPQD vesicles	100 nm −33.5 ± 1.9 mV —	PDT and immunotherapy	*In vitro*: 4T1 and MCF-7 *In vivo*: 4T1-tumor-bearing mice	CpG	-A vesicle-like carrier was synthesized based on BPQDs which were responsive to ROS and light -After laser irradiation, the ROS generated from the BPQDs caused a structural change and release of the immune adjuvant -The synergism of PDT and immunotherapy blocked the primary tumors' growth and distant ones *in vivo*	166
Surface-modified BP nanosheets	55 nm — —	Photoacoustic therapy and immunotherapy	*In vitro*: 4T1, 4T1-MCF-7, and MCF-7 *In vivo*: 4T1-tumor-bearing mice	Resiquimod	-BP nanosheets were modified with a peptide and triphenylphosphine to endow tumor- and mitochondrion-targeting, respectively -In the presence of the adjuvant and photoacoustic shockwaves, the nanoparticles triggered tumor-associated antigens with a strong antitumor immune response -Besides prevention of primary and metastatic tumor suppression, the *in vivo* studies confirmed the existence of memory T cells in the spleens after the synergistic treatment inhibiting the tumors' recurrence	167
Cypate-BP nanosheets-Hyaluronic acid	187 ± 7.4 nm −40.2 ± 3.3 mV 49.12%	PTT and PDT	*In vitro*: 4T1 and human dermal fibroblasts *In vivo*: 4T1-tumor-bearing mice	—	-A dual stimuli platform based on BP nanosheets was designed for breast PDT/PTT -Cypate was loaded on the sheets followed by an outer layer of hyaluronic acid on the nanosheets -The combination of ROS generation and hyperthermia derived from light irradiation had a strong anticancer effect *in vitro* and *in vivo* than each approach alone	168
PEG-BP nanosheets-Au-Polypyrrole	180 ± 75 nm −1.46 mV 42.5%	PTT and SDT	*In vitro*: 4T1 *In vivo*: 4T1-tumor-bearing mice	—	-In order to improve the SDT potential of pure BP nanosheets, Au nanoparticles, and polypyrrole were conjugated into them -The nanocomposite showed enhanced electron transfer capacity, desirable biocompatibility, and photothermal conversion against 4T1-tumor-bearing mice	169
Magnetic BP microbubbles	1.7 ± 0.2 μm −20 mV —	PTT and magnetic hyperthermia	*In vitro*: MCF-7 *In vivo*: MCF-7-tumor-bearing mice	—	-This study has put effort into endowing BP nanosheets with a targetability capacity by combining them with a magnetic compound -The chain lengths of PEG were manipulated to optimize the stability and magnetic yield -In the presence of the external magnetic field, the microbubbles could more effectively reach the tumor site and the NIR irradiation caused them to explode and rapidly increase the tumor's temperature *in vivo*	170
BP nanosheets	200 nm −21 mV —	PTT, PDT, and chemotherapy	*In vitro*: 4T1, HeLa, L929, and A549 *In vivo*: 4T1-tumor-bearing mice	DOX	-This study is one of the pioneers of BP nanosheets for cancer therapy -The synergistic effects of PTT, PDT, and chemotherapy were exhibited *in vitro* and *in vivo* -NIR with two wavelengths was applied to obtain PDT and PTT and the nanosheets could load DOX molecules in much higher quantity than that of graphene and MoS_2	171

Table 4 (*continued*)

Nanovehicle	Particle size (nm) Zeta potential (mV) Photothermal conversion (%)	Type of therapy	*In vitro* and *in vivo* models	Cargo	Remarks	Ref.
BP nanosheets-poly-dopamine)-PEG-manganese	312 nm — 34.90%	PTT, PDT, and chemotherapy	*In vitro*: MCF-7 and drug-resistant MCF-7 *In vivo*: Drug-resistant MCF-7-tumor-bearing mice	DOX and phenethyl isothiocyanate	-This study has focused on multi-drug resistant breast cancer and used a natural compound called phenethyl isothiocyanate to deplete mutant p53 -The combination of PTT, PDT, and chemotherapy plus the p53 suppressor not only inhibited the tumor growth rate but also decreased the size *in vivo*	121
BP nanosheets-poly(dopamine)-hyaluronic acid	175 ± 6.1 nm −11.4 ± 1.6 mV —	Chemotherapy (pH and redox) and PTT	*In vitro*: 4T1 *In vivo*: 4T1-tumor-bearing mice	Cisplatin	-A triple-responsive nanocarrier carrying cisplatin was synthesized for breast cancer therapy -The loaded cisplatin was released faster in the presence of low acidic medium, hydrogen peroxide, and NIR irradiation -The drug release and PTT together decreased the migration and invasion of 4T1 2D monolayers and reduced the self-regeneration of 3D tumor spheroids *in vitro* -The carrier inhibited the growth rate of primary tumors and lung metastasis *in vivo*	172
Violet phosphorus	155 ± 4.97 nm — 29.14%	PTT, PDT, catalytic therapy	*In vitro*: 4T1, CT26, U87-MG, and MCF-10A *In vivo*: 4T1-tumor-bearing mice	—	-Violet phosphorus was derived from BP with higher stability in physiological solutions -The shelf-life of violet phosphorus was measured around 10 days which is competitively higher than that of bare BP -The combination of PTT, PDT, and catalytic therapy resulted in the eradication of cancerous tumor cells *in vitro* and *in vivo*	173

temperature up to nearly 38 °C. Since BPQDs are very small in size (3 nm), they can be easily cleared from the bloodstream through the renal pathway, whereas the combination had a size of around 100 nm which is more suitable for enhanced permeation and retention. The other reason can be regarded as the bare BPQDs' oxidation, which should have weakened the optical properties and so the PTT ability, but the PLGA could stabilize the BPQDs against the harsh environment of the body.[102]

The PTT efficacy of BP is known to be affected by different parameters; apart from the composition, the dimension and particle size play an important role. BP nanomaterials different in size were developed to assess if there was any effect on the PTT against breast cancer. The screened BP nanomaterials were classified as large (394 nm), medium (118 nm), and small (4.5 nm), obtained by varying the ultrasound time and the centrifugal speed. The cytocompatibility of BP nanomaterials was first assessed *in vitro* against human normal hepatocyte cells at different time intervals (12, 24, and 48 h) with different concentrations (6.3, 12.5, 25.0, and 50.0 μg mL^{-1}). It was found that neither any increase in the concentration up to 50 μg mL^{-1} nor prolonging the assay up to 48 h affected the cell viability in a negative way, and the viability of all samples remained above 80%. The PTT potential of samples (12.5 and 25 μg mL^{-1}) against MCF-7 cells was determined by exposing NIR (808 nm, 1 W cm^{-2}) to the cell plates *in vitro* for 15 min. The size effect was more evident when the applied concentration was 12.5 μg mL^{-1}, and the PTT potency is as follows: large BP > medium BP > small BP. All samples have been shown to kill the MCF-7 cells with higher concentrations.[146] Considerable attention has been paid to the functionalization of BP for better stability and surface modification to improve PTT-assisted targeted breast cancer therapy and imaging.[147–149] Through diazonium chemistry, Nile Blue was conjugated to the surface of BP nanosheets to improve the stability, rendering fluorescence properties for breast cancer therapy and imaging. The *in vitro* results showed acceptable biocompatibility, potent PTT, and desirable NIR imaging. The imaging made the tracking of nanoparticles possible (the tumor was marked in red fluorescence) and through *in vivo* studies, the surface-modified nanoparticles efficiently reached the tumor's site and led to the tumor ablation under NIR irradiation.[147]

Via solventless high-energy mechanical milling, BP nanoparticles were synthesized and surface-modified with poly(ethyleneimine) and dextran *in situ* to improve the nanoparticles' stability, solubility, and biocompatibility, and also forming functional groups on the surface. The functional groups were then used to interact with folic acid and a fluorescent dye. The *in vitro* cell viability of nanoparticles was tested against mouse embryo fibroblast cells (3T3) and murine breast cancer cells (4T1) with different concentrations (3.125, 6.25, 12.5, 25, 50, and 100 μg mL^{-1}) up to 12 h. There was no difference visible between the healthy and cancer cell lines and both of them showed a decrease in the viability as the concentration went up. The PTT efficacy of modified BP nanoparticles was tested *in vivo* as well against 4T1 tumor-bearing BALB/c mice. The nanoparticles were first injected intravenously (200 μL, 2 mg mL^{-1}), and although it was sufficient for imaging purposes, the PTT was found ineffective. Therefore, one-quarter of the suspension was injected intravenously for imaging and the rest was intratumorally injected. Within 6 min of irradiation of NIR, the tumor's temperature reached 64 °C, which is too strong for tumor ablation.[148] Recently, a novel approach has been reported to reverse the epithelial–mesenchymal transition in breast cancer cells through functionalized BP nanosheets (Fig. 3). This approach is able to convert highly invasive and metastatic mesenchymal-type MDA-MB-231 into an epithelial phenotype, which can inhibit the cell migration. Through different imaging techniques including super-resolution and advanced nanomechanical, the phenotypic switch was validated; the alteration of cell morphology, actin organization, and the increase in the specific protein markers of epithelial cells confirm this (Fig. 3(A–C)). After the mechanical exfoliation of BP nanosheets, they were coated with a protein layer (streptavidin) and then CD146 antibodies were conjugated (Fig. 3(A)). The breast cancer cells were treated with the functionalized BP nanosheets and those cells experienced a decrease in the ezrin/radixin/moesin phosphorylation, which resulted from the downregulation of membrane CD146 by about 40%. Applying the mild hyperthermia was synchronized with a sharper decrease in the ezrin/radixin/moesin phosphorylation (80%) rooted in the heat stress induced by the hyperthermia perturbing the phosphorylation of ezrin/radixin/moesin, thus synergistically hindering the Rho-guanine nucleotide dissociation inhibitory factor α sequestration.[150]

Removing a tumor throughout the breast tissue *via* surgery is a well-accepted approach, but the surgical intervention is not sufficient enough to get rid of all cancer cells, while the adipose tissue in the vicinity of tumor will be lost.[176] Regarding adipose regeneration, there are surgical tissue reconstruction approaches available but limited in terms of donor and/or foreign body response. Therefore, developing biomaterials which can simultaneously eradicate the remaining cancer cells and stimulate the regeneration of adipose tissue is of particular interest.[177]

Among various research studies performed on BP nanomaterials for cancer therapy and regeneration, only one so far has targeted breast cancer therapy and adipose regeneration. A bifunctional composite scaffold composed of gelatin and BP nanosheets was fabricated through freeze drying and the pore formation was adjusted through pre-prepared ice particles. The PTT of the composite was assessed *in vitro* and *in vivo* against MDA-MB-123 cells. The breast cancer cells were seeded on the composite scaffold for the *in vitro* study and it was ensured that about 95% of the cells were successfully seeded with minimum leakage. The tested scaffolds included pure gelatin and modified ones with BP nanosheets; the cell viability of those scaffolds without NIR was nearly 100% after 24 h showing the cell compatibility of substrates, whereas applying NIR decreased the viability down to 13% after 5 min followed by being completely eradicated after 10 min due to the temperature increase. The *in vivo* results showed how applying the NIR

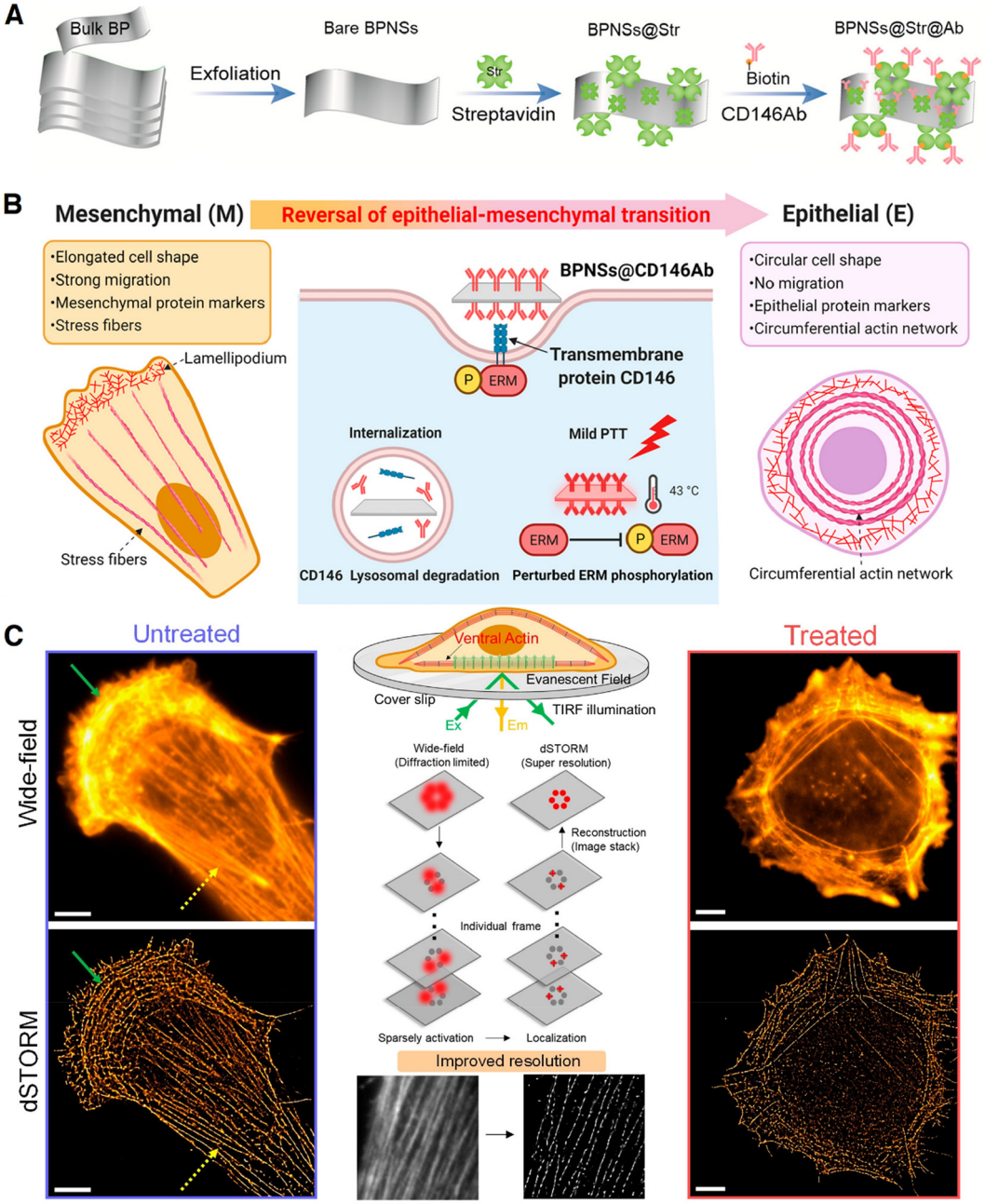

Fig. 3 Blocking breast cancer invasion through reversing the epithelial–mesenchymal transition. (A) Synthesis and surface functionalization of BP nanosheets. (B) Schematic of how the surface-modified BP nanosheets and mild PTT change a mesenchymal-type breast cancer cell into an epithelial cell. (C) Direct stochastic optical reconstruction microscopic images taken from the treated and untreated cells (the green and yellow arrows point at the ventral stress fibers and the lamellipodia, respectively; the scheme in the middle shows total internal reflection fluorescence mode to take images from ventral actin and the workflow of the direct stochastic optical reconstruction microscopy). Scale bar: 5 μm. Abbreviation: black phosphorus nanosheets: BPNSs, streptavidin: Str, ezrin/radixin/moesin: ERM, direct stochastic optical reconstruction microscopy: dSTORM, total internal reflection fluorescence: TIRF. Reprinted from[150] with permission from the American Chemical Society.

laser to BP-included scaffolds was synchronized with the increase in the local temperature followed by the tumor removal. Noteworthy, the BP nanosheet concentration applied in the scaffold's preparation was 100 and 200 μg mL^{-1}. The difference in the PTT efficacy of BP-loaded scaffolds is visible in the *in vivo* results and the scaffold with the higher content of BP could increase the local temperature up to 48 °C after 10 min of laser exposure. To prepare the scaffolds for adipose regeneration study *in vivo*, human mesenchymal stem cells were cultured in an adipogenic induction medium containing the scaffolds 1 week before the implantation. The implantation lasted for 28 days, after 21 days the implants were found robust without fragmentation or breakage showing the stability of the scaffold in the subcutaneous environment. Performing histological analysis revealed that the cells were

homogenously distributed throughout the scaffolds and the expression of adipogenesis-related genes was improved in the BP-included scaffolds rather than the pure gelatin. Moreover, an increase in the BP content up to 200 μg mL^{-1} showed higher levels of gene expression than the scaffold with lower BP exhibiting the potential of BP for the regeneration of fat tissue.[151]

One of the prominent advantages of BP nanomaterials is their high surface area endowing them with high drug and/or gene-loading efficiency.[16] Based on BPQDs, a platform was designed and synthesized for breast cancer therapy by carrying a chemotherapeutic drug called hederagenin. This drug is an antineoplastic natural compound with promising potential in cancer therapy but suffers from poor targeting and efficacy. The BPQDs (5 mg) were first put into the drug solution (2.8 mg) for 24 h followed by removal of the free drugs. Platelets from female BALB/c nude mice were separated throughout the whole blood *via* centrifugation and rinsing for being combined with the drug-loaded BPQDs. The combination of platelets and drug-loaded BPQDs was prepared through the fusion of platelets *via* ultrasound irradiation (Scheme 8(A)). The resulting nanomaterial was platelet-coated drug-loaded BPQDs. Platelets are capable of binding to tumors through P-selecting and CD44 receptors, which, on the one hand, enhances the targeting potential of the platform, and on the other hand, this surface coating increases the retention time of the carrier in the bloodstream and improves the colloidal stability since there are surface glycans on the platelets. The *in vitro* anticancer potential of

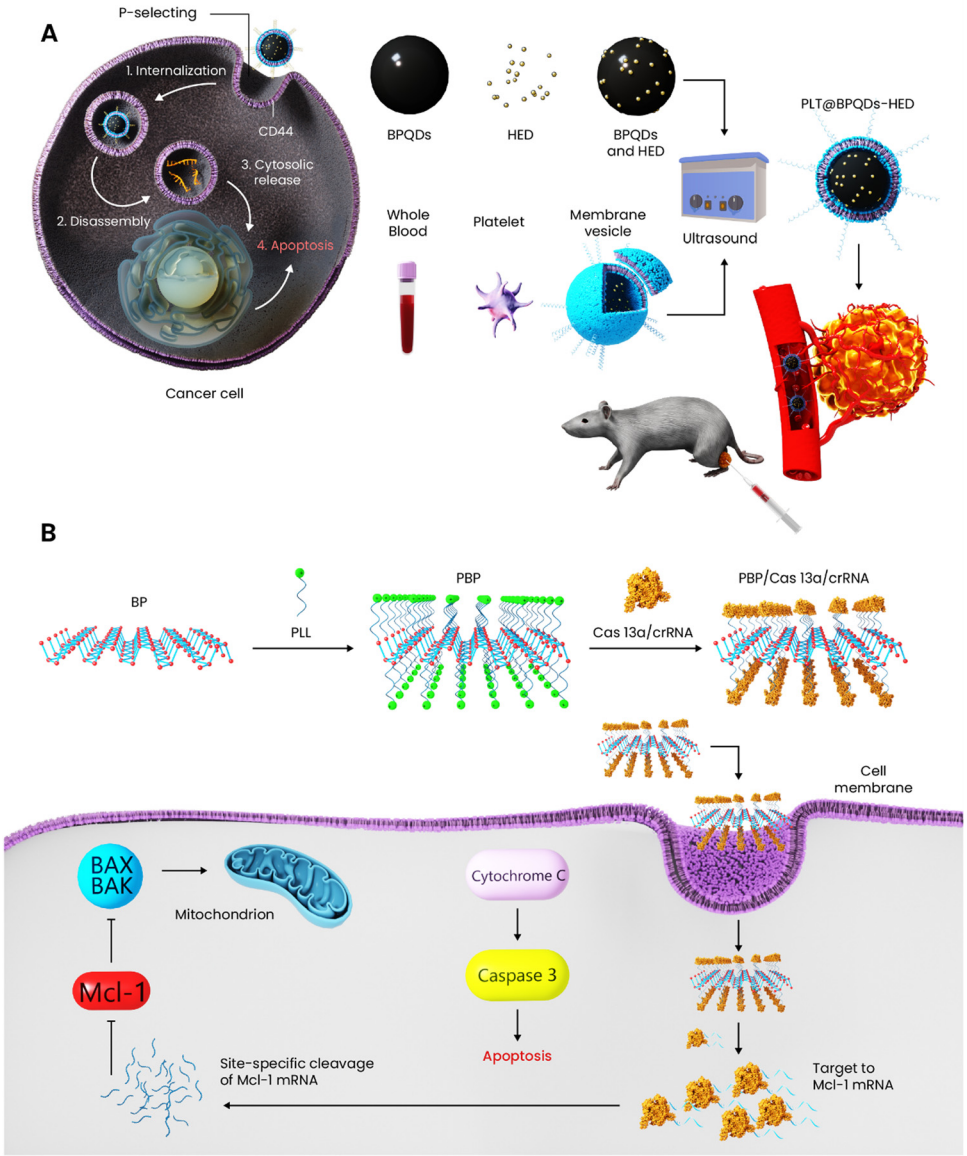

Scheme 8 BP nanomaterials for gene and drug delivery applied for breast cancer. (A) Platelet-membrane-coated BPQD preparation and its internalization into the breast cancer cells, inducing apoptosis. (B) Delivery of Cas13a/crRNA through BP nanosheets to inhibit Mcl-1 for breast cancer therapy.

nanomaterials including BPQDs, platelets-BPQDs, hederagenin, BPQDs-hederagenin, and platelets-BPQDs-hederagenin was assessed against MCF-7 cells for 48 h without mentioning the concentration of applied nanomaterials. It was found that neither pure BPQDs nor platelet-coated BPQDs induced anticancer activity, while after drug loading, the carrier (platelets-BPQDs-hederagenin) showed the highest anticancer activity and reduced the cell viability down to 39.9%. The viability of the pure drug and BPQD-hederagenin was 67.9 and 53%, respectively, and flow cytometry revealed that the carrier could generate more ROS inside the cell than the pure drug, and hence, a higher anticancer activity was obtained. The targetability potential of a carrier for cancer therapy is of great importance and the *in vivo* targeting potential of nanoparticles with and without platelet modification was evaluated at 6, 24, and 48 h post-injection. The tumor accumulation of platelet-BPQDs at each time interval was greater than that of BPQDs and after 48 h, the surface-modified nanoparticles were less likely to accumulate through the kidney and liver. The *in vivo* antitumor study on the MCF-7-bearing mice up to 20 days showed no effect on the tumor size from BPQDs alone and platelet-BPQD nanomaterials, whereas the best anticancer performance is related to platelet-BPQDs-hederagenin, which significantly increased the anticancer activity of the drug.[152]

Cancer gene-therapy is a well-known approach by which specific nucleic acids are carried into a cancer cell in order to reverse the metastatic state through affecting the genetic errors and/or directly eliminating the cancer cells.[178] Regarding the high surface area of BP nanomaterials, the nanosheets were functionalized with poly-lysine to deliver a gene complex to target a key determinant factor in breast cancer cells.[153] As a member of the B-cell CLL/lymphoma 2 family, Mcl-1 has been targeted for cancer therapy as it showed resistance over traditional chemotherapy.[179] In the case of breast cancer, Mcl-1 is known as a key determinant, but developing effective inhibitors of Mcl-1 is still a challenge. The gene complex was composed of CRISPR/CRISPR associate 13a and CRISPR RNA; notably, binding of the former to the targeted RNA can occur with specificity under the guidance of CRISPR RNA. At first, the BP nanosheets which had a negative surface charge were coated with cationic poly-lysine; this polymer had three roles here: (i) stabilizing the BP dispersity in the physiological media, (ii) facilitating the endocytosis of carrier into the cells, and (iii) playing an intermediate role between the substrate and the gene complex, both of which are negative in surface charge. Once the gene-loaded carrier reaches the breast cancer cells, it undergoes degradation at a faster rate than that of the normal cells because of higher ROS and acidity of cancer cells, leading to the release of the gene complex. Under the function of the gene complex, Mcl-1 RNA could be targeted and knocked down at the transcriptional level, which at last results in cell apoptosis (Scheme 8(B)). The efficacy of gene-loaded carrier plus bare BP and the gene complex alone was tested *in vitro* against MCF-7 and MDA-MB-231 up to 48 h. Neither bare BP nor the gene complex showed the anticancer effect on any of the cells, but it is not mentioned how long the bare BP and gene complex were exposed to the cells. However, the gene-loaded carrier showed a time-dependent cytotoxicity against both cell lines and the cell viability reduced from 100% to nearly 85, 70, and 40% after 12, 24, and 48 h, respectively. The *in vivo* studies performed on nude mouse tumor xenografts established through using MDA-MB-231 revealed that only the gene-loaded carrier exhibited a significant tumor growth inhibition; to further analyze the mechanism of action, the transcription and expression levels of Mcl-1 were determined through PCR, western blotting, and qRT-PCR all of which unanimously agreed on the downregulation of Mcl-1, which subsequently led to tumor cell death.[153]

PDT is an anticancer therapy technique which is relatively less invasive than most common treatments but with higher efficacy. Through this technique, a photosensitizer, organic/inorganic origin, or a combination of both is adopted to generate cytotoxic ROS, which upon exposure to external light irradiation leads to cancer cell death. Briefly, the excitation of the photo-responsive agent leads to the transfer of energy to the oxygen molecules, turning them into cytotoxic species.[180] The first report on the use of BP in PDT against breast cancer was published in 2015. Since BP nanomaterials, at that time, were competitively better in terms of quantum yields, biocompatibility, and biodegradability than most common photosensitizers in PDT, it attracted considerable attention soon after. The PDT potential of BP nanosheets was assessed *in vitro* against MDA-MB-231 cells for 4 h with and without NIR irradiation. The applied concentrations were 0.025, 0.05, 0.1, and 0.2 μg mL^{-1} and the results indicated no effect in the case of non-irradiated samples, while the counterpart inhibited the growth in a concentration-dependent manner; upon NIR irradiation, 0.09 μg mL^{-1} is the concentration which induced the cell viability reduction down to 50%. Having gained promising results from the *in vitro* studies, they progressed towards *in vivo* analysis by injecting the BP nanosheets (30 μL (500 μg mL^{-1})) to MDA-MB-231 tumor-bearing mice. Regarding the PDT, after 12 h post-injection intratumorally, NIR was irradiated (660 nm, 20 min). It turned out that the BP nanosheets without NIR could not inhibit the tumor growth, whereas the one exposed to light successfully suppressed the tumor growth.[154]

To improve the PDT potential of BP nanosheets, Liu *et al.*[155] have shown that C_{60} covalently grafted onto the edges of nanosheets improved the stability and physiological dispersibility of BP and promoted the ROS generation capability of the nanosheets. The *in vitro* cell growth inhibition analysis was performed with and without NIR for 24 h against 4T1, MCF-7, and healthy cells (Huh-7, U937, and RAW 264.7). Regarding the light irradiation, it was applied to 4T1 cells 6 h after the incubation for 5 min (5 W cm^{-2}, 650 nm), and no irradiation was applied to healthy cells and MCF-7. Notably, different samples including BP, C_{60}, and the hybrid with different concentrations were used in the cell viability assay. The hybrid (BP/C_{60}) could inhibit the cell growth after light irradiation by about 90%, whereas the BP alone could only reach 30% showing the positive effect of C_{60} on the PDT efficacy. In the absence of light irradiation, all the samples showed nearly 90% cell viability, even at the highest concentration (140 μg mL^{-1}) to

both healthy and cancer cells. The *in vivo* antitumor effect of samples was tested against the 4T1 mouse model for up to 2 weeks. The nanomaterials were injected both intratumorally and systematically through the tail vein. The NIR was applied 30 min right after the injection for 10 min and repeated every 2 days up to 14 days and the concentrations were 70 and 140 μg mL^{-1}. The results related to the former approach exhibited an inhibition rate of 88.2% for the hybrid and the BP and C_{60} alone inhibited the growth by about 36.6 and 30.7% respectively. Although the systemic administration of nanomaterials was found with less antitumor efficacy, the hybrid still showed an inhibition rate of 35.9 (70 μg mL^{-1}) and 65.6% (140 μg mL^{-1}) in a dose-dependent manner.[155] It has also assessed the SDT potential of the C_{60}-BP nanohybrid for breast cancer therapy *in vitro* and *in vivo*.[156] SDT is a non-invasive cancer therapy approach in which a sonosensitizer agent gets activated *via* ultrasound and produces cytotoxic ROS the same way as PDT. However, one of the criticisms revolving around PDT is the limited tissue penetration depth of NIR compared to ultrasound; ultrasound waves are known to penetrate several tens of centimeters culminating in higher efficacy and efficiency of the cancer treatment.[3] In this study, C_{60} was anchored on the BP nanosheets covalently and on the edge of sheets. Moreover, the BP nanosheets were surface modified with benzoic acid and these samples were compared in terms of SDT potency. In the presence and absence of ultrasound, all samples were exposed to 4T1 cancer cells with 25, 50, and 100 μg mL^{-1} for 4 h. Without ultrasound irradiation, no decrease in the cell viability of all samples was observed while the triggered samples caused the viability to drop. In comparison with the bare BP nanosheets, only C_{60}-edge-functionalized BP showed inferior SDT efficacy and the other two outperformed the bare BP. The benzoic acid-functionalized BP had the highest suppressing effect on the cancer cells after ultrasound exposure resulting from the functionalization effect on the conduction and valence band energy levels of BP, which were measured through synchrotron radiation photoemission spectroscopy. Nonetheless, the authors have prolonged the cell viability assay without ultrasound up to 72 h reported in the supporting information and only the bare BP (50 μg mL^{-1}) was able to decrease the 4T1 cell viability down to 50% due to its inherent anticancer potential, but the authors have mentioned this as the cytotoxic effect of BP, not the selective anticancer potential.[156]

5.2. Dual therapy

To improve the developed single-therapy approaches, combinational therapy has been introduced to open new doors in fighting various types of cancer.[181] There are three categories of combinational therapies generally as follows: internal-based, external-based, and internal–external-responsive agents. Internal or endogenous-responsive carriers relate to those that carry a chemotherapeutic/bioactive material to an organ/tissue in a passive or targeted manner. These materials undergo a change in their structure once exposed to a specific stimulus—pH, redox, temperature, *etc.*—and release the cargo to the intended destination.[182] The second group, in contrast to the internal-responsive carriers, is responsive to external triggers including magnetism, light, and ultrasound. As mentioned briefly before, this category can induce hyperthermia and/or ROS to kill cancer cells. The internal–external group takes advantage of both internal and external triggers simultaneously and comes up with more functional anticancer agents.[183] It is critical to bear in mind that it is possible to design dual and triple-responsive agents only based on internal or external stimuli. For instance, there are different carriers that are simultaneously equipped with two internal stimuli such as pH-redox and pH-temperature or magnetic-light, light, and ultrasound. In this section, the BP biomaterials designed to induce dual therapy against breast cancer are discussed in detail.

The combination of chemo- and thermo-therapy has been a well-known anticancer treatment so far. Within this context, a few studies have focused on BP nanomaterials for breast cancer therapy with a dual therapeutic approach based on chemo- and thermo-therapy. BP nanosheets were combined with DOX, poly-L-lysine, and hyaluronic acid to design a chemo-phototherapy agent for breast cancer therapy. *In vitro* drug release was tested in physiological and acidic media in order to simulate the mildly acidic environment of tumors and/or intralysosomal/endosomal pH and if the pH change has an effect. After 24 h of soaking into an acidic medium (pH 5.5), the release rate reached nearly 77%, while 59% of the drug was released at pH 7.4 under the same conditions. Moreover, the effect of NIR irradiation on the release rate was assessed *in vitro* by applying the light for 5 min; the release rate had a rapid increase from 29 to 72%. The *in vitro* anticancer activity of samples against MCF-7 and MDA-MB-231 was evaluated for 48 h. The samples included free DOX, the modified BP without DOX and with DOX. The nanomaterials without DOX kept the viability higher than 80%, whereas the DOX-loaded one decreased the cell viability in a concentration-dependent manner starting from 0.01 to nearly 100 μg mL^{-1}. The IC_{50} value of both cell lines was reached when the concentration had been increased to 1 μg mL^{-1}. The NIR irradiation was also applied to improve the anticancer effect further. In the case of *in vivo* studies, the nanomaterials were injected intravenously through three cycles in MDA-MB-231 tumor-bearing mice, and after 24 h post-injection, the NIR was applied as well. The highest tumor suppression belonged to the DOX-loaded modified BP plus NIR followed by the same sample but without NIR and then free DOX. In this manner, it is visible how the combination of these two therapies culminated in more desirable outcomes.[157]

Using a layer-by-layer coating strategy, a drug carrier based on BP nanosheets was developed for breast cancer therapy. Two chemotherapeutic drugs were co-delivered into the cancer cells; DOX molecules were first loaded on the nanosheets *via* electrostatic interactions between the cationic drug and the negative surface charge of BP followed by coating of poly(dopamine) on the drug molecules. Next, the poly(2-ethyl-2-oxazoline) ligand was conjugated on the poly(dopamine) to not only prolong the blood circulation time and improve the cellular uptake *in vivo*, but also provide a suitable position for the loading of the

second drug (bortezomib). One of the prominent advantages of this carrier was charge reversal upon exposure to the acidic environment of the tumor, facilitating the cell internalization; the surface charge undergoes a change due to the ionization of amide groups of the outer layer from negative (−10.2 mV) at a physiological medium of pH 7.4 to positive (2.4 mV (pH 6.8) and 5.2 mV (pH 5.0)). Through the cell viability assay, the drug-free carrier was found biocompatible, whereas applying the NIR (808 nm) to the nanoparticles (50 μg mL^{-1}) killed over 80% of MCF-7 cells. The DOX-loaded nanomaterials showed pH-dependent cytotoxicity; at acidic pH, the release of drug molecules was intensified. The drug release was also assessed *in vitro* in the presence of NIR (808 nm, 1 W cm^{-2}) for 6 min at each pulse and the light irradiation was applied four times up to 48 h. Compared to the non-irradiated samples, NIR led the release kinetic of both drugs to rise significantly stemming from the decomposition of the poly(dopamine) layer. *In vivo* studies were performed on MCF-7-induced tumor-bearing mice and the nanoparticles were injected intravenously (5 mg kg^{-1} in 100 μL PBS). At 24 h post-injection, the tumors were irradiated with NIR (808 nm, 1.5 W cm^{-2}) for 5 min and IR images plus the temperature changes were collected and determined. The drug-loaded sample was found to increase the local temperature up to 50 °C, which is the tumor ablation range, after 300 s.[110]

Tamoxifen is a well-known drug used against breast cancer with the potential to decrease the mortality rate and reduce cancer recurrence in estrogen receptor-positive patients, but this drug similar to most anticancer drugs suffers from low bioavailability, toxicity, *etc.* In this way, BP nanosheets were adopted as not only a substrate for tamoxifen delivery, but also a sonosensitizer agent for SDT. Through *in situ* polymerization, dopamine was conjugated onto the nanosheets and then the drug molecules and folic acid were electrostatically attached to the surface. The loaded drug molecules were observed to release faster when the carrier is in a mild acidic medium and also when ultrasound irradiation had been applied to the nanoparticles. The nanoparticle internalization rate was assessed against tamoxifen-sensitive and -resistant MCF-7 cells and in both cell types, the internalization was excellent. The drug-loaded nanosheets induced about 94% cytotoxicity to the cancer cells while bare tamoxifen showed about 30% cytotoxicity, both at the concentration of 5 μg mL^{-1}. The SDT could add 15% more cell death to the antitumor efficacy of the nanoparticles.[184] Generally speaking, designing smart drug carriers for cancer therapy responsive to pH has been at the epicenter of nanomedicine research followed by redox-responsive carriers. The former experiences structural changes in the acidic medium, while the latter bondages with loaded drug molecules will break in the presence of reductive agents.[185]

Due to the rapid growth of tumors, ROS and free radicals are found in their microenvironment in large quantities and so the cancer cells must generate reductive agents such as glutathione to compensate the free radicals causing the microenvironment to become reductive. This feature has been taken to design drug carriers with reduction-responsive ability through which the chemotherapeutic drug is conjugated to the carrier with disulfide, di-selenium, and other bonds. Once the carrier reaches the tumor's site and is exposed to glutathione, the bondage breaks resulting in the increased drug concentration in the targeted site.[186] A dual-responsive (redox- and light-responsive) drug delivery system composed of BP nanosheet and poly-L-lysine was designed for breast cancer therapy. The DOX molecules were first loaded on the BP nanosheets followed by a coating of the polymer to improve the stabilization of nanoparticles in the physiological medium, on the one hand, and prevent the premature leakage of the drug molecules, on the other hand. Through both *in vitro* and *in vivo* studies, it was revealed that the combination of chemotherapy and PTT was not only biologically safe but also yielded potent anticancer outcomes. The cytotoxicity of BP and modified poly-L-lysine was tested *in vitro* against 4T1 cell at various concentrations (0.0625–4 μg mL^{-1}) for 48 h; notably, these concentrations were chosen based on free DOX since the drug at 4 μg mL^{-1} completely killed the cells. The cell viability assay showed that neither BP nor the polymer had any negative effect on the viability. Besides these compounds, the BP + NIR, DOX, and the dual-responsive carrier with and without NIR were assessed in terms of cytotoxicity against the same cell line. The strongest effect belonged to free DOX, which showed IC_{50} in the range of 0.5–1 μg mL^{-1} followed by the carrier + NIR which at the highest concentration (4 μg mL^{-1}) reduced the viability down to 10%. Surprisingly, the BP + NIR (4 μg mL^{-1}) could only reduce the viability down to nearly 80%. The most important advantage of the carrier was revealed through the *in vivo* study in which intravenous injection of free DOX was synchronized with a decrease in the mouse weight without desirable tumor suppression efficacy, whereas the carrier did not show the side effects of free DOX and completely prevented the tumor growth rate up to 13 days.[158] Different from the previous studies which applied surface modification to BP nanosheets, another one encapsulated BPQDs and docetaxel as a well-known breast cancer drug inside PLGA for PTT and chemotherapy. The synergistic therapeutic effects were tested against primary and lung metastatic tumors and the NIR irradiation led to photothermal tumor ablation, but also liberated the drug molecules at a higher rate.[125]

The combination of PTT with immunotherapy is of great importance because, on the one hand, immunotherapy can compensate the low tissue penetration depth of NIR, and PTT as an easy and cost-effective approach can establish tumor vaccine *in situ*, on the other hand. It is known that tumor ablation through photothermal treatment is able to induce immunogenic cell death by delivering tumor-associated antigens. Moreover, the increase in the local temperature by PTT has some benefits for immunotherapy, improving the blood flow and vascular permeability, both of which result in the recruitment of more immunocytes.[187,188] In 2019, a study reported the preparation of biomimetic BPQDs to first induce breast cancer cell apoptosis through PTT followed by activation of the immune system to get rid of both residual and metastatic cancerous cells. The anticancer agent was designed in the form

of nanovesicles and BPQDs were coated with erythrocyte membranes; this coating provided a long circulation time through the bloodstream and improved the tumor accumulation *in vivo*. Once the cancer cells have undergone apoptosis through PTT, dendritic cells were recruited and took the antigens, which subsequently led to a strong T cell response ($CD8^+$) in already treated tumors and distant ones. The administration of programmed cell death protein 1 (PD-1) antibody reinvigorated the T cells and along with the nanovesicles successfully prevented both primary and secondary tumors *in vivo*.[160] Somewhere else and through manipulating the PTT parameters and an immunologic adjuvant, the antitumor immunity was optimized. BP nanosheets were modified with PEG and then the immunologic adjuvant (CpG) was grafted onto the surface. Different concentrations of the nanomaterials (30–80 μg mL^{-1}) were exposed to 4T1 and HepG2 cells for 6 h and NIR (808 nm, 2 W cm^{-2}) was applied for different time intervals (100–200 s) and the cell viability was assessed after 24 h. To precisely understand if the necroptotic cell death occurred, the necroptotic inhibitor had been applied in the cell viability assay. It turned out that the 4T1 cells co-incubated with the inhibitor had a competitively higher viability than those without it, showing the important role of necroptosis in the PTT-mediated breast cancer. The highest necroptotic rate was nearly 73% under an optimized condition (60 μg mL^{-1}, irradiation time = 180 s); under this condition, the cell temperature was mentioned to reach 45 °C by which an effective antitumor immune response was activated without melting the tumor tissue. Western blotting assay was also performed to verify if the necroptosis was the dominant cell death pathway. Since necroptosis is caspase-independent and its activation relies on RIP1 and 3, the expression levels of caspase-3 and 8 were assessed and did not experience any change, but the RIP1 and 3 proteins were expressed highly in the cells treated with NIR. *In vivo* studies on the 4T1 breast tumor model were in agreement with the *in vitro* studies and except for the control group, which was treated with PBS, other groups rapidly saw an increase in the tumors' temperature up to 45.6 °C, which had been revealed in the *in vitro* studies as the suitable temperature to induce necroptosis. The histological analysis clearly confirmed necrosis-like morphology through the slices of primary tumors containing the nanoparticles.[161] The same group did come up with another cancer vaccine based on BP and loaded CpG oligodeoxynucleotide onto the BP nanosheets-Au and together with an indoleamine 2,3-dioxygenase inhibitor, they were co-encapsulated into a cancer cell membrane for the elimination of primary and metastatic breast tumors. The membrane could improve the targetability of nanovaccine and the combination of PTT and immune adjuvant resulted in tumor-specific immunity. One of the highlighted advantages of this anticancer agent over the one developed in their previous study was that the nanovaccine not only showed effective therapeutic effects on the primary and metastatic breast tumors, but also produced a systemic immune memory which prevents tumor recurrence.[164] Indeed, these nanosystems functionalized with anti-PD-1 antibodies and irradiated with NIR were able to block metastasis and recurrence in a 4T1-luc breast tumor model. These nanovaccines, when combined with anti-PD-1/PDL1 antibodies, stimulated a favorable tumor immune response in both *in vitro* and *in vivo* models.[163] Based on the photothermal immunotherapy strategy, BPQDs and anti-PD-L1 were coated with cancer cell membranes against triple-negative breast cancer. As indicated in Scheme 9, the BPQDs were synthesized from bulk BP through probe sonication and applied for photo-immunotherapy. NIR irradiation to the tumors was synchronized with killing the cancer cells directly *via* temperature increase and through affecting and maturation of dendritic cells. Moreover, anti-PD-L1 improves T-cell immune response and blocks PD-1/PD-L1 pathways, leading to the recognition of cancer cells and killing them by T cells.[163] In the case of CTLA4 inhibitors, it was possible to observe a block of regulatory T cells (Tregs), which allow the immune escape of tumor cells. It has been shown that the presence of BP enhances CTLA4 inhibitor activity in Tregs-mediated immunosuppression inhibition, thus increasing the ratios of $CD8^+$ CTLs/Tregs and CD4+ Teff/Tregs and promoting a memory of CTL immune response useful in recurrence and metastasis of tumor prevention.[167] Apart from PTT-mediated immunotherapy, other approaches were used as well like PDT- and photoacoustic-mediated immunotherapy. A recent study has developed a dual-responsive vesicle composed of BPQDs grafted with PEG and ROS-sensitive poly(propylene sulfide). The main idea behind designing such a compound was to trigger the BPQDs with NIR to generate ROS followed by the disassembly of the vesicles due to a change in the structure of poly(propylene sulfide) in the presence of ROS (Scheme 9). To improve the effect of immunotherapy by PDT, CpG oligodeoxynucleotides were loaded into the cavities of vesicles. The vesicles were exposed to MCF-7 and 4T1 cells in the presence and absence of NIR at different concentrations (10–150 μg mL^{-1}) for 24 h. None of the treated cells without NIR saw cytotoxicity proving the biocompatibility nature of vesicles, while applying NIR has shown concentration-dependent cytotoxicity. The $^1O_2$ probe 2′, 7′-dichlorofluorescein diacetate was used to track ROS formed during the process and revealed the direct effect of vesicle concentration on higher ROS concentration. To understand the effect of PDT on the immune response, *in situ* levels of calreticulin as a molecular pattern that raises the dendritic cells' recruitment were analyzed. Excessive expression levels of calreticulin were observed when the vesicles with NIR were combined, showing that the dual-responsive carrier can activate and recruit dendritic cells for a stronger antitumor immune response. The same effect was also confirmed on 4T1-tumor-bearing BALB/c mice *in vivo*. The vesicle containing the immune adjuvant exposed to NIR outperformed the others and completely suppressed the tumor growth.[166]

Photoacoustic therapy is an anticancer approach that uses photoacoustic shockwaves to destroy cancer cells. Once the photo-responsive agent gets stimulated, the nano- and microbubbles around it undergo growth and collapse, leading to the formation of shockwaves. The explosion of those bubbles causes a mechanical disruption locally to the primary tumors with minimal negative effects on the healthy tissues.[189,190]

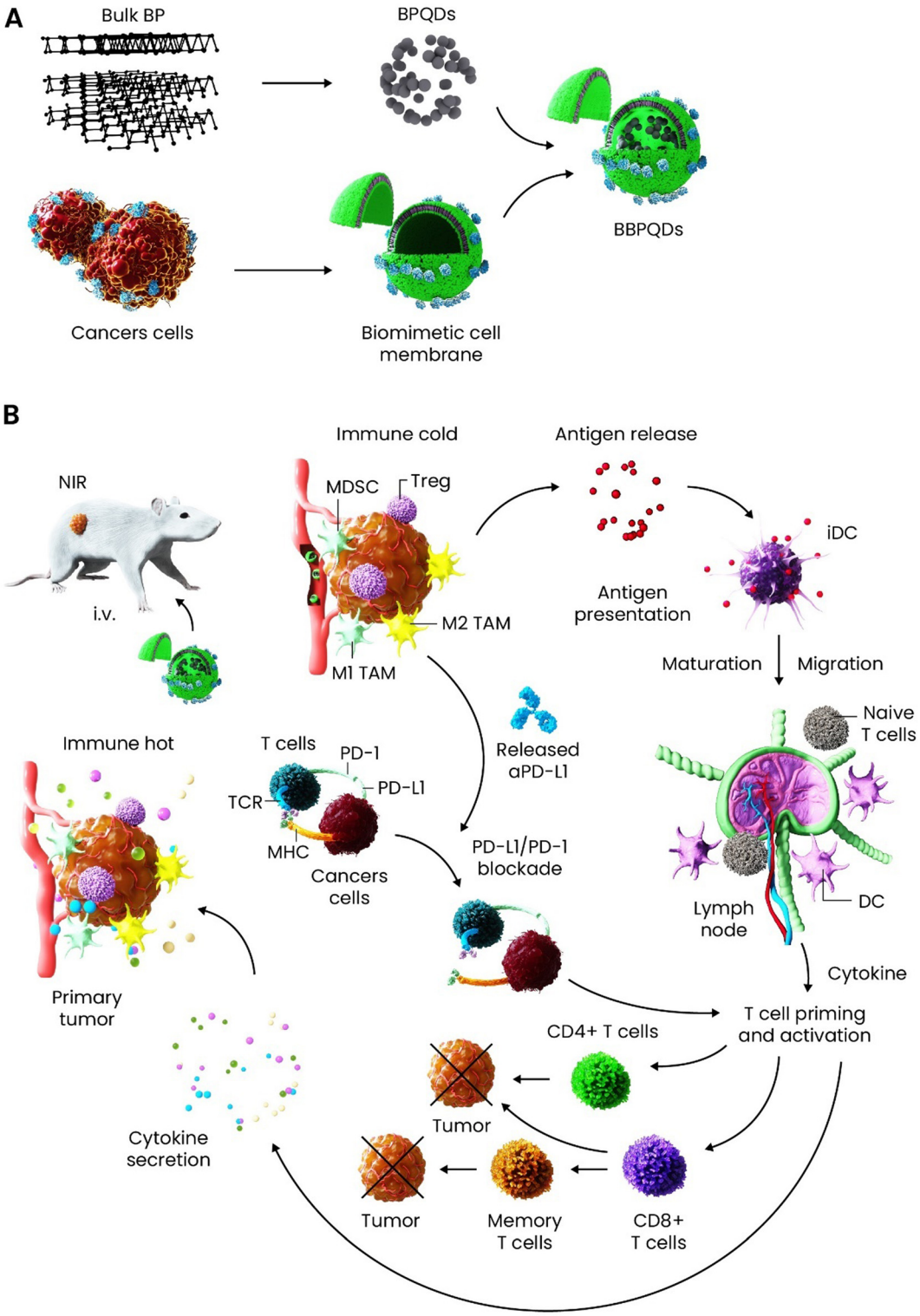

Scheme 9 Combination of immunotherapy with PTT. (A) Preparation of BPQDs from bulk BP and encapsulation inside biomimetic cancer membranes. (B) Process of dendritic cells' activation and maturation in the presence of NIR and anti-PD-L1 for the eradication of primary and metastatic breast tumors. Abbreviation: Biomimetic black phosphorus quantum dots: BBPQDs, Myeloid-derived suppressor cell: MDSC, tumor-associated macrophages: TAM, the regulatory T cells: Treg, and immature dendritic cell: iDC.

However, there is limited data available on the effect of photoacoustic therapy on the immunology system. In combination with a peptide, mitochondrion-targeting triphenylphosphine, and an immune adjuvant, BP nanosheets were used for

photoacoustic immunotherapy of breast cancer. The primary tumor eradication was achieved since the nanoparticles had been modified with tumor-targeting cyclic Arg-Gly-Asp peptide and triphenylphosphine; the former facilitated the nanoparticles' internalization towards the cancer cells and the latter helped the targeting of mitochondrion to induce the generated shockwaves after light stimulation to this organelle. To assess the effect of photoacoustic therapy on the immune response, the nanoparticles were injected intravenously into 4T1-tumor-bearing mice and then the laser was applied to induce the shockwave effect. At 72 h post-injection, the mice were sacrificed and their spleens were taken for flow cytometry. The levels of CD80 and 86 were found to upregulate after the treatment and the sample, which had the adjuvant and laser treatment, elicited higher levels of dendritic cell maturation than the one which only carried and released the immune adjuvant. One of the possible problems of this study was the interference of heat to the photoacoustic effects when the BP had been exposed to NIR since BP turns NIR light heat. Therefore, a pulsed laser irradiation was applied and the temperature change had been carefully checked during the process and a minimal heating effect was observed.[167]

Designing anticancer platforms responsive to two external stimuli has some advantages, which have attracted considerable attention. Well-known external stimuli are light, magnetism, and ultrasound from which PTT, PDT, SDT, and magnetic hyperthermia have been derived. The combination of these approaches can compensate the weakness of each and result in more efficacious therapeutic outcomes. For example, a drawback related to PDT/SDT is the lack of oxygen and this is specifically the case when it comes to the hypoxia regions of tumors causing the ROS generation to fall; the existence of hyperthermia from PTT/magnetism can increase the blood flow and oxygenation overcoming the mentioned drawback. However, the cytotoxic ROS generated through PDT/SDT has the potential to increase the sensitivity of cancer cells to PTT/magnetic hyperthermia.[188,191] Inspired by the benefits of combined PDT/PTT therapy, BP nanosheets were used as a substrate to load cypate as an FDA-approved photo-responsive agent followed by coating with hyaluronic acid to improve the accumulation of nanoparticles into the cancer cells; the high affinity of hyaluronic acid towards CD44 receptors which are found in triple-negative breast cancer in high quantity was one side of choosing this polymer and the other side was to improve the chemical stability and physiological dispersibility of cypate-loaded BP nanosheets. The anticancer activity of surface-modified BP nanosheets was tested in 2D cells and 3D organoids *in vitro* and in 4T1-tumor-bearing mice *in vivo*. The cytotoxicity of the platform was assessed *in vitro* against 4T1 and human dermal fibroblasts from 1.6 to 200 μg mL^{-1} for 24 h, and no significant changes were observed. One of the interesting points of this study was *in vivo* safety assessment of the BP with and without hyaluronic acid's coating for 24 h. The samples at 10–50 mg kg^{-1} were intravenously injected in Balb/c mice and although BP is known to degrade to harmless phosphate ions, the BP alone at 25 mg kg^{-1} decreased the survival rate down to 67% followed by 0% when the highest concentration had been applied (50 mg kg^{-1}). This shows that the mice were overdosed by phosphate ions, but the samples modified with hyaluronic acid showed a survival rate of 84% at 50 mg kg^{-1} and the body weight of those mice remained with minimal changes up to 30 days. The *in vitro* studies in the presence of NIR irradiation on the mentioned cell lines plus 3D tumorspheres revealed the efficacy of surface-modified BP nanosheets, which took advantage of simultaneous PDT and PTT. The role of hyaluronic acid became evident in the *in vivo* antitumor studies in which the distribution was determined and the highest accumulation and antitumor efficacy belonged to the surface-modified BP. Cypate could also elevate the ROS concentration upon stimulation with NIR and its anticancer inhibitory effect was assessed separately from the BP nanosheets *in vivo*; it outperformed the PBS (control) and the BP nanosheets without NIR but was not effective enough to suppress the growth rate. However, the combination of cypate + BP + hyaluronic acid with NIR culminated in complete suppression of tumor up to the end of study.[168] Another study chose the combination of hyperthermia and ROS generation for breast cancer therapy but through PTT and SDT. Since the electron recombination occurs fast in BP nanosheets, they were integrated with Au nanoparticles and polypyrrole. The *in vitro* studies exhibited superior sonodynamic and photothermal conversion against cancer cells. The nanocomposite's cell compatibility and anticancer activity were assessed *in vitro* for 24 h against 4T1 cells with and without the stimuli. Regarding the viability of nanocomposites without any external stimulus, the agent was applied at different concentrations (0–200 μg mL^{-1}) and concentration-dependent cytotoxicity was observed, but the results were not statistically significant. However, the same experiment was performed at only one concentration (50 μg mL^{-1}) in the exposure of ultrasound, NIR, and a combination of both. The PTT and SDT separately reduced the viability by about 40% and 50%, respectively, whereas the combination showed a strong effect and resulted in 90% reduction of 4T1 cells. The same conditions produced the same results (complete suppression of 4T1 tumors) *in vivo* up to 14 days, proving the potency of dual therapy.[169]

Magnetism has developed modern applications in nanomedicine—magnetic resonance imaging, directing a magnetic compound to the targeted tissue/organ through an alternating magnetic field, and inducing magnetic hyperthermia. The most highlighted advantage of magnetic nanoparticles over other external-stimuli-responsive nanomaterials is the independency of the applied magnetic field from penetration depth, which implies that these nanoparticles can also induce their properties even throughout the deep-seated tumors.[192,193] BP nanosheets obtained through liquid-phase exfoliation were conjugated to a magnetic compound (streptavidin-coated Fe_3O_4 nanoparticles and biotinylated microbubbles) to be delivered to cancer cells in a targeted manner. The effect of PEG chain lengths on the stability and magnetic responsiveness was assessed, which turned out that the longer chain lengths improved the stability and magnetic yield better than that of

shorter ones. Through an external magnetic field, the nanoparticles were accumulated in the site of action and once being saturated, the local temperature rapidly increased *in vitro* and *in vivo*. Moreover, the PTT studies *in vitro* and *in vivo* demonstrated that the magnetic compound required less incubation time than that of bare BP nanosheets to reach the cancer cells and induce anticancer activity under magnetic field and NIR irradiation.[170]

5.3. Triple therapy

Improvement in efficacy and decreasing the risk of tumor recurrence have further encouraged researchers in cancer therapy to design more successful solutions. Here, triple-responsive BP anticancer agents for breast cancer therapy will be discussed. These platforms were synthesized in a way to respond to both external and internal stimuli, which together obtained more promising results in terms of tumor growth suppression and recurrence. Chen *et al.* reported a combined therapeutic package (chemotherapy + PTT + PDT) comprising BP nanosheets. The authors discovered the strong light-responsivity of BP nanosheets to generate both ROS and heat besides a higher drug loading capacity than that of most 2D materials—950% in weight DOX loading ability on the surface of nanosheets. The BP nanosheets were prepared by a simple liquid exfoliation technique and exposed to a DOX solution (2.5 mg mL^{-1}) with a concentration of 50 μg mL^{-1}. The cell viability of BP nanosheets (25, 50, 100, and 200 μg mL^{-1}) was assessed *in vitro* against 4T1, L929, A549, and HeLa up to 24 h. Notably, the NIR light with two wavelengths of 660 and 808 nm was applied for inducing ROS and heat, respectively and NIR, DOX, BP, and each laser wavelength were applied separately and in combination to exactly understand their specific anticancer effect. The DOX was the only agent that reduced the viability down to 60% after 24 h, and neither NIR (660 and 808 nm) nor BP changed the viability. Speaking of combinatory effects, the BP + DOX + 808 nm NIR showed a stronger anticancer effect than the same one with 606 nm NIR, showing the potency of PTT over PDT here. However, the combination of BP + DOX + PTT + PDT had the strongest cytotoxic effect against 4T1 cells, and the viability was reduced to nearly zero.[171] BP nanoflakes incorporated with the transformation growth factor-b inhibitor were prepared and then coated with the neutrophil membrane. Applying both PTT and PDT caused acute inflammation in the tumor and enhanced the accumulation of the nanoparticles in the tumor tissue. Moreover, the combination of PTT, PDT, and the transformation growth factor-b inhibitor induced a potent immune response (the T cell infiltration and activation), which prevented lung metastasis.[194] Using hybrid membrane-camouflaged liposomes, a multifunctional platform was designed against breast cancer to stay longer in the blood circulation and accumulate more efficiently in the tumor tissue. In this regard, BPQDs as the photothermal agent, paclitaxel as the chemotherapeutic agent, and poly metformin as an immunomodulator agent were encapsulated inside these nanocarriers. Since the coating layer was derived from the fusion of cancer cells and red blood membrane, it was endowed with excellent tumor-targeting ability and long blood circulation features. The release of the immunomodulator agent boosted an immune response and increased dendritic cells along with T cell activation. Testing the antitumor potential of nanoliposomes in the 4T1 breast tumor model showed successful elimination of primary tumors and inhibition of lung metastasis as a result of combination therapy.[195]

One of the major problems of chemotherapy is the development of resistance, which causes a tumor cell to resist toxic drugs. It is known that the tumor suppressor p53 undergoes mutation in multi-drug-resistant tumors, enhancing tumorigenesis as well as anti-apoptosis ability capable of resisting chemotherapeutic drugs like DOX.[196,197] An innovative study has targeted this problem and come up with a modified BP platform, carrying an agent to reverse drug-resistant breast cancer.[121] In this regard, BP nanosheets have undergone step-by-step surface modification; DOX molecules were first loaded on the nanosheets followed by applying dopamine and PEG coatings one after another. Finally, the surface was decorated with manganese and phenethyl isothiocyanate, which is able to selectively deplete the mutant type of p53, not the natural one. The *in vitro* anticancer potential of samples containing different amounts of DOX (5, 10, and 20 μg mL^{-1}) was tested against MCF-7 and drug-resistant MCF-7 up to 24 h. MCF-7 cells showed a decrease only in the presence of DOX and the viability was concentration dependent; notably, this study was performed in the absence of NIR. However, the drug resistance was analyzed by the exposure of the platform to different conditions including NIR with two wavelengths—with DOX, NIR 660 nm, NIR 808 nm, DOX + 660 nm, DOX + 808 nm, 660 + 808 nm, and DOX + 660 + 808 nm. The combination of PTT, PDT, and chemotherapy outperformed the rest in terms of induced cytotoxicity, but the authors have also made a comparison between the platform with and without the mutant p53 suppressor. The one carrying the phenethyl isothiocyanate caused stronger toxicity towards the drug-resistant MCF-7. For *in vivo* studies, the drug-resistant MCF-7 cells were injected subcutaneously into the front flank of mice to establish the tumor model. Similar to the *in vitro* anticancer study, different samples were injected and the NIR (808 nm, 1.2 W cm^{-2}) was applied 6 h post-injection for PTT (5 min). For PDT, 30 min after the PTT treatment, the tumor region was exposed to NIR (660 nm, 0.5 W cm^{-2}) for 15 min. The same trend as *in vitro* study was repeated here, but one of the prominent results here was the antitumor potential of the DOX-loaded sample carrying the p53 suppressor which was irradiated with NIR at two wavelengths; this sample not only inhibited the growth rate but also decreased the size of the tumor.[121]

Apart from the discussed triple-responsive platforms combining two external stimuli-based therapies like PTT and PDT and one internal, some studies have adopted two internal triggers and one external. The endogenous or internal triggers were pH, temperature, and redox, and by combining the agents, for example, pH and redox can improve the efficacy and accuracy of treatment. A recent study has developed a cisplatin-loaded BP platform responsive to pH and H_2O_2 for combination therapy against triple-negative breast cancer and lung metastasis.

The cisplatin (20 mg mL^{-1}, 200 μL) was added to the BP nanosheets' suspension (1 mg mL^{-1}, 10 mL) and sonicated for 30 min and then dopamine hydrochloride solution was added to this one for another 4 h in the dark. Eventually, the hyaluronic acid which had been modified with a disulfide bond was added to this solution to obtain the pH- and redox-responsive carrier. The *in vitro* cisplatin release was assessed at different pH values and in the presence of H_2O_2 and NIR; the acidic medium resulted in a faster release than physiological pH and the presence of H_2O_2 even increased the drug molecule liberation. Above these, the combination of NIR + pH 5.0 + H_2O_2 had the strongest effect with the release of about 80% of the loaded drug after 96 h. Complete *in vitro* studies were performed regarding cell cytotoxicity, 2D migration, 3D invasion, and 3D tumor spheroids. In the H_2O_2-rich and acidic conditions of tumor microenvironment, the liberation of cisplatin and degradation of BP was reinforced by NIR and the temperature elevation itself increased the therapeutic outcomes. With all the platform's anticancer potential in effect, 4T1 cells were successfully killed, the growth rate and self-regeneration of tumor spheroids were suppressed, and the metastatic ability of 4T1 cells was limited.[172] Immune checkpoint blockade therapy along with chemotherapy and PTT were combined against breast cancer therapy. Poly metformin as a cationic chemotherapeutic agent was self-assembled around BP nanosheets by bridging the electrostatic interaction between them. Then, the immune checkpoint inhibitor anti-PD-L1 antibody was added to the platform through physisorption. Based on immune checkpoint blockade therapy, the nanoparticles could precisely target the primary tumor through the interaction of programmed death-ligand 1 and anti-programmed death-ligand 1 antibodies. Moreover, the upregulation of programmed death-ligand 1 increased gradually and the therapy potency was reinforced when the PTT had been applied, indicating the efficacy of combinational therapy. The synergistic effects of PTT, immunotherapy, and chemotherapy led to strengthened antitumor effectiveness, inhibited primary and abscopal tumor progression, and induced a long-term tumor immune memory establishment.[198]

Derived from BP, violet phosphorus was first proposed in 1865 as an allotrope of BP.[199] Violet phosphorus is considered the most stable phosphorus allotrope and it has attracted considerable attention recently thanks to its high stability,[200] unique cross structure,[201] and various derived structures.[202,203] Thus far, violet phosphorus has been assessed in different biomedical-related applications, including anticancer activity,[173,204] anti-infection,[205] periodontitis treatment,[206] and sensing.[207] However, a comprehensive assessment of the mechanism of action at the molecular and cellular levels is pivotal for biomedical applications. A recent paper on the synthesis and anticancer potential of violet phosphorus has targeted the effect of the physical properties of violet phosphorus on its anticancer activity *in vitro* and *in vivo*. A chemical vapour transport method was adopted to synthesize the violet phosphorus by using amorphous red phosphorus as feedstock and Sn + SnI_4 as the transport agent. Violet phosphorus was yielded with three different lateral sizes and thicknesses—the sizes: 176.7 ± 46.4 nm, 287.1 ± 71.6 nm, and 1–3 μm, and the thicknesses: 22, 40, and 140 nm. Nonetheless, cold atmospheric plasma treatment along with the violet phosphorus was applied *in vitro* and *in vivo* for more effective therapeutic outcomes. The cell viability of violet phosphorus against cancer cells was assessed *in vitro* for up to 24 h at different concentrations (5–82 μg mL^{-1}); a concentration-dependent suppressive effect was observed and the violet phosphorus with the smallest size had the strongest effect. Upon applying the cold plasma treatment in combination with the violet phosphorus, the anticancer effect got stronger. The violet phosphorus with the smallest size induced IC-50 in combination with cold plasma at a concentration of 10 μg mL^{-1}. Based on the obtained results, the cold plasma treatment elevated intracellular ROS levels, whereas the violet phosphorus did not affect the ROS levels. Mechanistic analysis indicated that the violet phosphorus treatment suppressed arachidonic acid metabolism *in vivo* and led to the antitumor effects.[204] Under the category of tumor nanomedicine, there is a subdiscipline called nanocatalytic medicine which is based on introducing a nano-sized catalyst in the tumor microenvironment to consume or generate substances for cancer elimination.[208] Generally, ROS is generated catalytically which can destroy cancer cells' structure and function followed by inducing apoptosis. These nanocatalysts can be activated by external and/or internal stimuli and BP nanomaterials are among those nanocatalysts that are responsive to both stimuli. However, some challenges restrict the treatment outcomes such as tumor hypoxia.[209,210] Violet phosphorus quantum dots, calcium peroxide, polyacrylic acid, and sodium hyaluronate were synthesized by a one-pot method as a self-catalyst for ROS generation. Given the hypoxic environment of the tumor and insufficient amount of hydrogen peroxide, calcium peroxide was added to the platform to address this issue and improved the treatment efficacy. As a result of violet phosphorus quantum dots and calcium peroxide metabolism, phosphorus and calcium ions were released and led to cell calcification (Fig. 4(A)). The cell viability of different nanomaterials was assessed at various concentrations against breast cancer cells (4T1). The nanomaterials are as follows: violet phosphorus quantum dots, calcium peroxide, and a combination of both. It was found that calcium peroxide significantly reinforced the suppressive growth effect on the cancer cells due to generating hydrogen peroxide, oxygen, and calcium ions; the first two substances reinforced the ROS generation capability of the quantum dots and the overload of calcium ions led to ROS-induced cell death and calcification. The efficacy of this platform was assessed *in vivo* through tail vein injection of the nanomaterials in 4T1 xenograft tumor-bearing mice. Following a single-dose injection, the multifunctional platform outperformed calcium peroxide, saline, and violet phosphorus quantum dots in terms of antitumor activity. After 14 days of administration, the tumors were dissected and sectioned to be analyzed through TUNEL staining and alizarin red staining; it was implied that the multifunctional platform had the highest antitumor activity among all the groups (Fig. 4(B)).[211] Since the physicochemical stability of violet phosphorus is higher than BP, it has attracted

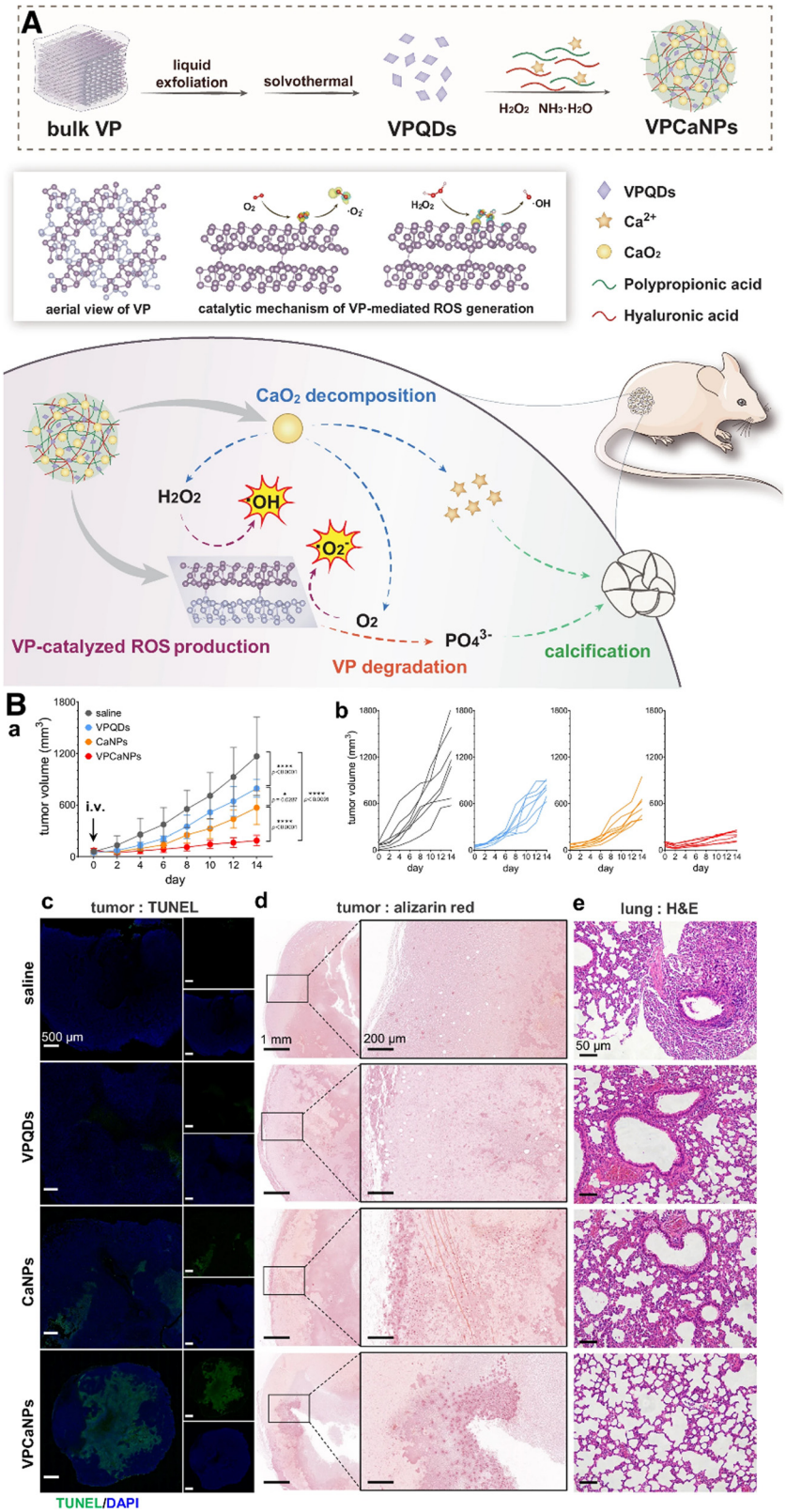

Fig. 4 Catalytic activity of violet phosphorus quantum dot nanosystems for cancer therapy. (A) Schematic of violet phosphorus quantum dot preparation through the liquid exfoliation followed by an ST technique; the multifunctional platform composed of the quantum dots, calcium peroxide, sodium hyaluronate, and polyacrylic acid was synthesized *via* a one-pot method under ultrasonic bath in the presence of hydrogen peroxide and ammonia solution. Once the multifunctional nanoparticles are internalized in a tumor cell, they undergo degradation and release calcium and phosphorus ions; the antitumor properties are violet phosphorus-catalyzed ROS generation, oxygen-mediated violet phosphorus degradation, and calcification. (B) *In vivo* experiments on 4T1 tumor-bearing mice and checking on the lung metastasis for two weeks. (a) and (b) Antitumor performance

of different samples including violet phosphorus quantum dots, calcium peroxide, saline as the control group, and the multifunctional nanocomposite after being intravenously injected in tumor-bearing mice. (c) TUNEL and (d) alizarin staining tumors along with (e) the histological analysis related to the lung of treated mice. Abbreviation: Violet phosphorus quantum dots: VPQDs; calcium peroxide: CaNPs; and the multifunctional platform: VPCaNPs. Reproduced under the terms of the Creative Commons Attribution License.[211] Copyright 2024, Nature.

considerable attention in stimuli-responsive cancer therapy. A recent study has successfully prepared 2D violet phosphorus for combined cancer therapy—PDT, PTT, and catalytic therapy (Scheme 10). The 2D nanosheets were synthesized through liquid exfoliation and after being dispersed into water for 10 days, violet phosphorus had kept its functionality, which is an added value to take into account compared to BP. At specific time intervals including 0, 3, 6, and 10 days, the PTT potential of violet phosphorus and BP was examined *in vitro*. The results indicated that gradually, BP had lost its photocatalytic properties due to oxidation. In contrast, the violet one indicated the same PTT ability during the treatment period without any sign of weakening in the catalytic properties. The cell viability of 2D nanosheets was assessed with and without light irradiation under the exposure of different cells—4T1, CT26, U87-MG, MCF-10A—at concentrations of 0, 1, 2, 5, 10, 25, and 50 μg mL^{-1} for 24 h. In the absence of light radiation, 25 and 50 μg mL^{-1} induced a small reduction in the cancer cell viability without affecting the healthy ones, and the authors have attributed this phenomenon to the GSH-consumption ability of violet phosphorus. The light irradiation has significantly reduced the cell viability of cancer cells down to 14% at the highest concentration. The anticancer activity of nanosheets was further assessed *in vivo* on 4T1-tumor-bearing mice for two weeks and tumor necrosis was obtained only in the case of violet phosphorus + light irradiation. The combination of PTT and PDT plus the consumption of GSH with the temperature increase caused the inhibition of tumor growth and induction of tumor necrosis *in vivo*.[173]

6. Brain cancer

Dismal prognosis and high recurrence rate are two prominent features of glioblastoma, making it a lethal malignant tumor. Surgery is the main treatment approach towards a brain tumor but complementary treatments including radio- and chemotherapy are of great importance because the entrapment of glioma cells through the brain tissues is highly probable, which is rooted in the infiltrative nature of these cells. It is critical to bear in mind that applying diagnostic and therapeutic operations in the brain is highly challenging due to the blood–brain barrier, which plays a restrictive role against the transportation of foreign substances unless they are ultra-small.[212,213] The brain tumor's formation is synchronized with the remodeling of the extracellular matrix (Scheme 11). The matrix of a normal adult brain (left) comprises hyaluronic acid, proteoglycans (aggrecan, brevican), collagen IV, and tenascins (mainly tenascin R). However, in the case of glioblastoma, an increase in the density and stiffness of the matrix occurs. Moreover, it is worth mentioning that the presence of neurodevelopmental proteins (tenascin C), metalloproteases (MMPs), and the absence of aggrecans promote invasion and angiogenesis. In recent years, BP nanomaterials have been applied in neurodegenerative

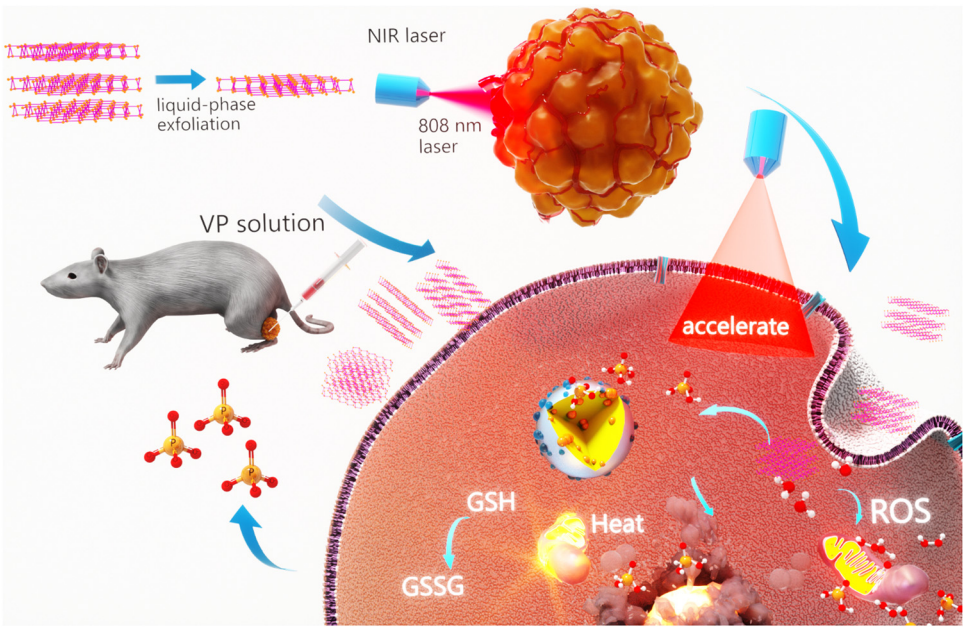

Scheme 10 Violet phosphorus for combined cancer therapy. Schematic of violet phosphorus 2D nanosheet preparation and light responsivity, which eradicate cancer cells while leaving behind no negative effects on the healthy cells.

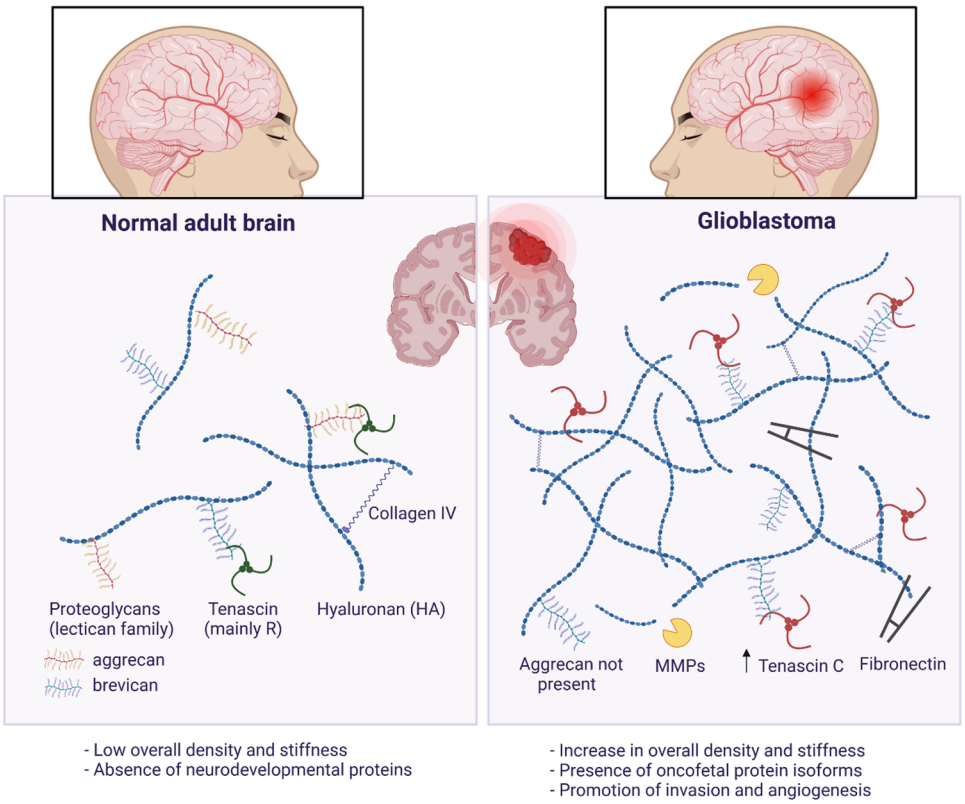

Scheme 11 Difference in the extracellular matrix of normal adult brain and glioblastoma. Created with BioRender.com.

diseases such as Parkinson and Alzheimer, showing the potential of this material for glioblastoma.[214–216] Thus far, a few studies have targeted glioblastoma through BP nanomaterials, which will be discussed in this section.

The first study focused on targeting glioblastoma through BP nanomaterials was published in the year 2020, in which BPQDs were first encapsulated in PLGA and then loaded with mesenchymal stem cells.[217] These cells have recently attracted more attention in cancer therapy because of low immunogenicity and excellent tumor tropism. The great tendency of mesenchymal stem cells towards tumor cells comes from the expression of CXCR4.[218] One of the most important aspects of mesenchymal stem cell-based targeted drug delivery systems is to preserve the migratory ability of these cells even after encapsulation of a therapeutic/bioactive cargo. The migratory potential and tumor tropism capacity of cells after encapsulation of PLGA-BPQDs were assessed *in vitro* through U251, NIH3T3, and DEME cell media. The unloaded and PLGA-BPQDs-loaded cells exhibited similar tumor tropism capability towards the chamber with U251 cells and easily migrated to the lower surface of the membrane showing that the nanoparticles did not negatively affect the mesenchymal stem cells. The cell viability of BPQD and PLGA-BPQD nanoparticles against the same cell lines was performed *in vitro* at different concentrations (0–100 μg mL^{-1}) up to 24 h; as a result, no significant changes in the viability compared to the control were observed. For *in vivo* studies, U251 cells were subcutaneously injected into the right axillary region of mice and once the tumors reached the desired size, the samples were injected through the tail vein at a concentration of 500 μg mL^{-1}. Two days post-injection, the tumors were irradiated with NIR (808 nm, 1 W cm^{-1} for 5 min) for 16 days. The PTT procedure applied on the PLGA-BPQD-loaded mesenchymal stem cells accumulated in the tumors led to an increase in the temperature up to 58.84 °C, and this treatment was implemented until the tumors were completely eradicated, whereas PLGA-BPQDs + NIR just inhibited the growth rate.[217]

A nanocomposite hydrogel was prepared by using a chitosan solution loaded with BP nanosheets functionalized with 3 nm copper nanoparticles. This temperature-sensitive hydrogel was developed for wound healing and anticancer purposes. The nanocomposite was found to cross the blood tumor barrier thanks to the photothermal effect of BP nanosheets and the copper nanoparticles could induce chemodynamic therapy. Moreover, the PD-L1 antibody was included into the package to introduce immunotherapy and reinforce the therapeutic outcomes. The biodegradable hydrogel was observed to be uniformly distributed around the blood tumor barrier and NIR irradiation facilitated the penetration rate, resulting in the liberation of more copper nanoparticles capable of inducing redox reactions in the presence of O_2 and H_2O_2. To investigate the therapeutic effects *in vivo*, U87MG-Luc cells were injected into the brains of mice to form the glioblastoma model. The thermal cameras which took images of the treated mice brains with the hydrogel revealed a temperature above 50 °C when the NIR (808 nm) was applied for 5 min, causing the

death of the tumor cells. It is worth mentioning that this study has simulated the penetration of nanocomposite through the blood–brain barrier *in vitro* as well as through the formation of a layer (human umbilical vascular endothelial cells) in transwells where the nanoparticles' ability to cross the chamber from inside to outside was considered as the permeability. This test also proved that the NIR could improve the penetration rate by about three times compared to the non-irradiated one.[219]

A novel strategy was proposed and applied for glioblastoma through a combination of PTT, tumor starvation, and nitric oxide therapy. Through an esterification reaction, L-arginine was conjugated onto the surface of BP nanosheets followed by the introduction of glucose oxidase to the nanocomposite through amidation, thus creating a multimodal nanodrug (BPAG). This chemical modification induces a major BP stability under physiological conditions and stimulates H_2O_2 and NO production through the cascade oxidation of glucose and L-arginine that is accelerated by PTT. To promote tumor targeting with BPAG, the macrophage membrane was functionalized with the nanoparticles under ultrasonic conditions. Thus, the membrane-coated BPAG (M@BPAG) increased penetration through the blood–brain barrier for GBM targeting that combined with H_2O_2-NO release. PTT effect is able to reprogram tumor immune microenvironment (M@BPAG with NIR irradiation converted cold tumors to hot ones) by high infiltration of $CD8^+$T cells and M1 macrophages. A macrophage coating was adopted to facilitate and improve the penetration of nanocomposites through the blood–brain barrier. The *in vivo* studies were performed on GL261-Luc tumor-bearing C57BL/6 mice through injection of the nanocomposite (4–6 mg kg^{-1}, 100 μL) in the tail vein just once throughout the whole process. At 8 h after the injection, NIR was applied to the tumors for 15 min. The biodistribution study revealed that the membrane coating was able to improve the penetration and accumulation of nanocomposites in the tumor and the combination therapy was the most effective strategy with the highest tumor growth inhibition among all samples.[220]

Another combined therapeutic package for glioblastoma was developed through the coordination of neodymium with BPQDs. The neodymium has improved second-window NIR absorption of BPQDs, which has been used for imaging in this study, by induced X-ray photodynamic performance. Upon NIR irradiation, photon energy was absorbed by BPQDs and then transferred to the neodymium ions culminating in the enhancement of NIR imaging. At the same time, X-ray photon energy was converted and transferred by coordinated neodymium ions to BPQDs resulting in the formation of singlet oxygen species. In order to make the platform targetable to the brain tumor, cyclic RGD peptides were added to the surface modification. The anti-glioblastoma performance of nanoparticles was evaluated *in vivo* in a glioblastoma nude mouse model. A dramatic suppression of the intracranial tumor growth for the peptide-modified neodymium-BPQDs was obtained, while the performance of rest was unfavorable. The mice which were left untreated experienced weight loss and decreased survival rate, whereas the nanoparticles irradiated with X-ray significantly improved the survival rate and only insignificant weight changes were observed.[221]

Anticancer therapy through mechanical shockwaves can be obtained by laser light known as photoacoustic therapy or microwave (microwave-induced thermoacoustic therapy). The former approach was introduced briefly in the previous sections. The mechanism of treatment is the same but the latter is preferred over optical treatment strategies since it has a deeper penetration depth.[222] A recent study has reported the development of an imaging-guided microwave thermoacoustic therapy agent. BP nanosheets were first modified with Fe^{3+} ions and then encapsulated into PLGA-COOH (Scheme 12). The carboxylic groups present on the surface of PLGA were favorable for the amide reaction between them and RGD peptides to target U87-MG cells. The cell viability of nanoparticles (15–240 μg mL^{-1}) was evaluated up to 24 h against U87-MG cells and compared with pulsed microwave, control, and the nanoparticles + the pulsed microwave. The nanoparticles at a concentration of 120 μg mL^{-1} induced IC_{50} after triggering with the microwave. The nanoparticles alone did not affect the cell viability negatively even at the highest concentration. The thermoacoustic therapy was also performed *in vivo* on U87-MG tumor-bearing nude mice for 14 days and the tumors were grown into the back of mice (a dorsal transplantation tumor model). The nanoparticles were injected intravenously as a suspension (100 μL, 0.5 mg kg^{-1}); the treatment cycles (pulsed microwave) were applied every 2 days for 15 min. The biodistribution study showed that the nanoparticles accumulated in the tumor site thanks to the peptide conjugation after 3 h post-injection. Then, gradually, the signal weakened showing the renal clearance of nanoparticles. The temperature of the tumor, which had been exposed to microwave, was assessed frequently after the treatment and revealed no change; this measurement was important to show that the therapeutic outcomes came from mechanical shockwaves and not heat. Both the targeting ability of nanoparticles and the generation of mechanical shockwaves after stimulation with microwave resulted in the reduction of tumors' size and the histological analysis performed on the tumor sections exhibited large amounts of cell necrosis and nuclear lysis. However, the tumors treated with other groups including the nanoparticles without stimulation, pulsed microwave alone, and control saw an increase in size up to 12 times bigger than that of the initial one.[223]

7. Skin cancer

Skin cancer is one of the lethal threats to human life globally and the new cases found each year are increasing at an ever-increasing rate. Melanoma is about 5% of all skin cancers but accounts for more than 75% of deaths under this category. If melanoma is localized (98%) or regional (64%), the survival rate differs, but it drops down to 23% when melanoma progresses to metastatic.[224,225] There are four stages for melanoma as follows (Scheme 13): (I) at the first stage, the cancer cells are in both the dermis and epidermis and the melanoma is less

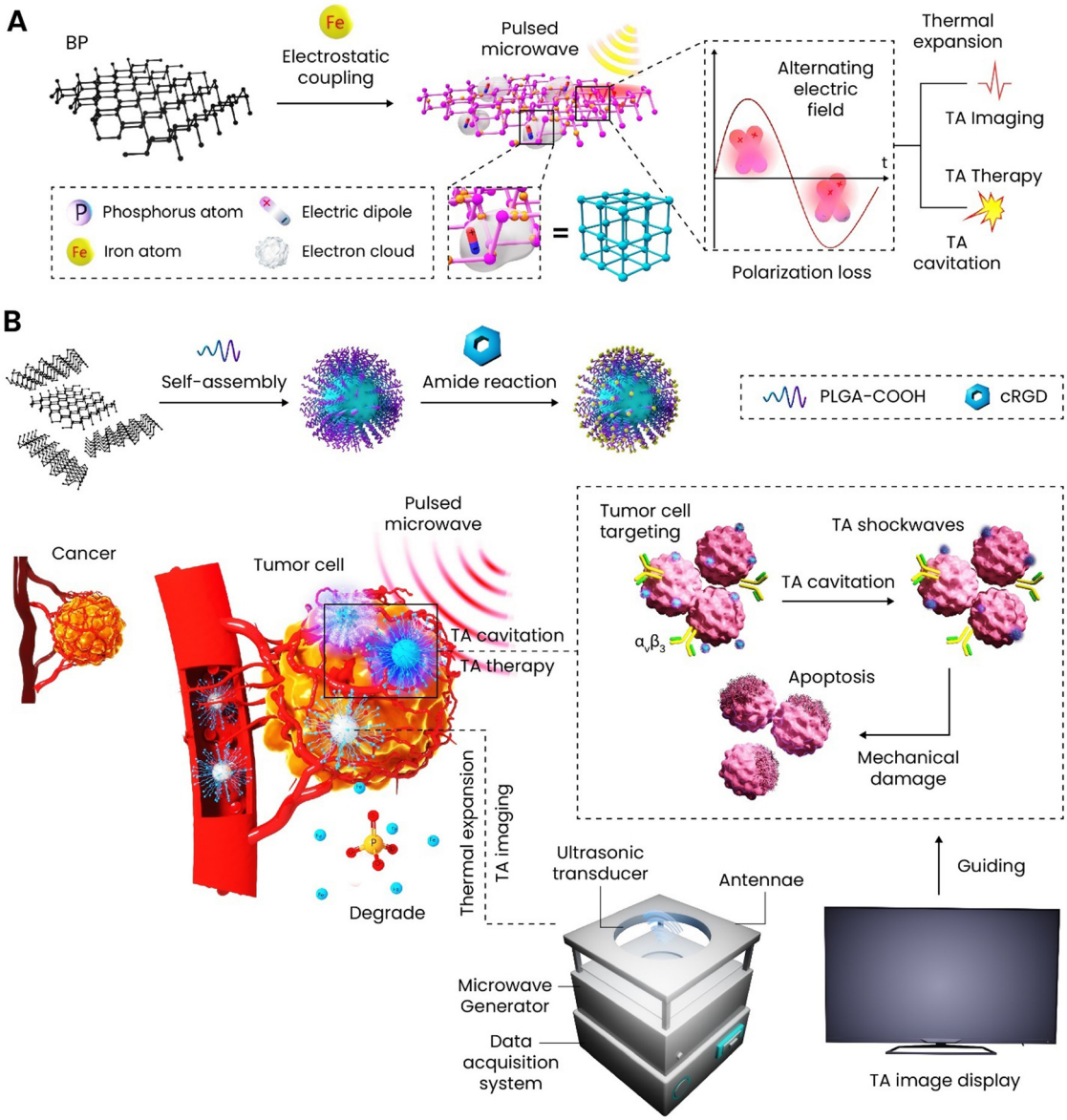

Scheme 12 Microwave-induced thermoacoustic therapy through surface-modified BP-encapsulated PLGA for glioblastoma. (A, B) Preparation process of Fe^{3+}-conjugated BP nanosheets followed by encapsulation in PLGA; the amidation of cRGD on the surface of nanoparticles gave them the targeting ability towards glioblastoma cells for both thermoacoustic imaging and therapy.

than 1 mm in size with or without ulceration. Spreading to distant sites or lymph nodes is not evidenced. (II) This stage is defined based on the tumor thickness and ulceration; the tumor thickness increases and reaches to the range of 1–4 mm but still there is no evidence related to spreading. (III) Progression to the third stage is synchronized with the involvement of regional lymph nodes while not spreading to distant sites. (IV) At the final stage, distant skin and lymph nodes got involved followed by spreading to other organs among which the lungs, brain, liver, bone, and/or intestines can be enumerated.[226,227] Surgery is considered as the most common treatment of skin cancer through which the lesions are excised. In the case of melanoma, the surgeon may remove larger areas due to the highly infiltrative nature of this type creating large wounds that put more problems on the shoulder of patients—infection and prolonged healing rate.[228]

BP in any form has been widely applied in skin cancer therapy and regeneration because of eradicating the cancerous cells at the first stage and then accelerating the regeneration rate. Here the focus is on the potential of BP nanomaterials in skin cancer therapy and Table 5 contains detailed information about the BP nanomaterials applied in skin cancer therapy.

Various therapeutic approaches have been applied in skin cancer therapy through BP nanomaterials—radiotherapy, PTT, PTT-chemodynamic therapy, PTT-immunotherapy, and PTT-chemotherapy. Radiotherapy is a well-known anticancer therapeutic method adopting high-energy X-rays or γ-rays to induce DNA damage and cell apoptosis in a tumor. Moreover, the

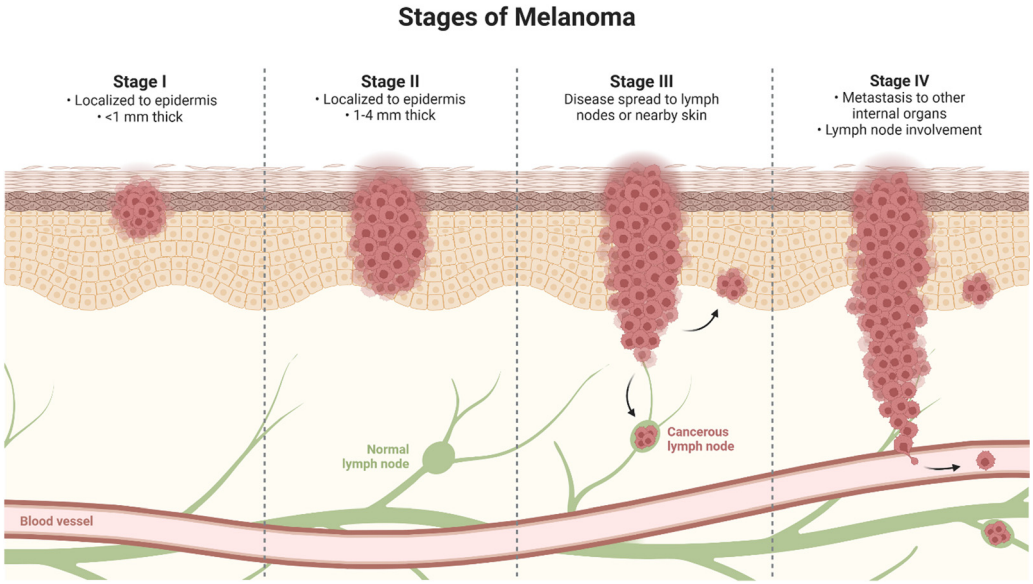

Scheme 13 Different stages of melanoma. Created with BioRender.com.

radiation alone has potential to turn water molecules into cytotoxic ROS reinforcing the cell apoptosis. However, this approach clearly suffers from some drawbacks including different radiosensitivities of individuals, radiation resistance, and unfavorable side-effects requiring more efficacious radiosensitizers.[235,236]

In 2018, a nanosystem composed of BPQDs and PLGA was synthesized for precise tumor radiosensitization. The nanoparticles were responsive to the acidic pH of tumor for a charge reversal followed by facilitating the cells' internalization and also glutathione for release of the encapsulated BPQDs. By tracking the absorbance changes in 1,3-diphenylisobenzofuran in the presence of $^1O_2$, the ROS generation capability of samples was assessed with and without X-ray irradiation *in vitro*. In the absence of irradiation, the efficiency of ROS was low and stable while applying X-ray increased the production of $^1O_2$ species of nanosystem in a dose-dependent manner. This radiotherapy was applied to the nanosystem exposed to the A375 human melanoma cell line and L02 as the normal cell line and a significantly higher ROS content was generated in the cancer cell medium than that of the normal cells. Using an A375 subcutaneous tumor model, *in vivo* studies were performed for 21 days and the combination of nanosystems with X-ray had the highest inhibition rate among the tested samples, but it is important to mention that the X-ray irradiation caused the mice to lose weight over the duration of study.[229] Another radiosensitizer was developed against melanoma through the formation of ultrasmall Bi_2O_3 on BP nanosheets. The decoration of nanosheets surface was found to prevent rapid degradation of BP and stabilize the water dispersibility. Both BP and Bi_2O_3 overproduced $^1O_2$ species upon external X-ray irradiation and induced cell apoptosis. This study has also performed *in vivo* tests and reported the inhibition of tumor growth by the combination of decorated BP and X-ray, but did not assess the body weight changes. The major organs were analyzed after 21 days of studying and revealed no pathological changes.[230]

Chemodynamic therapy is among effective supplementary anticancer approaches, which in combination with other methods yields much more therapeutic outcomes.[181] An innovative study has stabilized copper ions on the surface of BP to not only stabilize the photothermal stability of nanosheets, but also take advantage of copper ions to produce ROS in the tumor microenvironment due to inducing Fenton-like reaction. The deposition of copper was reported to improve the composite's photothermal performance and accelerate the degradation rate *via* redox reactions. The cell viability of samples at different concentrations (1–100 μg mL^{-1}) against B16F10 cells was assessed up to 48 h. Despite the increase in the concentration of bare BP up to 100 μg mL^{-1}, no significant changes in the cell viability were observed. However, the copper-modified BP started to decrease the cancer cells' viability from 20 μg mL^{-1} and IC50 was achieved at 80 μg mL^{-1} thanks to copper ions to turn H_2O_2 to hydroxyl radical ions. The strongest anticancer effect belonged to the surface-modified BP plus NIR, which induced IC50 at 50 μg mL^{-1}. To improve the tumor uptake of nanocomposites, a polypeptide was also conjugated and applied *in vivo* against the B16F10 tumor model; applying NIR to the tumors led to a rapid increase in the local temperature from 30 to 56 °C in 5 min resulting in the tumor ablation, whereas the samples without the polypeptide only elevated the local temperature by about 16 to 19 °C. The peptide used here could dramatically increase the accumulation of nanoparticles in the tumor and enhance the PTT.[26] Inspired by the desirable anticancer outcomes of PTT and chemodynamic therapy, a 3D scaffold was designed and fabricated for skin cancer therapy and regeneration. This multifunctional platform was supposed to eradicate the remained cancerous cells left in the wound, prevent potential infection, and accelerate the regeneration rate.

Table 5 Physicochemical and biological properties of BP-based materials in skin cancer therapy

Nanovehicle	Particle size (nm) Zeta potential (mV) Photothermal conversion (%)	Type of therapy	*In vitro* and *in vivo* models	Cargo	Remarks	Ref.
PLGA-BPQDs	150 nm −7.78 mV —	Radiotherapy	*In vitro*: A375, HeLa, and L02 cells *In vivo*: A375 tumor model	—	–A nanosystem was designed and modified with a polypeptide for targeted radiotherapy –The nanoparticles' surface charge underwent a change from negative to positive in the tumor microenvironment facilitating cells' internalization –Applying X-ray irradiation to the accumulated nanoparticles into the target-induced cell apoptosis and tumor growth inhibition *in vitro* and *in vivo*	229
Bi_2O_3-decorated BP nanosheets	300 ± 80 nm +34 mV —	Radiotherapy	*In vitro*: A375 and H9C2 cells *In vivo*: A375 tumor model	—	–Bi_2O_3 was conjugated onto BP to stabilize and improve the dispersibility of the nanosheets –The surface modification resulted in the reinforcement of singlet oxygen species production and better anticancer outcomes	230
BP nanosheets	916 ± 185 nm −20 ± 4 mV —	—	*In vitro*: NIH3T3, nHDF, and HT1080 cells *In vivo*: —	—	–The cytotoxicity of BP nanosheets against three different fibroblast cells was assessed *in vitro* –Various concentrations spanning from 0.3 to 125 μg mL^{-1} were applied for 48 h −3.9 μg mL^{-1} was enough to induce IC50 against fibrosarcoma cells whereas the same effect on the healthy cells took place at the concentrations of 62.5 and 125 μg mL^{-1}	231
PLGA-collagen-BP nanosheets	—	PTT	*In vitro*: SK-Mel-28-Luc and NHDFs cells *In vivo*: SK-Mel-28-Luc tumor model	—	–A composite mesh was fabricated for skin cancer therapy and regeneration –The scaffold showed excellent photothermal conversion against melanoma cells *in vitro* and *in vivo* –The adhesion and proliferation of dermal fibroblasts were promoted	232
Copper-doped BP nanosheets	60–120 nm — 35.4%	PTT and chemodynamic therapy	*In vitro*: B16F10, MDA-MB-231, SCC VII, and U87MG cells *In vivo*: B16F10 tumor model	—	–The surface of BP nanosheets was decorated with copper ions to improve the photothermal stability and degradation –The copper incorporation also introduced chemodynamic therapy and positron emission tomography imaging to the nanosheets –The combination of PTT and chemodynamic therapy had the strongest antitumor effect *in vivo*	26
Decellularized matrix-BP nanosheets-poly(dopamine)-Ag	225 nm and −20 mV for BP-poly(dopamine)-Ag	PTT and chemodynamic therapy	*In vitro*: A375 and HaCaT cells *In vivo*: A375 tumor model	—	–A multifunctional scaffold was designed to eradicate remained cancerous cells left from the surgery through PTT and chemodynamic therapy and accelerate the regeneration rate –The combined therapy led to 33% inhibition of tumor recurrence followed by prevention of infection and triggering the regeneration rate *in vivo*	111
PEGylated BP nanosheets	120 nm −8.34 mV 36%	PTT and immunotherapy	*In vitro*: B16, L929, and 4T1 cells *In vivo*: B16 tumor model	Imiquimod	–The combination of PTT and immunotherapy was adopted against B16 melanoma –A much greater release of cytokines was obtained when the PTT had been applied and the immunoadjuvant had been released together	162
Gelatin-PCL-BP nanosheets	— — 38%	PTT and chemotherapy	*In vitro*: NIH-3T3 and B16F10 cells *In vivo*: B16F10 tumor model	DOX	–An electrospun scaffold containing BP nanosheets was fabricated through an electrospinning technique –The nanosheets were modified with melanoma-targeting folic acid-based ligands to selectively prevent the growth of cancer cells –Upon NIR, the BP release from the scaffold got faster and the internalized DOX-loaded BP then killed cancer cells through the combination of PTT and chemotherapy	233

Table 5 (*continued*)

Nanovehicle	Particle size (nm) / Zeta potential (mV) / Photothermal conversion (%)	Type of therapy	*In vitro* and *in vivo* models	Cargo	Remarks	Ref.
Biomimetic erythrocyte membrane-camouflaged BPQDs	50 nm / −16 mV	PTT and glucose oxidase activity	*In vitro*: B16 and CNE-2 cells *In vivo*: B16 and CNE-2 tumor models	—	–Nanozyme containing BPQDs were synthesized and modified to reach the melanoma cells in a targeted manner –The internalized nanozymes could successfully BPQDs inside the tumors and upon NIR, the local temperature raised up to 50 °C, and also glucose activity was enhanced leading to the generation of ROS	234

The scaffold was composed of decellularized small intestinal submucosa as the matrix and surface-modified BP nanosheets; the nanosheets were first coated with poly(dopamine) followed by the deposition of Ag nanoparticles on the surface. By subjecting to A375 cells, the scaffold's anticancer potential was assessed *in vitro* with and without NIR and only the PTT caused a high decrease in the cell viability and not the chemodynamic effect. Using the same cell line, a hypodermic transplant was established *in vivo* and then most of the tumor mass was excised through conventional surgery. Next, the scaffold was implanted in the wound bed and got irradiated for 6 min and a temperature elevation of 27.1 °C was observed while the scaffold without BP did not make any changes in the local temperature. The tumor recurrence rate of the scaffold with NIR was 33% stemming from both PTT and chemodynamic therapy, whereas the counterpart without NIR saw a 67% recurrence rate.[111]

PEGylated BP nanosheets in combination with imiquimod were adopted against melanoma for photoimmunotherapy. The PEGylation improved PTT performance and the PTT reinforced the generation of tumor-associated antigens, which concomitantly induced a strong anticancer effect against B16 melanoma *in vitro* and *in vivo*.[162] Nanozymes have attracted considerable attention in monitoring and therapy applications because of their high stability and tunable catalytic properties.[237] Recently, a nanozyme carrier encapsulating BPQDs has been developed, which could induce both PTT and glucose oxidase activity in a tumor microenvironment. After being intravenously injected, the nanozymes were found to accumulate in the tumor region thanks to homing peptide iRGD. Upon NIR irradiation, the improved glucose oxidase activity of BPQDs in the presence of cellular glucose led to the generation of cytotoxic ROS. The synergistic effects of both therapeutic approaches were effective and successful against B16 and CNE-2 cells *in vitro* and the tumor models *in vivo*.[234] Furthermore, Huang *et al.* have prepared a multifunctional core–shell package with BP in the inner side, capable of releasing nitric oxide (NO) to obtain cancer multimodal therapy. Upon exposure to NIR irradiation, the BP induced PTT which in combination with the release of NO led to immunogenic cell death, thereby stimulating an antitumor immune response. Contemporarily, the authors have demonstrated BP-capability to reverse tumor immunosuppression *via* Treg inhibition, M2 macrophage restraint, and PD-L1 downregulation. Hence, this drug-free multimodal therapeutic approach (NO gas therapy, immune therapy, PTT) constitutes a valid tool with strong curative properties against primary and metastasis in B16F10 tumor models thanks to their novel mechanism to destroy immune cold tumors by NO-potentiated immunogenic cell death and immunosuppression reversal.[238]

8. Prostate cancer

Among all the cancer types diagnosed in men, the prostate is the second on the list in terms of fatal malignancy in the USA

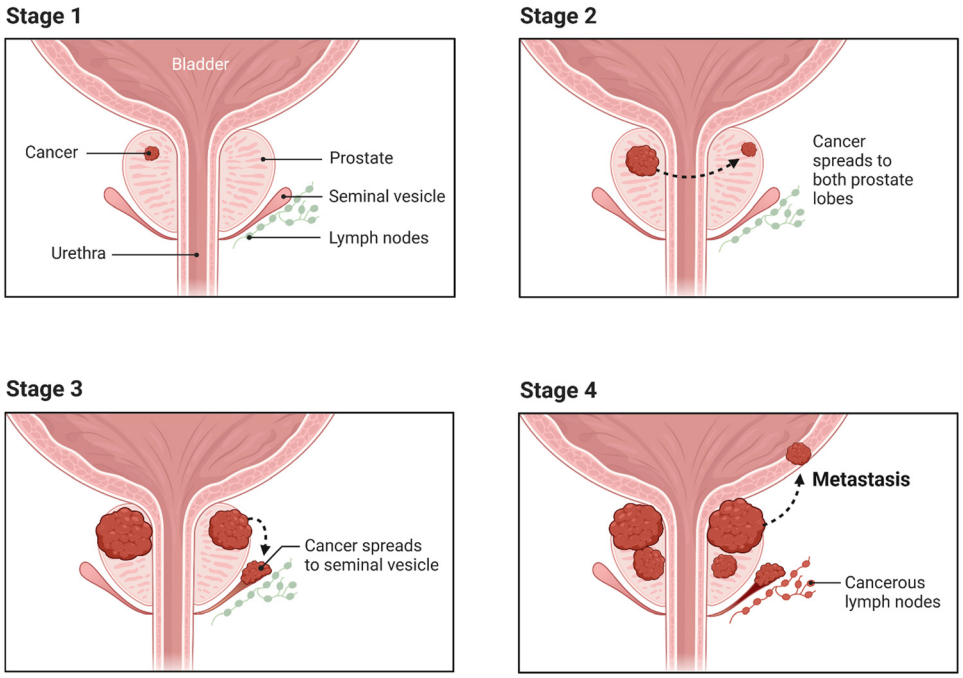

Scheme 14 Different stages of prostate cancer. Created with BioRender.com.

and is on top of the list in some parts of Europe and Africa. Referring to US 2022 statistics, about 27% of confirmed cancer cases account for prostate cancer.[239,240] Although it is known that obesity, family history, aging, and some specific gene mutations are related to prostate cancer, the precise mechanism is unknown.[241] The status of prostate cancer can be recognized through the stages that had been set as follows (Scheme 14): (I) The tumor is only on one side of the prostate and no lymph node involvement and metastasis are observable. (II) The tumors are confined in the prostate glands and they can be on both sides. (III) At this stage, the cancer is regarded as locally advanced and the tumors have progressed and are more likely to spread. (IV) The tumors have spread to lymph nodes and other organs. In the case of moderate to low-risk patients, surgical or radiation therapy is applied as the first treatment option, but for patients with high-risk diseases, the mentioned approaches are at risk of failure.

One of the most common treatments is androgen deprivation therapy which is combined with paclitaxel-based chemotherapy. This approach usually is able to suppress prostate-specific antigens and generate an objective response in bone metastases and soft tissue.[240] Nonetheless, chemotherapy is applied in prostate cancer and the well-known effective drugs for this type are docetaxel, paclitaxel, cyclophosphamide, cabazitaxel, *etc.* However, the clear and common drawbacks are low bioavailability, drug resistance, negative effects on normal cells, and short circulation time.[242,243] However, for unresectable localized prostate cancer, the most advanced radiotherapy is represented by brachytherapy consisting in placing the radioactive sources close to the tumor side. However, brachytherapy provokes several side effects of external-beam radiotherapy such as erection problems, inhibition of ejaculation, infertility, bowel problems, and obstacles in urine passing with pain.[244] Nanotechnology has addressed some of these problems and new formulations with promising clinical results are approved; these formulations and the ones, which are in progress towards being clinically approved, can be found in a recently published review paper.[245]

In 2018, a study with the aim of cytotoxicity assessment of BP nanosheets was published; two cell lines—human ovarian cancer cell line A2780 and human prostate cancer cell line PC-3—were chosen and the cell viability assessment was performed for 24 h through four different methods—MTT, WST-8, resazurin, and LDH assays. Although the objective of this study was not anticancer purposes, it gave an initial clue about the BP behavior in the exposure of prostate cancer cells. All methods revealed that BP nanosheets showed low cytotoxicity against both cell lines up to the concentration of 15 μg mL^{-1}. Except for the MTT assay, the other methods exhibited that the cell viability of PC-3 cells dropped below 40% when the concentration was increased to 400 μg mL^{-1}.[246]

Prostate is known to contain the highest level of zinc and this ion is able to inhibit the activity of mitochondrial aconitase maintaining the normal function of this organ.[247] The malignancy in the prostate was reported to diminish the zinc concentration, as discussed by some papers showing the anticancer potential of zinc against prostate cancer. Still, the mechanism has yet to be fully understood.[248,249] Zinc ions were conjugated onto BP nanosheets to compensate for the lone pair on the surface, leading to more chemical stability and improving the therapeutic effects of BP against prostate cancer. The BP

nanosheets were first modified with amine-contained PEG and an aptamer to improve the accumulation of nanosheets in the tumor's cells and then zinc ions and DOX molecules were attached to the surface for the combination of PTT and chemotherapy. The DOX release accelerated at an acidic medium and upon NIR irradiation. Various concentrations of zinc and DOX were used to modify the BP and tested against the prostate cancer cells up to 72 h; a concentration-dependent cytotoxic effect was observed when the content of both had been raised. The tumor models were established through subcutaneous injection of PC-3 cells into the right flank area of each mouse and the best anticancer performance belonged to the surface-modified sample with zinc and DOX plus NIR which completely eradicated the tumors *in vivo*.[250] In a different study, the same research group assessed the anticancer potential of zinc-modified BP nanosheets for prostate cancer focused on immunotherapy. DOX was again loaded on the surface-modified BP nanosheets and the combination of chemotherapy and PTT on the maturation of dendritic cells; the results indicated that this combined therapy stimulated the immunogenic cell death process in prostate cancer cells followed by the maturation of dendritic cells.[251] Our group has also studied the effect of BP nanosheets with and without NIR on healthy and cancerous prostate cells *in vitro*. Three concentrations—5, 25, and 75 μg mL^{-1}—were exposed to cells for 72 h and in the absence of NIR. As a result, the lowest concentration was able to reduce the cell viability of PC-3 cells after 72 h compared to the control, and the concentration of 25 μg mL^{-1} had a stronger anticancer effect than 5 μg mL^{-1}. However, there was no significant difference between the viability of 25 and 75 μg mL^{-1}. The middle value of concentration (25 μg mL) also induced cytotoxicity in the healthy cells after 72 h. Upon NIR irradiation, even 5 μg mL^{-1} could significantly induce a reduction in the cell viability due to both PTT and PDT.[252] Additionally, this study showed that 2D BP is capable of leading to the production of anti-inflammatory cytokines (IL-10) and simultaneously inhibiting the release of pro-inflammatory cytokines (IL-6) in healthy prostate cells. Additionally, COX-2 expression in PNT-2 cells stimulated by lipopolysaccharide was also inhibited, which is the most crucial target for standard non-steroidal anti-inflammatory drugs used to treat inflammation and pain. Additionally, it was demonstrated that 2D BP can inhibit the superoxide dismutase decline brought on by lipopolysaccharide. Superoxide dismutase is a well-known enzyme that specifically inhibits the superoxide anion free radical ($O_2^{\bullet -}$), which reduces the formation of nitrite and inhibits the activation of the inflammatory cascade.[253] Superoxide dismutase also plays a significant role as an antioxidant defense in the pathogenesis of many inflammatory diseases by preventing the production of ROS, which is responsible for tissue destruction.[254] A complementary study on the effect of 2D BP on prostate cancer cells also exhibited that after 24 h, some flakes were located near the nucleus. The oxidation of nanosheets gradually caused an apoptotic state of the cells. However, the same material in the exposure of healthy cells did not induce any change and remained stable.[100]

9. Bone cancer

Bone cancer is a rare disease, and its primary types include osteosarcoma, Ewing sarcoma, and chondrosarcoma. The mentioned bone cancers account for less than 1% of total cancers diagnosed annually but the morbidity is significant. However, bone can host metastasis from other malignancies including lung, breast, and prostate. Osteosarcoma is the most common type and about 60% of total cases belong to this type; it is more likely to occur during childhood rather than adolescence. Osteosarcoma is known to originate from malignant primitive mesenchymal stem cells differentiated into osteoblast cells followed by the production of a malignant osteoid matrix.[255] The cancer cells worsen the bone's condition through increasing the proliferation of osteoblasts and so they secrete RANKL; it binds to osteoclasts and stimulates their proliferation. Therefore, not only bone absorption gets faster, but also the osteoclasts secrete growth factors (IGF-1 and TGF-beta), increasing the cancer cells (Scheme 15). The possible treatment pathways for osteosarcoma are surgery and chemotherapy. Since bone tumors generally appear in long bones, the surgical excision would leave a defect; the remaining cancer cells in the defect have potential recurrences.[256] A more up-to-date therapeutic approach is to apply therapeutic and regenerative materials to the bone defect to simultaneously address both issues.[257] BP has strong anticancer potential besides its regenerative properties, making it a promising biomaterial for bone cancer therapy and regeneration.

Since addressing bone cancer and regeneration at the same time is of great importance, the related studies have assessed both properties *in vitro* and *in vivo*. Bioactive glass scaffolds were fabricated through 3D printing and then surface-modified with 2D BP nanosheets for bone cancer therapy and regeneration (Fig. 5(A)). Once the bioactive glass scaffolds had undergone sintering, they were soaked in a BP solution (200 μg mL^{-1}), and this procedure was repeated three times. Through digital photographs, SEM images, and TEM images, it was revealed that the nanosheets were deposited onto the surface of scaffolds and the bare scaffold changed from white to darker colors. The anticancer potential of scaffolds was tested *in vitro* against Saos-2 cells in the presence of NIR with various power densities; increasing in the power density from 0.2 to 1 W cm^{-2} resulted in a significant decrease in the cell viability from 40 to 98%. To develop the osteosarcoma model *in vivo*, Saos-2 cells were injected subcutaneously into the neck of mice. Once the tumors reached an appropriate size, the scaffolds were implanted into them and the NIR irradiation (808 nm, 1 W cm^{-2}) was applied. During the 14 days of *in vivo* study, the surface-modified scaffold was the only sample achieving tumor ablation, while the rest did not inhibit the growth rate. One of the interesting points of this study was the assessment of *in vitro* bioactivity in the simulated body fluid as a sign of bone-bonding ability of the scaffold. The surface-modified scaffold could form calcium phosphate on the surface as a result of BP degradation in the medium which turned into PO_4^{-3} and provided a suitable condition for the calcium deposition and formation of hydroxyapatite.

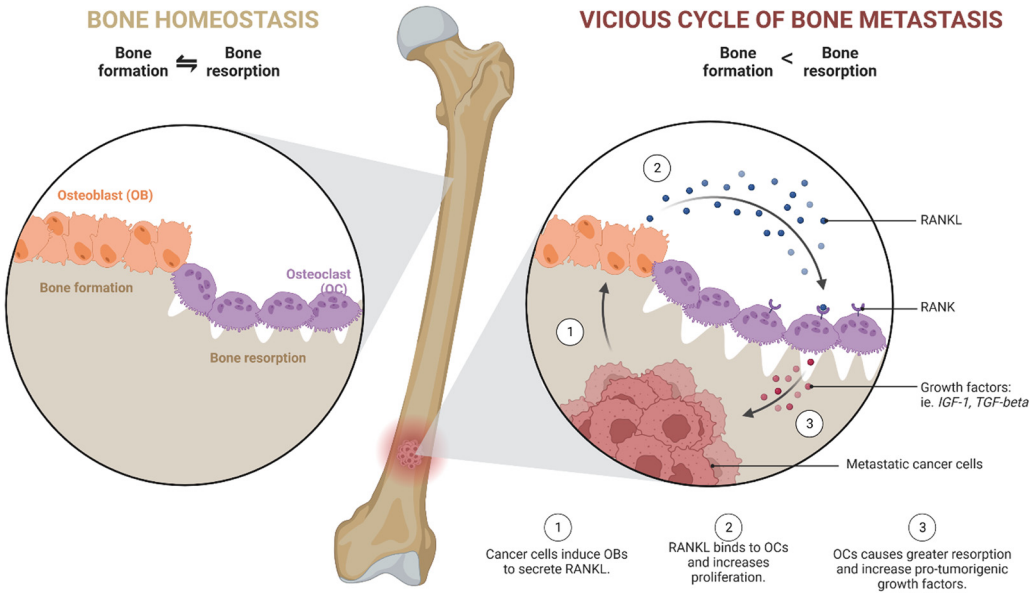

Scheme 15 Schematic of bone homeostasis and bone metastasis. Created with BioRender.com.

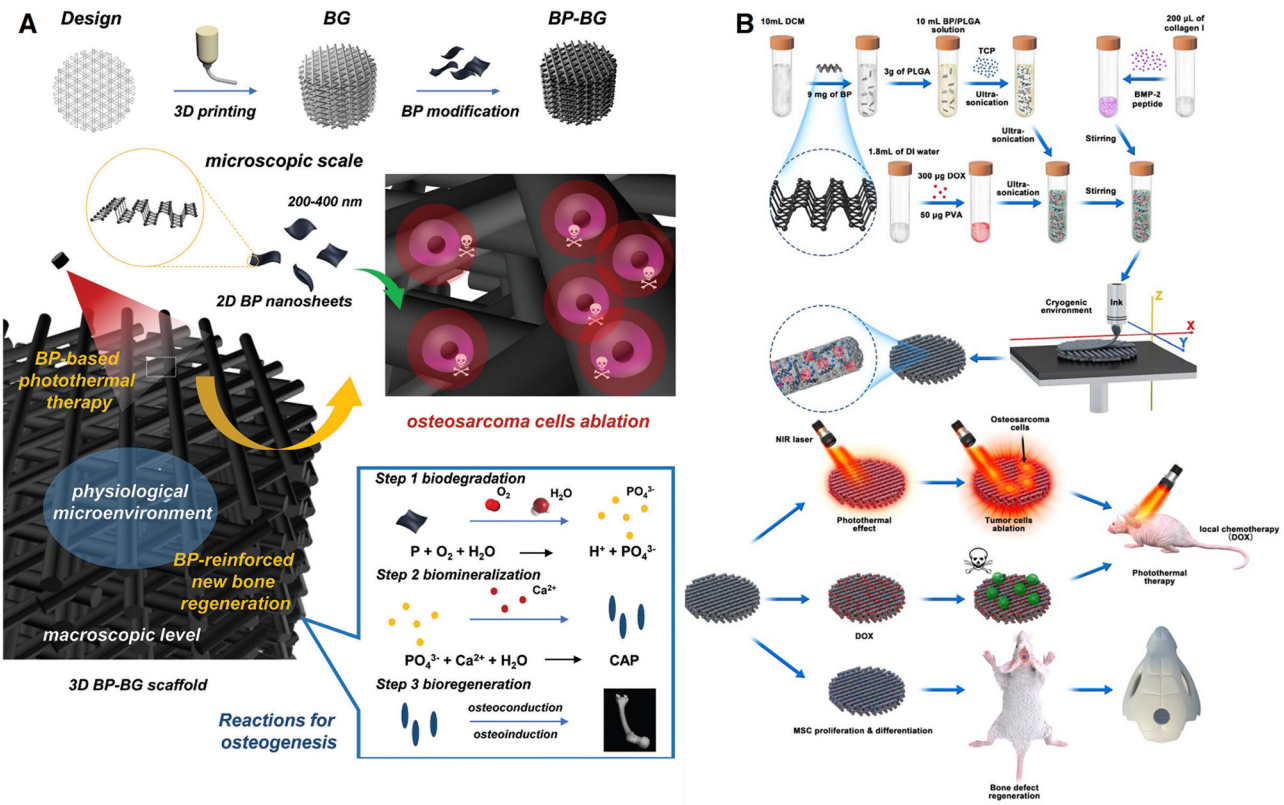

Fig. 5 Multifunctional bone scaffolds containing BP for bone cancer therapy and regeneration. (A) Schematic of bioactive glass scaffold 3D printing and surface modification of scaffold with BP nanosheets for osteosarcoma ablation and osteogenesis. Reprinted from ref. 12 with permission from Wiley. (B) Illustration of preparation and application of a multifunctional scaffold composed of PLGA, BP nanosheets, a peptide, tricalcium phosphate, DOX, and poly(vinyl alcohol) for simultaneous bone cancer therapy and regeneration. Reprinted from ref. 258 with permission from IOP.

In this term, it can be deduced that BP is not only considered as an anticancer agent but also can reinforce the bone-bonding ability of the scaffold.[12] Using the 3D printing technique, another multifunctional bone scaffold was developed to eradicate the osteosarcoma cells followed by inducing accelerated bone tissue regeneration. Three solutions were prepared to obtain the 3D

printing ink: (i) BP nanosheets were encapsulated into PLGA particles and then tricalcium phosphate particles were added to this solution; (ii) a mixture of poly(vinyl alcohol) and DOX molecules; and (iii) combination of collagen I and BMP-2 peptide. Once all solutions were prepared and mixed, 3D printing under cryogenic conditions was performed (Fig. 5(B)). Important information was obtained by examining the tumor volume treated with various samples. The scaffold without DOX exposed to NIR almost eradicated the tumor after 4 days, but tumor recurrence took place. However, the scaffold without BP, which was endowed with only chemotherapeutic potential, could not induce significant inhibitory effects. The combination of chemotherapy (release of DOX) and PTT thanks to BP nanosheets resulted in the reduction of tumors' size *in vivo* after 16 days of treatment.[258] Our group has also assessed the therapeutic and regenerative properties of BP nanosheets upon NIR against osteosarcoma and healthy osteoblast cells. The Saos-2 cells were found to undergo apoptosis due to ROS generation of BP in the exposure of NIR. However, the BP showed the opposite behavior against the healthy cells and stimulated their proliferation and osteogenic marker expression.[13] In another study performed by our group, a hybrid nanocomposite composed of bioactive glass, Pluronic F127, and BPQDs was developed for simultaneous bone cancer therapy and regeneration. With the aid of the surfactant-assisted sol–gel method, BP was encapsulated in the liquid crystals formed by F127 and after applying microwave irradiation, the nanosheets were turned into BPQDs and got encapsulated inside the liquid crystals. The BP-included hybrid showed a suppressive effect against osteosarcoma cells without NIR at a concentration of 150 μg mL^{-1}, while the same concentration did not leave negative effects on the healthy osteoblast cells. The inhibitory effects of nanocomposite on the migration and invasion behavior of bone, prostate, and breast cancers were assessed *in vitro* to evaluate if the nanocomposite was potent enough against primary and secondary bone cancers. Nonetheless, the nanocomposite showed regenerative properties in the exposure of mesenchymal stem cells and osteoblasts *in vitro*.[11]

Applying injectable hydrogels in cancer therapy has gained considerable interest in recent years as a minimally invasive approach; these hydrogels are able to deliver anticancer agents to tumor tissue, and preserve the drug's concentration in the therapeutic window while decreasing the systemic toxic side effects.[259] A recent study has reported the development of an injectable thermo-sensitive hydrogel based on chitosan incorporating BP and DOX for simultaneous bone cancer therapy and regeneration. This hydrogel was supposed to be injected between the interface of implant with the host bone after removal of the bone tumor to eradicate the residual cancer cells and promote osteogenesis. Five cycles of NIR irradiation were applied to the different samples to measure the PTT potential of hydrogels *in vitro*. The hydrogel including BP and DOX could ultimately increase the temperature up to 56.3 °C, which is high enough to damage the tumor tissue. The antitumor efficacy of hydrogel was also tested *in vivo* and it was injected subcutaneously into the tumors followed by exposing the mice to NIR (1.0 W cm^{-2}, 5 min). The temperature of tumors was found to increase rapidly during the 5 min and reached 51 °C. A comparison has been made through the *in vivo* studies and the hydrogels encapsulating DOX, BP, and BP + DOX were checked in terms of potency. The combination of PTT and chemotherapy was the only one which not only inhibited the growth rate but also reduced the size of tumors significantly.[260] A hybrid photothermal scaffold composed of chitosan/hydroxypropyl trimethyl ammonium chloride chitosan/hydroxyapatite/BP was designed and developed to address the residual cancerous bone cells, potential infection, and osteogenesis. This study with the aid of multistage PTT has achieved all the objectives. BP at three concentrations, namely 75, 150, and 300 μg mL^{-1}, was introduced through the hydrogel, allowing regulating the PTT capability. The anticancer and antibacterial activities were obtained when the photothermal stimulation had increased the temperature up to 50 °C; about 95% of osteosarcoma cells and more than 90% of *E. coli* and *S. aureus* bacteria were eliminated as a result of the applied temperature. However, mild hyperthermia was found to upregulate the expression of heat shock proteins. The studies regarding the osteogenesis ability of hydrogel revealed that the gene expression level of ALP, COL 1A1, and OCN after exposure to mild hyperthermia was significantly increased compared to the non-photothermal group *in vivo*.[261]

10. Other cancer types

In the previous sections, the anticancer potential of BP against different cancer types was discussed. These subcategories were based on the published studies. The following section belongs to other types of cancers including colorectal, bladder, liver, ovarian, and lung treated with BP, which has received less attention. The details of these studies are reported in Table 6.

Colorectal or colon cancer is a disease through which the cells in the colon system grow uncontrollably and result in the formation of polyps, which may turn into cancer. Traditional treatments such as surgery, chemotherapy, and radiotherapy are applied extensively with little success and efficacy encouraging more effective approaches to come into practice.[276] The first trial of using BP against colorectal cancer goes back to 2018 in which a study reported the synthesis of BP nanosheets from coarse BP flakes for the first time and used as a DOX carrier and made a surface modification with chitosan-PEG and a cancer growth inhibitor for chemo-PTT. Three different colorectal cancer cells including MC-38, HCT116, and HT29 were exposed to nanoparticles (5–20 μg mL^{-1}). Generally speaking, a concentration-dependent cytotoxic effect was observed against all the cells and the strongest effect was on the MC-38 followed by HCT116 and HT29. The carrier without DOX was found biocompatible and the free DOX had a weaker anticancer effect than that of the DOX-loaded nanoparticles, which was caused by the targeting ability of nanoparticles and an increase in the cytotoxicity. The combination of chemotherapy and PTT resulted in more than 80% cell viability decrease in the three cell lines. Further anticancer potential of samples was tested on

Table 6 Physicochemical and biological properties of BP-based materials in other types of cancer

Nanovehicle	Particle size (nm) Zeta potential (mV) Photothermal conversion (%)	Type of therapy	Cancer type and *in vitro* and *in vivo* models	Cargo	Remarks	Ref.
Chitosan-PEG-coated BP nanosheets	48 nm 23 mV —	PTT, chemotherapy, and immunotherapy	Colorectal cancer *In vitro*: HCT116, HT29, and MC-38 cells *In vivo*: MC-38 tumor model	DOX	–A synthesis route was proposed to continuously produce BP nanosheets from course BP flakes through ultrasonic bubble bursting –The nanoparticles were found to induce chemotherapeutic, PTT, and PDT effects and also the NIR-induced maturation of dendritic cells –The *in vivo* studies showed that the combined therapy was the only one that ablated the colorectal tumor model	262
Poly-L-histidine grafted BP nanosheets-coated with erythrocyte membrane	174 nm 6.08 mV —	PTT, chemotherapy, and immunotherapy	Colorectal cancer *In vitro*: A375 and H9C2 cells *In vivo*: A375 tumor model	Interleukin-1α siRNA and paclitaxel	–A core–shell nanosystem was designed in which poly-L-histidine-grafted BP formed the core and the erythrocyte membrane was the shell –The shell controlled the burst release of drug-loaded molecules and enhanced the tumor targetability and silencing potential of loaded siRNA	263
BPQDs-liposome coated macrophage	152.2 ± 0.989 nm −17.4 ± 0.424 mV —	PTT, PDT chemotherapy, and immunotherapy	Colorectal cancer *In vitro*: CT26, B16, and MCF-7 cells *In vivo*: CT26 tumor model	Abemaciclib	–An antitumor platform based on artificially assembled macrophages was prepared through a simple strategy –The nanosystem could accumulate in the tumor's site thanks to the macrophage coating –Upon NIR irradiation, the platform could activate a strong antitumor response through the promotion of dendritic cell maturation and T proliferation –The combination therapy led to a powerful antitumor effect *in vivo*	264
Gold-BP nanosheets	—	PTT and PDT	Lung cancer *In vitro*: HeLa, 293T, and A549 cells *In vivo*: Orthotopic human lung tumor xenograft	—	–Gold nanoparticles were deposited on the surface of BP nanosheets to come up with a PDT-PTT anticancer platform –The hybridization culminated in the higher production of singlet oxygen molecules and so stronger PDT plus hyperthermia –The combined therapy potential was tested *in vivo* against deep-seated lung tumors and complete tumor suppression was obtained	265
BPQDs	2–10 nm −16.26 ± 0.38 mV in PBS (pH 7.4) and −5.82 ± 1.34 mV in the cell culture medium (pH 7.4) —	—	Lung cancer *In vitro*: A549 and Beas-2B cells *In vivo*: —	—	–The cytotoxicity of BPQDs was assessed *in vitro* against two lung cell lines –A concentration-dependent cytotoxicity was obtained after 24 h –The reduction of cellular activity was attributed to induced oxidative stress by BPQDs	266
Cancer cytomembrane-BP	99.6 nm −22.5 eV —	PTT and chemotherapy	Lung cancer *In vitro*: LLC or NCI-H1299 cells *In vivo*: LLC tumor model	Gefitinib	–A platform was designed based on BP nanosheets to alleviate the side effects of gefitinib as a chemotherapeutic drug against non-small cell lung cancer –The drug molecules were loaded on the BP and then coated with cancer cytomembrane to improve the targetability –The delivery system facilitated the liberation of drug molecules and retention in the tumor's microenvironment –The combination of PTT and chemotherapy culminated in the suppression of cancer cells *in vitro* and the xenograft model *in vivo*	267

Table 6 (*continued*)

Nanovehicle	Particle size (nm) Zeta potential (mV) Photothermal conversion (%)	Type of therapy	Cancer type and *in vitro* and *in vivo* models	Cargo	Remarks	Ref.
BPQDs-loaded exosomes	100 nm −25 mV —	PTT	Bladder cancer *In vitro*: V-HUC1, T24, 5637, and BIU-87 cells *In vivo*: BIU-87 tumor model	—	–BPQDs were encapsulated into exosomes through electroporation method –The exosomes protected BPQDs from degradation in the physiological medium and enhanced the photothermal conversion –The *in vivo* studies performed on bladder tumor-bearing mice revealed a high accumulation of nanoparticles inside of tumor mass and induced strong anticancer activity upon NIR	268
Manganese oxide-BPQDs	300 nm — 36.30%	PTT, PDT, and chemotherapy	Liver cancer *In vitro*: LO2 and HepG2 cells *In vivo*: HepG2 tumor model	DOX	–A hollow mesoporous structure was synthesized from manganese oxide to load DOX and BPQDs against liver cancer –About 80% reduction of cancer cell viability was obtained when NIR with two wavelengths had been applied after 48 h *in vitro* –After 15 days of *in vivo* tumor therapy, the sample loaded with DOX in the presence of NIR was the only one that eradicated the tumor mass completely	269
BP nanosheets	160 nm — —	Chemotherapy	Ovarian cancer *In vitro*: A2780 cells *In vivo*: —	Cisplatin and oxaliplatin	–BP nanosheets were used as a drug delivery system against ovarian cancer –*In vitro* study showed that bare BP at the highest concentration (30 μg mL^{-1}) only induced about a 30% reduction of cell viability –The drug-loaded samples induced cytotoxicity from the lowest concentration (2.5 μg mL^{-1}) due to the released drug molecules	270
Polymer-coated BPQDs	58 nm −28.31 ± 1.38 mV —	Gene therapy	Ovarian cancer *In vitro*: PA-1 cells *In vivo*: —	siRNA	–BPQDs were surface modified with a polymer followed by being coated with siRNA against human ovarian cancer –The expression of lysine-specific demethylase 1 mRNA was suppressed by the gene-loaded carrier –Upon NIR irradiation, the combination of gene therapy and phototherapy culminated in the cancer cell growth inhibition by about 80%	271
PEGylated-BP nanosheets	100 nm −10.3 mV —	PTT and chemotherapy	Cervical cancer *In vitro*: HeLa cells *In vivo*: HeLa tumor model	DOX	–BP nanosheets were surface-modified with amine-functionalized PEG and then DOX, folic acid, and cyanine 7 –The modified BP nanosheets potential with and without NIR was tested against HeLa cells *in vitro* and the combination chemotherapy and PTT had the strongest anticancer effect –*In vivo* study on the HeLa-tumor-bearing mice revealed that the nanoparticles could ablate the tumor at the end of the study	106
Surface-modified BP	115 nm ∼−20 mV —	PDT	Cervical cancer *In vitro*: HeLa cells *In vivo*: HeLa tumor model	DNA duplex	–BP nanosheets were modified in order to address the hypoxia region of the tumor mass and improve the PDT potency –The Fe-protoporphyrin IX in the composition turned out to turn H_2O_2 to oxygen molecules and about 8-fold increased the PDT efficacy *in vivo*	272

Table 6 (*continued*)

Nanovehicle	Particle size (nm) Zeta potential (mV) Photothermal conversion (%)	Type of therapy	Cancer type and *in vitro* and *in vivo* models	Cargo	Remarks	Ref.
BP-encapsulated thermosensitive hydrogel	BP: 288.3 ± 122.4 nm	PTT	Cervical cancer	—	–A multifunctional thermosensitive hydrogel containing BP nanosheets was fabricated for post-operative cancer therapy	273
	—		*In vitro*: hMSCs, L929, MCF-7, and HeLa cells		–Upon NIR irradiation, the BP inside increased the temperature and turned the sol into a gel	
	—		*In vivo*: HeLa tumor model		–The PTT was able to eradicate the remained cancerous cells left behind after tumor excision *in vivo*	
BP nanosheets	150 nm	Selective anti-cancer activity	Cervical cancer	—	–This study did not involve PTT, PDT, drug delivery, and multimodal imaging abilities of BP nanosheets to understand the intrinsic anticancer potential of this material	15
	—		*In vitro*: HeLa, D551, A549, and Hek293 cells		–The *in vitro* and *in vivo* studies revealed that BP nanosheets reduced the cancer cells' activity while leaving no negative effects on the healthy cells	
	—		*In vivo*: HeLa and A549 tumor models		–The proposed mechanism of action was related to the increase in the phosphate anions due to the degradation of BP leading to the generation of cytotoxic ROS	
Charge reversal surface-modified BP	200–350 nm	PTT	Oral cancer	—	–A pH-responsive charge reversal platform composed of BP nanosheets was developed to oral cancer therapy	274
	pH 7.4 = –14.32 ± 1.35 mV		*In vitro*: CAL-27 and SAS cells		–A surface modification on the BP was made and improved the stability and biocompatibility also in the exposure of the tumor microenvironment, the surface charge turned positive followed by better cell internalization	
	pH 6.5 = 16.35 ± 1.96 mV pH 5.5 = 23.70 ± 1.76 mV		*In vivo*: CAL-27 tumor model		–The *in vitro* and *in vivo* studies exhibited that NIR irradiation triggered the nanoparticles to decrease the cancer cells' viability and increase the tumors' temperature to nearly 60 °C, respectively	
	—					
BP-gold nanoparticles	—	PTT and chemotherapy	Oral cancer	Cisplatin	–BP-gold nanoparticles composite was prepared and then loaded with cisplatin for oral cancer therapy	275
			In vitro: SCC-9 cells		–The *in vitro* study against SCC-9 cells showed that BP and gold nanoparticles at low concentrations had a significantly stronger anticancer effect than pure cisplatin	
			In vivo: 0.5% DMBA in acetone used to establish tumor tissues on the left cheek of golden hamsters		–*In vivo* process revealed that as the weight ratio of BP to gold increased in the composite's composition, the tumor inhibition growth got stronger due to the PTT	

MC-38 tumor-bearing mice for 28 days and 8 h after the intravenous injection and NIR laser (808 nm, 1.5 W cm^{-2}) was irradiated for 5 min. Similar to the *in vitro* studies, the combined therapy completely inhibited the growth rate and ablated the tumors. Histological analyses revealed that the tumor masses treated with these samples had the accumulation of $CD4^+$ and $CD8^+$ T cells and also the expression levels of Ki-67 or CD31, attributed to tumor cell proliferation and angiogenesis, were decreased significantly proving the potential of applied combined therapy.[262]

A chemo-photo-immunotherapeutic platform was constructed against colorectal cancer, which was composed of BP nanosheets, poly-L-histidine, interleukin-1α silencing small interfering RNA, and paclitaxel drug molecules as the core and ephrin-A2 receptor-specific peptide grafted erythrocyte membrane as the outer shell. The shell could effectively prevent the undesirable release of loaded chemotherapeutic drug molecules, and also the grafted peptide improved tumor targetability and endosomal escape. The nanosystem was found to trigger the antitumor immune response (activation of $CD8^+$ T cells, IFN-γ, and TNF-α) through abrogation of interleukin expression followed by limiting Treg cell accumulation in the tumor site.[263] Somewhere else and based on the macrophage concept, a nanosystem was designed which was supposed to imitate the tumor-targeting capability of macrophages. The system was prepared through the fusion of a liposome containing an anticancer drug and BPQDs and macrophage membrane. The nanosystem was found to reverse the immunosuppressive tumor microenvironment and activate the antitumor immune response. The *in vivo* studies on the colorectal tumor model exhibited that the combination of chemotherapy, PTT, and immunotherapy could successfully yield the highest tumor inhibition growth rate (~95%) among the samples.[264] To relieve hypoxia in solid tumors and increase the efficacy of therapy, a study reported on the development of an oxygen-independent platform for hypoxic tumors. BPQDs were conjugated to *E. coli* bacteria through an easy electrostatic adsorption technique (Scheme 16). Two therapeutic techniques were adopted for colon cancer: PTT and X-ray-mediated radiosensitization. The antitumor potential of this platform was assessed *in vitro* and *in vivo*. CT26 colon tumor-bearing mice were treated with different samples and also PTT, radiotherapy, and the combination were separately applied to understand the effect. In the case of mice exposed to the combination therapy, 24 h after the intravenous injection, the tumor was irradiated with NIR (0.5 W cm^{-2}, 5 min) followed by applying a low dose of radiotherapy (2 Gy) half an hour after the NIR. In this model system, it was revealed that neither PTT nor radiotherapy alone did not yield potent antitumor suppression. The most efficacious tumor suppression belonged to the combination of nanoparticles + PTT + radiotherapy.[277]

Lung cancer is the most common type of cancer among both genders in developed countries accounting for 18.4% of all cancer deaths.[278] To reinforce the PDT potential of gold nanoparticles, they have been hybridized with BP nanosheets for PDT-PTT combined therapy against lung cancer. Through inoculating A549 cells to the lungs of nude mice, orthotopic human lung tumor xenografts were developed *in vivo*. At 5 h after the injection of nanomaterials (100 μL per mouse, 200 μg mL^{-1}), the lung tumors were irradiated with NIR (808 nm, 2 W cm^{-1}) for 30 min and the therapeutic outcomes of gold nanoparticles, BP nanosheets, and the combination of both were assessed and compared. The tumors treated with PBS experienced a rapid increase in their size while each component alone could show an inhibition against the growth rate and the gold nanoparticles showed a bit stronger effect than that of BP nanosheets. However, none of them alone could completely block the tumors' growth rate. The combination of BP-gold completely suppressed the growth rate thanks to the synergistic effects of PDT and PTT. Notably, the metastasized tumors to the legs did not receive NIR irradiation and they grew and became large. Moreover, the efficiency of combined therapy was proved through histological analyses and the lungs treated with gold-BP + NIR had well-organized tissue with single-cell-layer alveoli.[265] The cytotoxicity of BPQDs at different concentrations (0, 5, 10, and 20 μg mL^{-1}) was tested *in vitro* for up to 24 h against two lung cell lines—human lung carcinoma epithelial and bronchial epithelial cells. Concentration-dependent cytotoxicity was obtained, and the results indicated that the quantum dots were internalized through phagocytosis; it is notable that the phagocytosis inhibitor could alleviate the reduction of cell viability and also the damage to the cell membrane caused by BPQDs. The main reason why such a decrease in the cell viability was induced is the oxidative stress through BPQDs.[266]

A recent study has reported the crosslinking of BP nanosheets with cytomembrane and gefitinib for lung cancer therapy. Due to intermolecular interaction between the components, the three parts were conjugated to each other successfully. Upon NIR exposure, the nanoparticles exhibited superior anticancer activity *in vitro* and *in vivo*. A nude mouse lung cancer tumor model was established and different samples including free gefitinib, PBS, and the nanoparticles with and without NIR irradiation were inoculated to compare if there was any difference. The injection of free chemotherapeutic drug caused weight loss in the treated mice while this effect was relieved in the groups of drug-loaded BP nanoparticles. The combination of PTT and chemotherapy was able to inhibit the tumor growth better than that of other samples, but still this sample failed to completely suppress the growth and even the tumors treated with drug-loaded BP + NIR reached a volume of approximately 600 mm^3 at the end of the study.[267]

Cervical cancer is considered the fourth most common gynecological tumor in women targeting its victims mostly aged less than 58 years old. Although cervical cancer has been recently observed to decrease, it is still a threat to young women around the world.[279] A study has developed a multifunctional BP-based nanosystem against cervical cancer. The BP nanosheets were first surface-modified with amine-functionalized PEG to improve biocompatibility and stability. Next, other molecular species including DOX, cyanine-7, and folic acid were conjugated to the surface to endow the platform with chemotherapeutic ability, NIR imaging, and targetability, respectively. HeLa

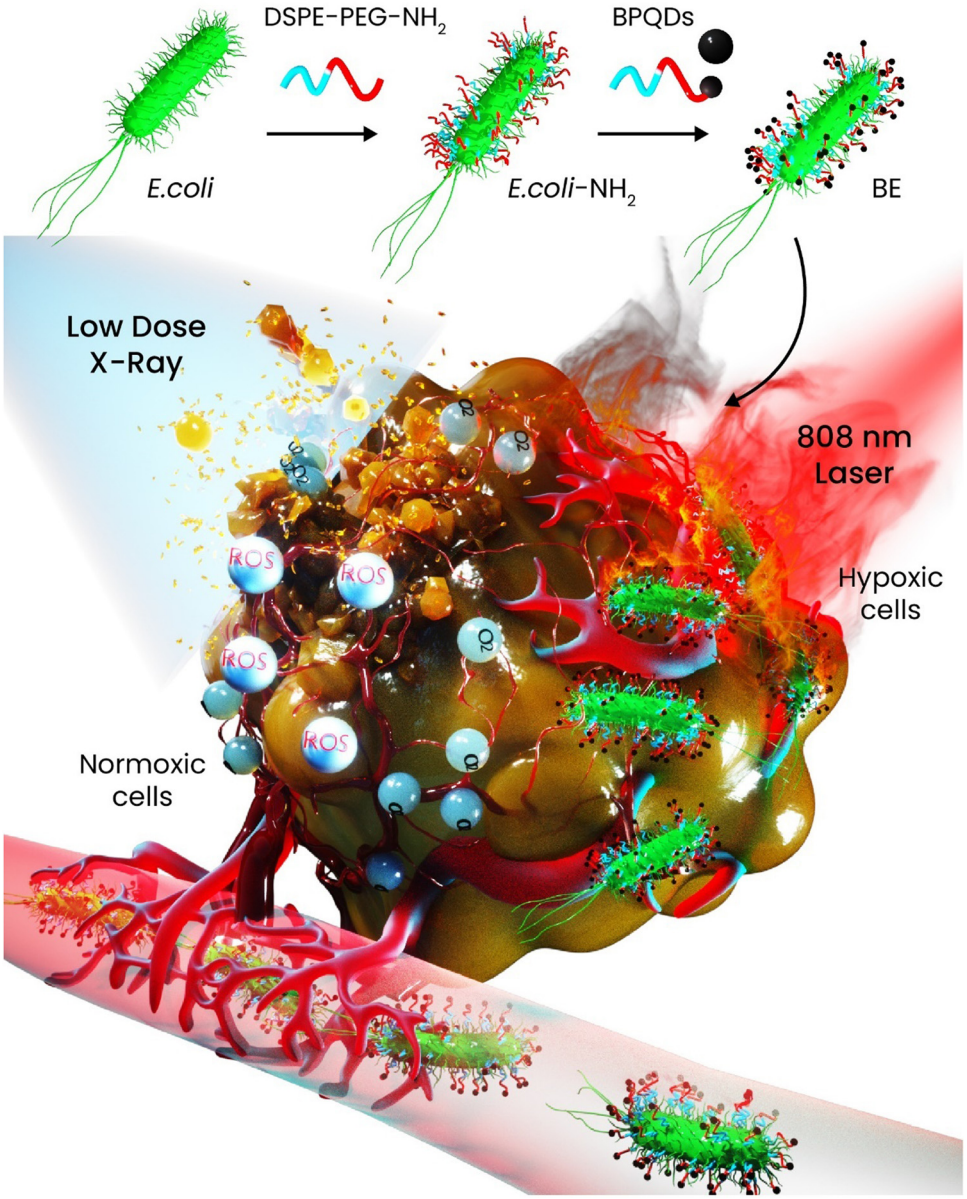

Scheme 16 BPQD-conjugated bacteria as an anticancer agent against colon cancer: Schematic of the conjugation of BPQDs onto *E. coli* and the platform exhibiting dual-responsivity potential to suppress the tumor growth.

cells were incubated and exposed with the samples at concentrations ranging from 5 to 25 μg mL^{-1}. The PEGylated BP nanosheets did not show any cytotoxic effect while applying NIR resulted in about a 40% decrease in the cell viability. Addition of DOX to this system has reinforced the cytotoxic effect significantly due to the combination of chemotherapy and PTT, but the highest decrease was caused by this nanosystem plus folic acid, which increased the targetability and so even at a concentration of 10 μg mL^{-1} the viability dropped to nearly zero. This sample also performed an excellent antitumor effect against the HeLa-tumor models up to 2 weeks and the accumulation was competitively higher than that of other samples thanks to folic acid.[106] To attenuate the hypoxia region of HeLa tumors and improve the efficacy of PDT, BP nanosheets were functionalized with folate and a blocker DNA complex containing a Fe-protoporphyrin IX dimer against cervical cancer. The dimer was found to passivate its peroxidase activity and the passivated nanosystem then activated the catalytic function turning H_2O_2 to oxygen molecules; this reaction led to reinforcing the PDT efficacy by about 8.7- and 7.5-fold in both the cancer cells *in vitro* and the tumors *in vivo*.[272]

A new sprayable hydrogel containing BP nanosheets was designed and fabricated for post-operative cancer therapy. The organic part of hydrogel was composed of poly(D,L-lactide)–poly(ethylene glycol)–poly(D,L-lactide) and upon NIR irradiation and increase of temperature due to light responsivity of encapsulated BP nanosheets, the sol–gel transition took place and turned into a gel (Fig. 6(A)). HeLa cells were subcutaneously

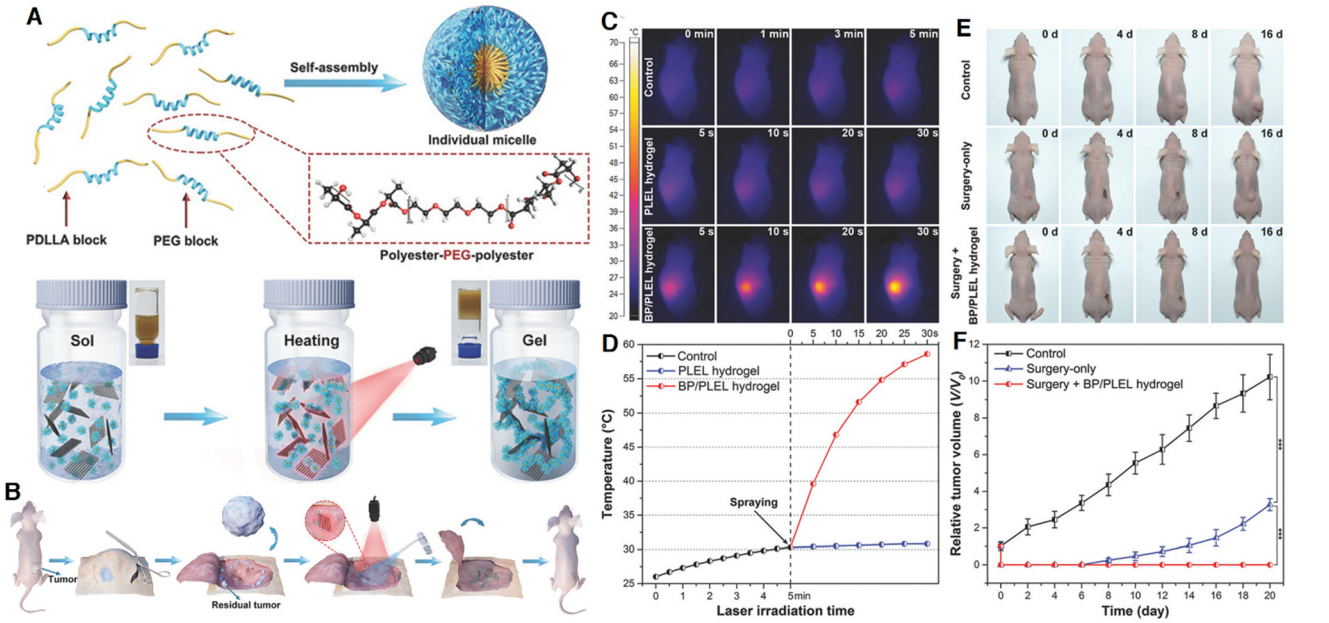

Fig. 6 Sprayable multifunctional hydrogels for post-operative cancer therapy. (A) Schematic of hydrogel preparation and its responsiveness to heat to become a gel. (B) Scheme of tumor surgery followed by spraying the hydrogel and applying NIR. (C) and (D) Thermal images and time-dependent temperature change of tumors treated with different samples *in vivo*. (E) and (F) Digital photographs were taken from the HeLa-tumor-bearing mice and the relative tumor volume of treated mice with different samples. Abbreviation: Poly(D,L-lactide): PDLLA, poly(D,L-lactide)-poly(ethylene glycol)-poly(D,L-lactide): PLEL. Reprinted from ref. 273 with permission from Wiley.

injected into the right rear flank of each mouse to establish the tumor model and assess the potential of sprayable hydrogel *in vivo*. Once the tumors reached approximately the size of 100 mm^3, the mice were divided into three groups—control, surgery only, and surgery followed by spraying the multifunctional hydrogel. Since the surgery of tumor mass would leave some cancer cells inside of the defect, they would increase the potential of tumor recurrence. The *in vivo* studies revealed that the tumors in the group of surgery came back after a few days and experienced constant growth, whereas the group treated with the hydrogel saw complete tumor growth suppression due to the ablation of remaining cancerous tissues through PTT (Fig. 6(B–F)).[273] In 2020, a study reported on the intrinsic anticancer activities of BP nanosheets and omitted the effects of PTT, PDT, drug delivery, and multimodal imaging. The selective anticancer activity of BP nanosheets was tested against HeLa and D551 cells *in vitro* for up to 48 h. The number of cancer cells was decreased when the concentration of PEGylated BP nanosheets had been increased, but the viability of normal cells was left intact at the same concentrations. Moreover, the same effect was tested for A549 cancer cells and Hek293 healthy cells, and the same results were obtained *in vitro*. This selective anticancer activity was attributed to the increase in the phosphate anion levels due to the degradation of BP nanosheets; these anions led to an increase in the lipid peroxidation followed by a decrease in the superoxide dismutase and this phenomenon resulted in the cytotoxic ROS generation. It is critical to bear in mind that the higher metabolism rate of cancer cells accelerates the degradation rate of BP and that is why BP turns down the cell viability of cancer cells, while it does not affect the healthy ones. The anticancer potential was tested *in vivo* against two tumor models, namely, HeLa and A549 xenograft tumor models. The nanoparticles accumulated in the tumors more than other organs followed by livers and kidneys. *In vivo*, immunofluorescence staining and FCM assay both confirmed that significant ROS generation in the tumor masses occurs by BP nanosheets. In contrast, the control treated with PBS did not experience the same effect. DNA damage and apoptosis were assessed through the FACS co-staining assay. ROS generation caused the high expression of caspase-3 and decreased the expression of a proliferation marker (Ki-67), both of which are the signs of increased apoptosis and tumors' growth inhibition.[15]

Oral cancer is a common disease in the neck and head and the number of patients diagnosed with this type of cancer has increased recently. The clinical treatment is based on surgery, but a complete tumor resection is required to prevent the tumors from spreading and this procedure may lead to the removal of the entire tongue and gum leaving a very serious impact on the patient's life.[280,281] A charge reversal system composed of BP nanosheets, polydopamine, and polyacrylamide hydrochloride-dimethylmaleic acid was synthesized for oral cancer therapy. The nanoparticles were negatively charged in blood circulation and underwent charge reversal towards positive once they reached the acidic regions of tumor tissues culminating in the enhanced uptake into the cancer cells (Scheme 17). *In vitro* studies against two squamous cell carcinoma lines (CAL-27 and SAS) at different concentrations (6.25–100 μg mL^{-1}) showed that the BP nanomaterials without being triggered with NIR did not affect the cell viability after 24 h,

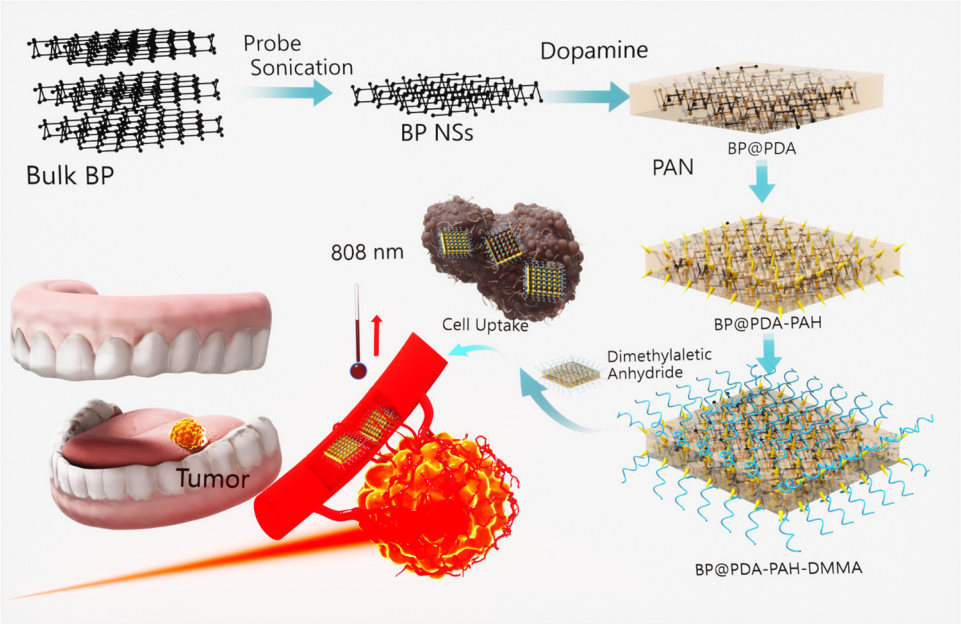

Scheme 17 Anticancer potential of BP nanosheets against oral squamous cell carcinoma. (A) Schematic of BP nanosheet preparation and surface modification with different polymers to turn it into a charge reversal platform. Abbreviation: poly(dopamine): PDA, polyacrylamide hydrochloride: PAH, dimethylmaleic acid: DMMA.

whereas applying laser irradiation in a concentration-dependent manner decreased the cell viability of both lines down to 20%. The nanomaterials were injected into CAL-27 tumor-bearing mice at a concentration of 0.54 mg kg^{-1} in 100 μL PBS and after 24 h, the tumors were exposed to NIR (808 nm, 1.5 W cm^{-2}) for 5 min. Notably, two different surface-modified nanoparticles were intravenously injected including a charge reversal system and the one without this modification and the former was found to accumulate more than the latter in the tumor mass showing the effectiveness of this surface modification on the internalization rate. The temperature of tumor mass was measured after NIR and the laser increased the local temperature up to 54.9 °C, which is high enough for tumor ablation, without affecting the other organs' temperature.[274]

To enhance the survival rate (5 years) of patients diagnosed with oral squamous cell carcinoma, a composite from BP nanosheets and gold nanoparticles was synthesized. *In vitro* and *in vivo* studies were performed on the human SCC-9 cells and golden hamster cheek cancer models, respectively. BP nanosheets (50 μg mL^{-1}), gold nanoparticles (50 μg mL^{-1}), and cisplatin (2 mg mL^{-1}) were exposed to SCC-9 cells and it was found that the nanomaterials even at this low concentration showed significantly stronger anticancer effects than that of pure cisplatin. The anticancer efficacy of BP nanosheets was better than that of gold nanoparticles, which was attributed to the easy internalization of nanosheets into the cancer cells followed by rapid degradation causing G2/M phase arrest. The *in vivo* tumor model was established by rubbing 7,12-dimethylbenz[*a*]-anthracene (0.5% in acetone) into hamsters' left cheeks and various samples including the drug-loaded composites with different BP-to-gold weight ratios were injected intratumorally followed by applying NIR (808 nm) for 5 min. The tumor inhibitory effect and even ablation got stronger when the ratio of BP to gold had been increased and the strongest effect belonged to the gold (1)-BP (5) loaded with cisplatin. The weight changes during the treatment were tracked and except for about 10% mass loss between the hamsters which may have been attributed to the individual differences, no other differences related to the samples were noticed.[275]

Other types of cancers including bladder, ovarian, and liver have received less attention from BP-assisted therapy, and in this part, these studies are discussed. BPQDs were packaged into exosomes *via* the electroporation method for PTT against bladder cancer. This encapsulation did not allow fast degradation of BPQDs and improved their photothermal activity. Moreover, the exosomes had prolonged blood circulation time and accumulated in the tumor tissue attributed to the good homing effect of the exosome membrane. The exosomes with different concentrations of BPQDs inside (0–300 μg mL^{-1}) were exposed to various cell lines to assess the cell viability. Even the highest concentration did not affect any of the cells negatively and the cells' survival rate stayed above 90%, whereas applying NIR with different power densities was synchronized with a significant decrease in the BIU-87 cells' viability. The BPQDs-loaded exosomes were intravenously injected through the vein of BIU-87-tumor-bearing mice. The nanoparticles + NIR had almost complete tumor suppression followed by bare BPQDs + NIR.[268] Hollow mesoporous manganese oxide was coated with two polymers (anionic and cationic), reacted with PEGylated-amine-functionalized BPQDs and finally loaded with DOX against liver cancer. Choosing manganese oxide was beneficial for three

reasons as follows: (i) the hollow mesoporous structure allowed high drug loading capacity and taking control over the drug release kinetic; (ii) manganese oxide offered contrast for magnetic resonance imaging; and (iii) this ceramic has potential to convert endogenous H_2O_2 to O_2 alleviating the hypoxia region of tumors and reinforcing the PDT potency. *In vitro* cell viability of nanoparticles (0–200 μg mL^{-1}) was performed against LO2 and HepG2 cells for 48 h. In the absence of NIR irradiation, there was no decrease in the LO2 viability even at the highest concentration while little cytotoxicity was observed for cancer cells, which was attributed to the release of loaded DOX in the presence of acidic medium of cancer cells. The same study was also performed with and without NIR (630, 808 nm, and a combination of both). It turned out that the anticancer effect of PTT obtained from 808 nm irradiation was stronger than that of PDT (630 nm), but the strongest effect (~80% reduction of viability) was obtained when the combination of both had been applied. *In vivo* chemo-phototherapy was applied on HepG2-tumor-bearing mice. An immunofluorescence assay using pimonidazole as a hypoxyprobe was adopted to understand if manganese oxide was able to alleviate the hypoxia region and it was revealed that due to the generation of oxygen molecules by the carrier, the hypoxia was decreased in the tumor mass. After 15 days of treatment *in vivo*, the DOX-loaded nanoparticles, which had been exposed to NIR with two wavelengths, could ablate the tumor completely, whereas the other samples with a single therapeutic strategy (PTT or PDT or chemotherapy) were able to decrease the growth rate.[269]

Ferritin is recognized as a well-known marker of liver cancer and early detection of it would improve curability chances in patients diagnosed with this type of cancer. Based on surface-enhanced Raman scattering technology, an immunoassay platform composed of magnetite, MoS_2, and BP nanosheets was developed. The deposition of MoS_2 onto BP nanosheets led to the formation of a matched interleaved energy band structure by which the surface of MoS_2 was enriched with photogenerated electrons; this phenomenon resulted in transferring of more Raman molecules and so detecting ferritin antigen with a concentration of 7.3×10^{-5}. The formation of magnetite nanoparticles on the surface through a secondary hydrothermal treatment made the platform magnetic-responsive and so separation and collection of the nanocomposite from the immune solution after photocatalytic activity were possible (Fig. 7). One batch was recommended for 7 times detection of ferritin.

BP nanosheets were turned into a targeted drug delivery system through the loading of two drugs with platinum agents—cisplatin and oxaliplatin—against ovarian cancer. The cytotoxicity of drug-bounded BP nanosheets was assessed against A2780 cells for 24 h. The applied concentrations were 2.5, 5, 7.5, 10, 12.5, 15, and 30 μg mL^{-1}, and up to the concentration of 12.5 μg mL^{-1}, BP alone induced little cytotoxicity and increasing the concentration led to a decrease down to 70%. Compared to bare BP, cell growth suppression occurred for the drug-loaded samples from the lowest concentration and the effect got stronger as the concentration went higher and the cell viability reached down to 40% (30 μg mL^{-1}).[270] BPQDs were functionalized with polyelectrolyte polymers to deliver genes into human ovarian cancer cells. PA-1 cells were chosen for this study due to their pluripotency as stem cells making them cancer stem cells. The BPQDs as the gene carrier exhibited a high

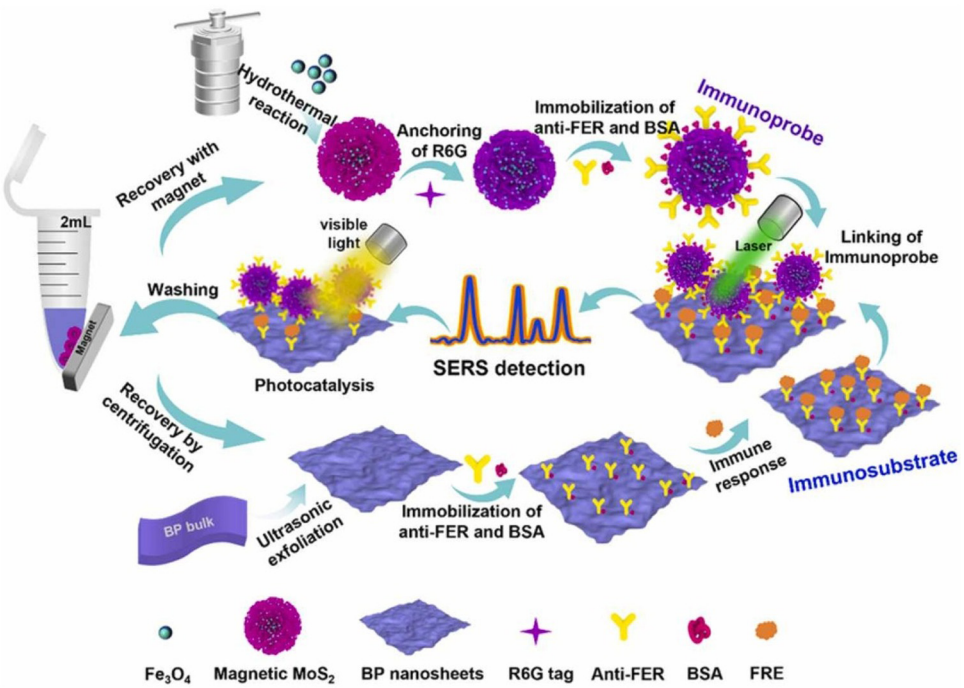

Fig. 7 Preparation of the mechanism of action of surface-enhanced Raman scattering-based platform for the detection of ferritin against liver cancer. Abbreviation: Bovine serum albumin: BSA, ferritin: FER, Rhodamine 6G: R6G. Reprinted from ref. 282 with permission from Elsevier.

rate of internalization into the cells and about 80% inhibition rate of proliferation was obtained under laser irradiation.[271]

11. Black phosphorus and protein interactions: protein corona

One of the most vital features of therapeutic agents is their circulation in the bloodstream long enough to reach target tissues. It is already known that nanoparticles can selectively diffuse throughout tumors with leaky vasculature through enhanced permeation and retention phenomenon. Moreover, surface functionalization of these nanoparticles with various antibodies, proteins, and peptides improves the targetability due to the overexpression of receptors in the tumor site, facilitating the binding of nanoparticles and uptake.[186] One of the challenges revolving around therapeutic agents is the binding of proteins on the nanoparticles, which is known as protein corona once they entered into the bloodstream. The attachment of these proteins on the surface is synchronized with the formation of a new identity for the nanoparticles distinct from the one they had been designed for (Scheme 18). Therefore, protein corona is recognized as a link between *in vitro* and *in vivo* studies and its effect on the fate of nanoparticles must be taken into account for developing successful therapeutic agents.[283]

Upon entrance of a nanoparticle into the bloodstream, it goes through interacting with various moieties of biological fluid, serum proteins specifically. These proteins bind to the surface of nanoparticles and form a soft corona, which is gradually being replaced with other proteins and leads to a hard corona. There are some methods applied to measure the protein corona *in vitro* and *in vivo*.[284] The *in vitro* studies were based on incubation of the nanoparticles in physiological media encompassing serum or plasma for a specific period of time followed by elution and digestion of those proteins and

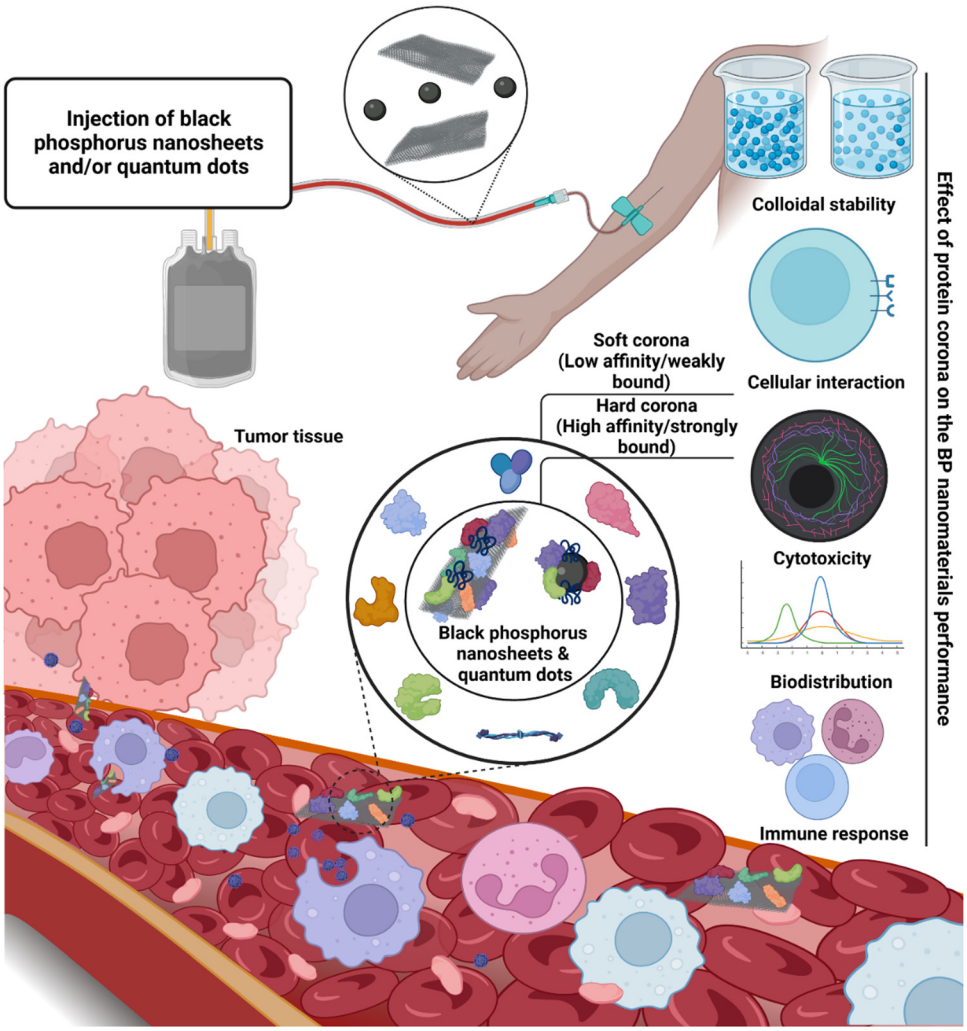

Scheme 18 Protein corona formation on BP nanosheets and BPQDs. The injection of bare BP nanomaterials in the bloodstream would be synchronized with the formation of protein corona followed by changes in their performance and fate as some of them would be caught by the immune system and some would reach tumor's tissue through enhanced permeation and retention effect. Created with BioRender.com.

analyzing through gel electrophoresis. Since this process is accompanied by centrifugation and rinsing of the nanoparticles prior to elution, it can measure the hard corona while inclusion of additional analytical tools including zeta potential analysis, microscopy, and spectroscopy can give valuable information about soft corona *in vitro*.[285] However, some studies have injected different nanoparticles intravenously *in vivo* and retrieved the nanoparticles through size exclusion chromatography and magnetic separation from blood for analysis.[286]

Similar to other nanoparticles, BP nanomaterials undergo coronation once soaked into body fluids, especially plasma proteins. A primary study published in 2018 investigated the protein corona formation on the BP nanosheets and BPQDs. Since the isoelectric point of most corona proteins is less than 7.4, these negatively charged proteins were mainly absorbed on both nanosheets and quantum dots, indicating that besides electrostatic interactions, other driving forces such as electron-transfer forces and van der Waals forces play important roles in the interaction between BP nanomaterials and these proteins. Characterization of the formation of protein corona over nanosheets and quantum dots showed that abundant plasma proteins were attached to nanosheets, whereas the BPQDs had more tendency to absorb low molecular plasma proteins. The size of BP nanomaterials was found decisive on the identity and quantity of protein corona formation; shape of ultra-small 2D nanosheets was observed to change while large 2D nanosheets have not undergone such a change. About 70% of proteins formed on the BP nanomaterials were immune proteins and other opsonins leading to an increase in the uptake of these nanomaterials by macrophages and also the cellular uptake pattern altered from the bare nanomaterials. Nonetheless, to assess if macrophage-like cells could affect the secretion of cytokines, the BP-corona complex was exposed to the cells. The amount of inflammatory cytokines was assessed after treatment and turned out to significantly increase the cytokines including IL-1β, IL-6, IL-8, and IFN-γ, exhibiting the proinflammatory effect induced by BP-protein corona complex (Scheme 19). However, the bare BP nanomaterials did not show any significant effect on the secretion of cytokines.[287] Another study has provided more details about the effect of BP-corona complex on macrophage polarization and immune modulation. Mechanistically, the BP-corona complex interacted with calmodulin and activated stromal interaction molecule 2, which facilitated the influx of calcium ions in macrophages; uptake of calcium ions was found to activate p38 and NF-κB followed by macrophage's polarization from M0 to M1 phenotype. This study then proved that the BP-corona complex effect on the macrophages made them migrate towards cancer cells significantly greater than that of the control and also the cellular cytotoxicity and phagocytosis of cancer cells by the macrophages were obtained nearly 2 times higher than that of the control.[288]

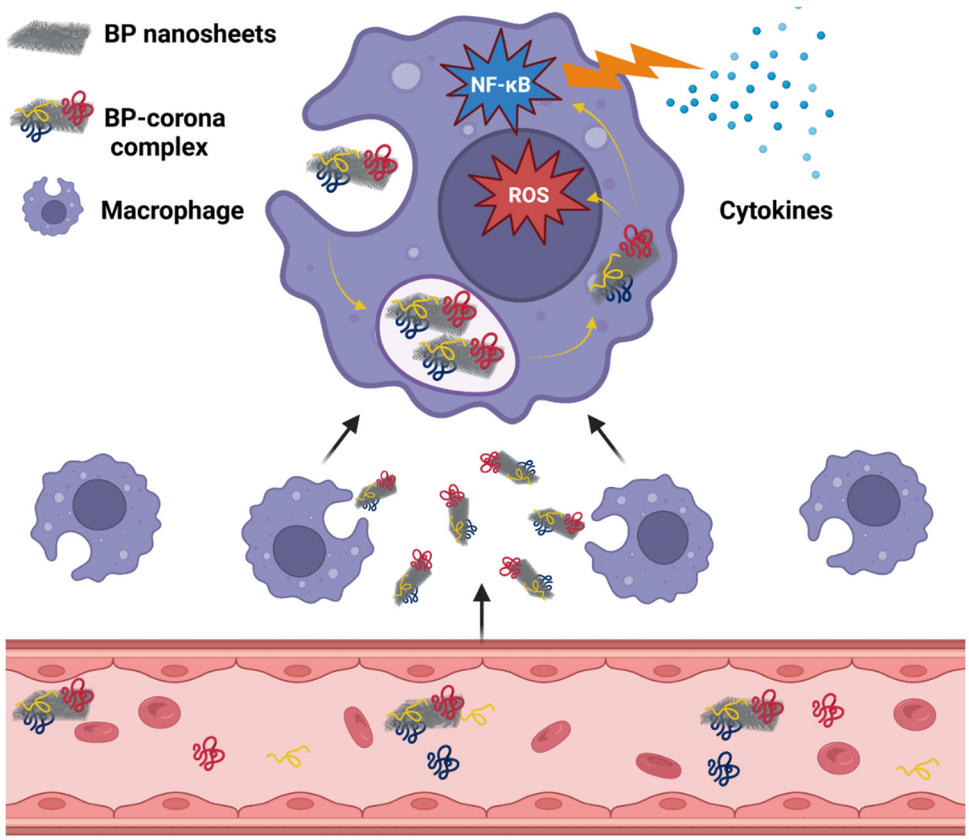

Scheme 19 Formation of protein corona on BP nanosheets in the bloodstream followed by induction of immunoregulation effect on macrophages. Created with BioRender.com.

A recent study has performed deep research on the interaction of BPQDs with bovine serum albumin and interpreted that BPQDs quenched the endogenous fluorescence of bovine serum albumin through van der Waals and hydrogen bond interactions. A stable ground-state construct was obtained when a strong interaction between Sudlow's site I of bovine serum albumin and BPQDs had been formed. Moreover, BPQDs in a concentration manner could decrease the thermal stability and α-helix structure content of the albumin.[289]

12. Biosafety of BP nanomaterials

Since the introduction of BP nanomaterials in biomedicine, various studies have been performed *in vitro* and *in vivo* to evaluate the biosafety and biocompatibility of BP. The general idea about the safety of BP was based on the fact that its biocompatibility was related to its intrinsic chemistry: it degrades to phosphates that are already considered non-toxic. Early studies on both nanosheets and quantum dots showed that none of these materials showed toxicity towards different mammalian cells even at concentrations as high as 1 mg mL^{-1}. However, there are some reports on the potential cytotoxic effects of BP as well. It is critical to bear in mind that different factors affect the biocompatibility of BP—size, thickness, surface modification, combination with other compounds, *etc.* As mentioned in previous sections, BP inherently induces selective anticancer activity in a concentration-dependent manner because it has shown a faster degradation rate in the exposure of these cancer cell types, but some papers took advantage of the light-responsivity of BP only or loaded an anticancer drug, or combined different therapeutic approaches in one package without considering the inherent anticancer activity of BP. In these papers, bare BP was put in the exposure of cancer cells for only 24 h and observed no decrease in the cell viability, whereas others have prolonged the assay up to 48 and 72 h and reported on cell growth prevention. These inconsistencies have thrown doubts on the biosafety of BP nanomaterials. In this section, different studies and points of view regarding the biocompatibility and biosafety of BP nanomaterials *in vitro* and *in vivo* will be discussed (Scheme 20).

A systemic cytotoxicity study on BP nanosheets was conducted against three healthy cell lines (HCoEpiC, NIH-3T3, and 293T) up to 48 h to check if the concentration and size of 2D nanosheets and type of cell can affect the viability. Three batches of BP nanosheets with different sizes and thicknesses were prepared as follows: BP-1 (thickness: 92 ± 32 nm, size: 566.5 ± 74.7 nm, zeta potential: −30.70 ± 0.53 mV), BP-2

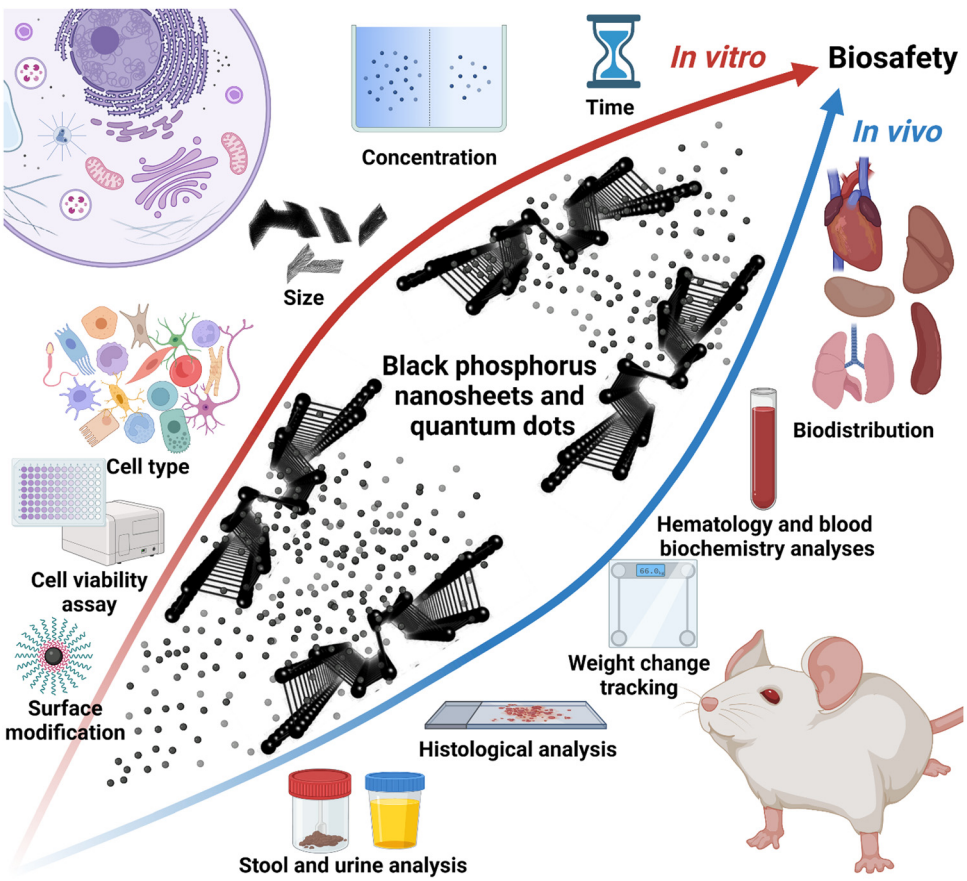

Scheme 20 Schematic of the decisive factors and analyses related to the assessment of biosafety of BP nanomaterials *in vitro* and *in vivo*. Created with BioRender.com.

(thickness: 27.0 ± 12.0 nm, size: 448.3 ± 18.6 nm, zeta potential: −26.57 ± 0.35 mV), and BP-3 (thickness: 17.4 ± 9.1 nm, size: 175.4 ± 0.5 nm, zeta potential: −26.57 ± 0.35 mV). It is worth mentioning that the hydrodynamic size of BP nanosheets after soaking into FBS significantly increased to 1124.0 ± 107.9, 722.3 ± 67.7, and 273.3 ± 5.3 nm for BP-1 to 3, respectively, due to protein adsorption on the surface of nanosheets, which led to their agglomeration. *In vitro* cytotoxicity assays performed for each material against the healthy cell lines indicated that BP-1 with the largest particle size and thickness could induce cytotoxicity at lower concentrations, while BP-3 showed moderate toxicity and even at the highest concentration of 200 μg mL^{-1}, the IC50 could not be measured toward HCoEpiC cells because of high cell compatibility. An interesting point to mention was about BP-2 and 3, which even induced cell proliferation at a low concentration of 1 μg mL^{-1}.[290]

In the case of cancer cells, inconsistent results are more highlighted like decrease in the cell viability of HeLa cells after 24 h down to nearly 36% when BPQDs with a concentration of 200 μg mL^{-1} had been applied,[74] whereas the same material with nearly 5 times higher concentration did not induce toxicity after 12 h towards the same cell line.[271] Somewhere else the BPQD viability was tested against Raw264.7 and turned out with no cytotoxicity, whereas the ATP level in J774A.1 treated with BPQDs was significantly decreased.[290] These differences might have resulted from different processes taken to synthesize the BP nanomaterials and also the incubation time which has been adopted only up to 12 or 24 h. Our group has assessed the cell viability of SAOS-2 and preosteoblast cells when exposed to different concentrations (10–500 μg mL^{-1}) of BP nanosheets up to 21 days and showed the stimulatory progressive effect on the osteoblast cells while causing the osteosarcoma cells to undergo apoptosis due to generation of excessive ROS. It is worth mentioning that during the initial incubation time, the results were not clear enough and after 72 h, the selective anticancer activity of BP nanosheets could be clearly deduced.[252]

Another factor which has potential to introduce discrepancy in the obtained results is the approach by which the cell viability is assessed. For instance, PEGylated few-layered BP exhibited a biocompatible nature measured by an MTT assay towards different cell lines—HeLa, HepG2, A375, PC3, and MCF7—up to a concentration of 100 μg mL^{-1}, while the same material showed selective anticancer activity towards HeLa cells when the Alamar Blue assay had been applied.[15] Previous studies have revealed that BP nanosheets can induce interference in the results obtained by MTT through adsorption or reduction of the assay reagent[291,292] and so a study has introduced an assay that does not need colorimetric or fluorescence reagents and showed that besides concentration and textural properties, time and the type of cell should be taken into consideration.[293] Surface modification is among physical properties shown to decrease the cytotoxicity of BP nanomaterials. BPQDs were surface-modified with Lanthanum titanate for biomedical applications and tested against Raw264.7 cells in terms of cell viability; the surface modification has led to a decrease in toxicity due to alteration in the zeta potential and higher chemical stability both of which affected the cellular internalization quantity and ROS generation and so less cytotoxicity.[290] Somewhere else it has been indicated that polyglycerol functionalization improved the cell viability of BP nanomaterials.[294,295] Nonetheless, Mohamad Latiff *et al.*[296] studied the effect of the synthesis approach on the toxicity of BP nanomaterials, and the exfoliation degree and oxidation content were manipulated; the results showed that the thinner nanoparticles plus the ones, that have undergone more oxidation, showed more cytotoxicity.

Despite reporting various studies on the biological effects of BP nanomaterials *in vivo*, we are still in the early stages. As indicated through Scheme 20, the applied analyses were histology, hematology, stool and urine analysis, weight change tracking, and checking on the biodistribution through fluorescence microscopy and histological staining. Based on the physicochemical properties of nanoparticles, their clearance pathways can be different but mainly through the immune system, leading to accumulation in the liver and spleen.[297] The biodistribution of BP nanomaterials can be tracked through different ways—fluorescence imaging using labeling or taking advantage of intrinsic NIR absorption of BP for photothermal and photoacoustic imaging.[298] Moreover, Raman spectroscopy provides an opportunity to examine the *ex vivo* tumor/organ distribution.[299] Referring to the studies on the biodistribution of BP nanomaterials, they can be found mainly in the liver and spleen after being arrested by macrophages and also in tumors thanks to enhanced permeation and retention effect.[299,300] It is noteworthy that the similarity between the structure of DNA and layer BP led the nanosheets to reach the kidneys.[298] Besides the mentioned organs, there are some studies reported on the distribution of BP nanomaterials in low quantities in the heart and lung.[298–300] The measurement of phosphate content *in vivo* is not an easy task due to the existence of intrinsic phosphorus in animals' body to directly understand the quantity after inoculation, but researchers based on the intensity of fluorescence or radioactivity have tracked BP nanomaterials and come up with pharmacokinetics of BP. The process of cleaning from blood stream followed by complete elimination has two phases; up to 1 h, a rapid decrease in the BP nanomaterials was observed from the bloodstream followed by up to 19 h, and clearance of BP from the circulation.[298–300] Previous studies have reported that the excretion of BP mainly takes place through the renal pathway; BP degrades into smaller species and gets excreted through urine.[74,301] To understand the effect of BP on the organs and biochemical levels, other parameters including hematological, histological, biochemicals, and change in body weight have been taken into consideration. In the case of histological analysis, major organs have been dissected and stained with hematoxylin and eosin to understand if any abnormality has occurred compared to the control, which has not received BP. Most of these studies have unanimously demonstrated that BP did not induce inflammation or damage to these organs.[223,268,302,303] However, there are some studies reporting on the negative effects of BP nanosheets

and BPQDs. Kidney impairment was observed for the mice treated with BPQDs, and through histological analysis, it was revealed that neutrophil infiltration increased and tubule degeneration had occurred.[304] In another study, BP nanosheets were observed in the lungs leading to cell apoptosis.[291]

The biosafety of BP has been evaluated *in vivo*, but these studies have not come up with definitive conclusions and the difference might have been raised from decisive factors such as BP's fabrication procedure, physical and chemical properties, surface modification, inoculation route, and dosage. These parameters must be taken into account and also lack of long-term *in vivo* studies can be felt, which requires to be addressed in the future.

13. Paving the way for clinical translation

Despite many studies that have been performed on BP nanomaterials' potential in cancer therapy, there is still no clinical trial ongoing. The fundamental models for clinical translation are *in vivo* animal models to understand the efficacy of therapy and biosafety profiles. The outcomes of this research are essential for anticipating the success rate in human studies. Among different types of animal models, the mouse model is considered reliable due to the similarity of human and mouse genes. Mice have become the main preclinical model in cancer research because of a wide variety of advantages over other animal models—small size, easy alteration in the gene, low maintenance costs, *etc.* However, there is still controversy about the reliability of preclinical data for the clinical translation of biomaterials. Step by step, BP has undergone *in vitro* and *in vivo* studies in terms of anticancer activity and biosafety, as indicated and discussed in the previous sections. *In vivo* studies emphasize the importance of understanding the relationship between the physicochemical properties of BP and its interaction with biological systems. For successful clinical translation, it is essential to formulate BP-based nanomaterials in a way that preserves their physicochemical properties after administration. However, the clinical use of BP is hampered by its poor stability under environmental conditions, as it rapidly degrades when exposed to oxygen and water, producing ROS and phosphoric acids. This instability not only decreases the shelf life of BP, but also reduces its therapeutic efficacy, as premature degradation may occur before it reaches the target site. However, the biodegradability of BP is a significant advantage in biomedical applications, as it allows safe degradation and elimination from the body once it has served its therapeutic function.

The key challenge is to strike a balance between the desirable biodegradability of BP and enhanced stability in biological environments. A potential solution is surface modification or coating with biocompatible materials, such as polymers, lipids, or inorganic compounds.[305] As discussed earlier, coatings such as PEG and polydopamine can protect BPs from environmental degradation while allowing controlled degradation within the body.[306] Additionally, doping BP with elements such as nitrogen or sulfur can help passivate its surface, improving stability while preserving its functional properties. Another approach is incorporating BP into hybrid materials, such as combining it with carbon-based materials (*e.g.*, graphene oxide) or encapsulating it within hydrogels,[307] which increases stability without compromising its biodegradability.

BP-based nanomaterials show immense potential in medicine, particularly for precise drug delivery systems, PTT, biosensing, and biodegradable implants. The controlled degradation makes it ideal for smart drug delivery, enabling the release of therapeutic agents in response to specific stimuli such as changes in pH or temperature. In cancer therapy, the photothermal properties of BP can be used to selectively target and destroy cancer cells, followed by natural degradation that minimizes long-term toxicity. Additionally, the electronic and optical properties of BP make it highly suitable for biosensing and bioimaging, facilitating real-time monitoring of disease markers. Despite these promising applications, several challenges must be addressed before BP can be used in clinical settings. Comprehensive toxicity studies are essential to fully understand the long-term effects of BP degradation products *in vivo*, and regulatory requirements must be met to ensure that BP-based nanomaterials adhere to the necessary safety and efficacy standards for medical use.

In terms of safety, a recent study by Zhang *et al.*[308] has revealed that BP nanomaterials follow a two-compartment model for clearance from the circulatory system. During the distribution phase, BP levels in circulation dropped rapidly, with a half-life in the range of a few minutes to approximately 1 hour. During the elimination phase, BP was cleared from the bloodstream over an extended half-life, ranging from a few hours to as long as 18 hours. The study also observed that BP initially accumulated in major organs after injection, reaching a peak within a few hours before gradually declining, as it was eliminated. Furthermore, experiments showed that BP is primarily cleared through the kidneys, with its breakdown products, mainly phosphate species, excreted in the urine.

Therefore, dose is a particularly critical factor in the safe application of BPNSs in biomedical contexts. A study by Qin *et al.*[309] demonstrated that the inflammatory response in mice was dose dependent. The research showed that BPNSs triggered oxidative stress and rapidly generated a large amount of ROS. The excessive ROS production activated the NF-κB signaling pathway, leading to inflammation, thereby enhancing the understanding of the molecular mechanisms underlying BPNS-induced inflammation.

It has also been reported that reducing the size of BP can lower its toxicity. A recent study has investigated the toxicity and oxidative stress caused by BPQDs *in vivo* at a dose of 0.34 mg.[74] The study observed lipid peroxidation, DNA damage, reduced catalase activity, and a decrease in the number of blood mononuclear cells, along with weight loss in mice. However, these symptoms reversed after 1 month, with the mice's body weight returning to physiological levels. Importantly, no damage to the liver, spleen, or kidneys was detected

during the *in vivo* experiments. Another study,[304] however, revealed that BPQDs may cause nephrotoxicity, linked to alterations in insulin response and the induction of endoplasmic reticulum stress in the kidneys. This toxicity was only observed within the first week, with no follow-up investigations to assess potential long-term recovery. These findings highlight the need for further research to thoroughly assess the biosafety of BP and ensure its suitability for clinical trials. The translation of exfoliated BP from laboratory research to therapeutic applications is a complex process that requires careful attention to detail and strict adherence to standards at every stage. Initially, the production process must be meticulously optimized and tightly quality-controlled, with each step fine-tuned, progress carefully monitored, and methods thoroughly documented to ensure consistency and reproducibility. Adhering to stringent quality guidelines, such as Good Laboratory Practice (GLP), is crucial, as it forms the foundation for regulatory compliance and eventual clinical application. Additionally, the process must be designed to smoothly transition to current Good Manufacturing Practice (cGMP), ensuring the production of materials that meet the highest standards of safety, efficacy, and quality for regulatory approval. Preclinical safety and toxicology investigations provide an important link between laboratory research and clinical trials. These investigations, which are commonly done on animal models, provide an accurate assessment of the compound's safety profile. Toxicity, pharmacokinetics, and biodistribution are evaluated to gain insights into the compound's behavior in live organisms. Pharmacokinetic studies are essential for investigating a compound's absorption, distribution, metabolism, and excretion characteristics. Understanding these factors is crucial for determining appropriate dosage regimens and predicting how the molecule will interact with the human body. To visualize the *in vivo* biodistribution of BP-based nanomaterials, fluorescence and photoacoustic imaging techniques are commonly employed, utilizing either NIR fluorescence dyes or the intrinsic NIR absorption properties of BP nanomaterials.[15,298] Single-emission computed tomography, combined with radioactive technetium-99m labeling, enables high-resolution analysis of biodistribution and pharmacokinetics.[300] Additionally, Raman mapping offers a direct method for examining *ex vivo* tumor accumulation without the need for labeling.[299] BP-based

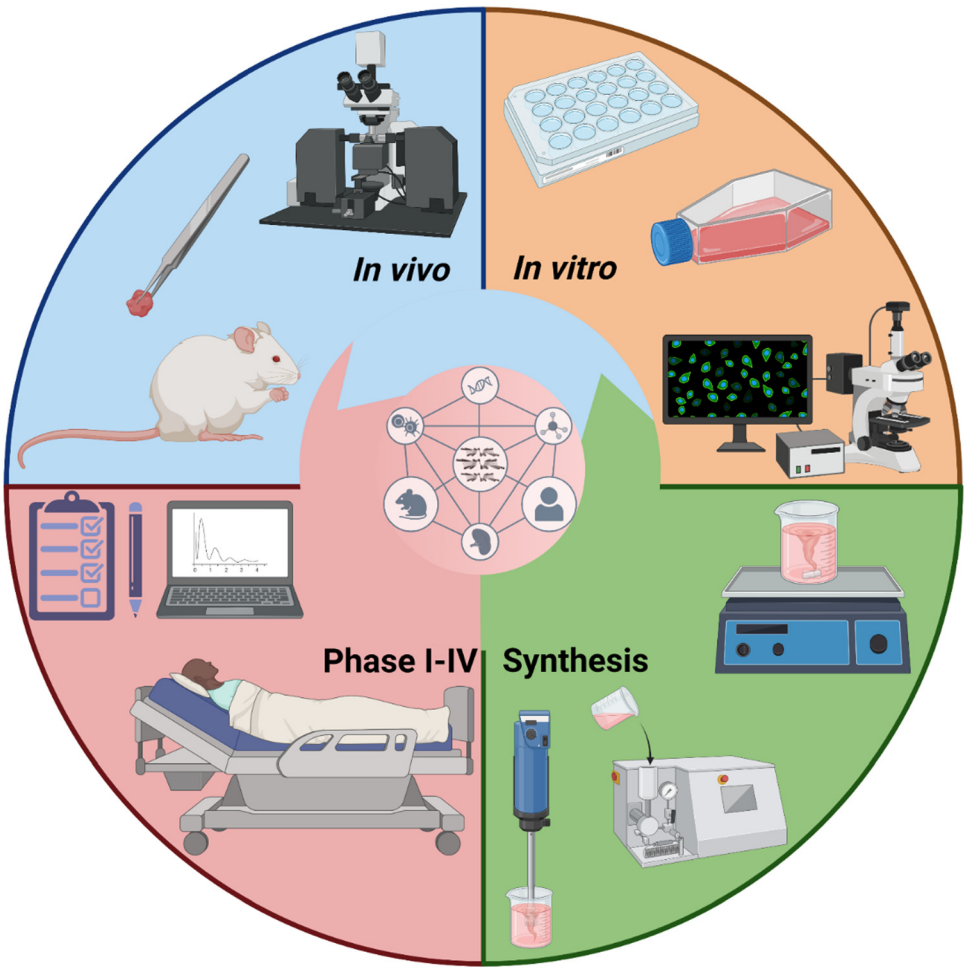

Scheme 21 Clinical translation of BP nanomaterials through four stages: synthesis, *in vitro* evaluations, assessment of BP interaction with the biological system *in vivo*, and finally, moving to human trials through phases I to IV. Created with BioRender.com.

nanomaterials primarily accumulate in the liver and spleen due to macrophage capture, as well as in tumor tissues through the enhanced permeation and retention effect. Interestingly, the structural similarity of layered black phosphorus to DNA nanostructures enhances its kidney targeting capabilities, while minor distribution is also noted in the lungs and heart.[298]

As the translation continues to clinical trials, careful planning and execution become increasingly important. Phase I studies aim to assess the compound's safety and tolerability in a small sample of healthy volunteers or patients. These trials yield vital information on dose, delivery routes, and potential adverse effects. Subsequent Phase II trials broaden the scope to evaluate the efficacy, fine-tuning dose regimes and treatment approaches. Phase III studies, which involve bigger patient groups, are designed to establish the compound's safety and efficacy when compared to existing therapies or placebo. Regulatory organizations, such as the FDA, carefully examine the collected data to evaluate if the compound passes the demanding safety and effectiveness requirements for market approval. Once authorized, exfoliated BP can be used in clinical settings, providing novel treatment and therapy options. Continuous post-market surveillance ensures that safety and efficacy are monitored in real-world clinical settings, providing a thorough understanding of the compound's long-term impacts. To achieve successful clinical translation, researchers, doctors, regulatory agencies, and industry partners must work together. Exfoliated BP appears as a potential and safe treatment option, providing hope to patients in need. To make the move from laboratory findings to clinical applications, rigorous adherence to exacting regulatory criteria is required.

We believe that a targeted study aimed at clarifying the physicochemical characteristics of BP and its interactions with numerous human organs would help to bridge the gap between *in vivo* investigations and clinical application (Scheme 21). Particle size, surface modification, biodistribution, tumor internalization rates, therapeutic effectiveness, and biosafety may all be investigated to acquire a better understanding of BP's therapeutic potential. Furthermore, using the volume of data generated through research activities, in addition to the advancement of modeling methodologies and the integration of artificial intelligence, holds enormous promise for closing the gap between the preclinical and clinical stages. These novel techniques have the potential to accelerate the use of BP in human cancer treatment, easing the transition from experimental to clinical practice.

In the end, successful clinical translation necessitates a collaborative effort among researchers, physicians, and regulatory authorities. Exfoliated BP can emerge as a safe and effective therapeutic solution, providing hope to patients in need, by carefully navigating each stage and adhering to regulatory criteria.

14. Conclusions and outlook

Research and development in the field of cancer therapy are in progress in an ever-increasing rate to devise and discover new anticancer agents and improve the already developed ones. BP nanosheets and quantum dots have been applied in this field since 2015 (referring to the pioneer publications) as a nanomaterial that has strong photocatalytic properties and is responsive to external NIR irradiation.[17,154] Gradually, the unique physicochemical and biological properties of BP were revealed to the research community. BP is prone to oxygen and this oxidation accelerates the degradation rate and affects the optical properties negatively. Generally speaking, this degradation is a double-edged sword; in the case of bone tissue regeneration, this release of phosphate anions stimulates the cells toward proliferation and induces calcium phosphate precipitation.[12]

However, when it comes to cancer therapy, prolonged circulation and tumor retention may be required, and hence, a fast degradation rate and loss of photo-responsivity are detrimental. In this regard, surface modification of BP can compensate for the physiological instability and endow the BP with additional functionalities.[10] Different strategies were taken to passivate BP's surface/protect it from oxidation and improve its functionality including encapsulation into hydrophobic polymers, coating of polymers, and doping of metallic ions to the surface all of which had made significant changes in the functionality. In the gap time between 2015 and 2017, there were publications relating to the anticancer potential of BP nanosheets and quantum dots, but none has reported if BP had solely anticancer activity. In 2017, it was reported that the elevation of phosphate anions in various cancer cell lines resulted in G2/M phase arrest followed by apoptosis, and the normal cells were not affected. This study was a turning point in the anticancer potential of BP because its capability was compared with DOX as a well-known anticancer drug and turned out to be superior to this chemotherapeutic drug.[14] From that moment on, BP has become a multifunctional platform due to its superior photoresponsivity, drug/gene delivery, biocompatibility, and selective anticancer activity. Another mechanistic study has proposed a complementary explanation about the BP selective anticancer potential and omitted using either NIR or any chemotherapeutic drug. An increase in phosphate anions concentration due to a faster degradation rate in cancer cells increases lipid peroxidation and then a decrement in the superoxide dismutase takes place resulting in the generation of excessive ROS.[15] The present review has put effort into covering the most recent advancements related to BP cancer therapy. We have shed light on BP's potential against each cancer type comprehensively and so each disease is divided into a separate section helping the potential reader to understand what has been done and where BP is going to be in the near future. Each disease differs from another one with specific obstacles and treatment outcomes, and understanding how applying BP affected the treatment procedure is of great importance.

Since the appearance of BP in anticancer applications, mostly it has been assessed against breast cancer cells and breast *in vivo* tumor models. In this regard, different therapeutic platforms based on BP, namely, mono-, dual-, and triple-therapeutic/responsive nanomaterials were designed and

applied, and they are covered here in detail. An interesting recent study has opened new doors to BP potential against breast cancer migration and successfully reversed highly invasive and metastatic mesenchymal-type MDA-MB-231 to an epithelial phenotype through a surface-modified BP + mild hyperthermia culminating in the inhibition of breast cancer cell migration. This study on its own is a unique one adopting a new approach towards BP cancer therapy and we expect to see more similar studies in the future. Other studies have focused on combinational therapeutic approaches with the aid of internal, external, and internal–external stimuli. A shiny example is the combination of chemotherapy and PTT against breast cancer, which had promising results, not only inhibitory growth effects but also tumor ablation. Other examples are the combination of PDT/PTT and PTT/immunotherapy. PDT alone suffers from weakened efficacy when it comes to hypoxia regions of tumors whereas applying PTT solely is not strong enough for a complete tumor ablation. A combination of PDT and PTT was shown to compensate for the drawbacks of each and yielded strong antitumor results. PTT derived from BP-based nanomaterials has also been shown to activate the host immune system to fight back cancer cells and distant tumors caused by breast cancer. Apart from dual-therapy, a few studies have stepped further to come up with triple-therapy packages including chemotherapy + PTT + PDT. Although the synthesis procedures are more complicated and time-consuming and the full potential requires applying laser irradiation with two wavelengths, the results are promising, and complete tumor eradication was obtained which cannot be seen in every study. Regeneration of breast tissue at the same time or after breast cancer therapy has received less attention through BP and it is expected that this point will be taken into consideration for future studies.

Followed by breast cancer, other types have recently been targeted through BP including glioblastoma, melanoma, prostate, and osteosarcoma, but the rest—liver, colorectal, lung, cervical—have yet to be fully assessed. The development of BP-based biomaterials for brain cancer has been impressive in recent years. The main obstacles can be crossing the blood–brain barrier and targeting glioblastoma cells and various strategies have been taken like conjugation of specific peptides and even applying NIR. A study has simulated the blood–brain barrier through the formation of human umbilical vascular endothelial cells in transwells to assess if the nanoparticles were able to diffuse throughout the membrane and an interesting outcome was an improvement in the penetration rate once the NIR had been applied and hyperthermia was induced by BP.[219] Other platforms and approaches were also designed for brain cancer like neodymium-doped BP, which showed improved NIR imaging and ROS formation, and Fe^{3+}-doped BP for photoacoustic therapy through inducing mechanical shockwaves. The overall outcomes show a bright future over BP-based brain cancer therapy. Skin and bone cancers are those for which BP has been applied as a therapeutic and regenerative platform. Generally speaking, tumors diagnosed in both cases are removed through surgery and the remaining cancerous cells could be successfully eradicated through the PTT potential of BP. Apart from this, BP is capable of accelerating tissue regeneration, which plays two important roles in these cases.

Despite these great advancements and developments BP cancer therapy, there are major problems and challenges that require careful scrutinizing to facilitate the clinical translation of BP. There are some contradictory *in vitro* and *in vivo* results among most studies which can be attributed to the physicochemical properties of synthesized BP. The thickness and size of yielded BP nanosheets cannot be controlled throughout the exfoliation procedure. Another problem relates to the low yield of BP with time-consuming and expensive procedures limiting its applicability; this should be addressed since large-scale production of BP requires minimization of batch-to-batch variation and quality control. Future studies must target this challenge besides the BP's application and come up with other synthesis routes and electricity-mediated approaches and microwave-assisted synthesis techniques should be more adopted because the parameters can be easily controlled with minimized variation.

Referring to the surveyed studies in the present review, the selective anticancer activity of BP may not be enough for tumor ablation. The injection route should also be taken into account; intravenous injection of bare BP throughout bloodstream cannot obtain desirable tumor accumulation and may require increase in the concentration. Despite the biocompatibility of BP, which has been frequently reported, it has been revealed that applying BP with a concentration of 25 mg kg^{-1} *in vivo* decreased the survival rate down to 67%, and doubling this concentration completely caused the mice to die (0% survival rate) due to phosphate overdose.[168] The injection of bare BP intratumorally may yield the desirable therapeutic outcomes with a competitively lower dose of BP, but significantly limits the BP applications. Therefore, the long-term effects (about half a year) of BP *in vivo* must be carefully tracked and the *in vivo* models should be gradually steered from mice towards larger animals before translation towards clinical settings and instead of single therapy, which no longer is capable of addressing the actual needs of a patient, combinational therapy must be substituted.

In tissue regeneration and cancer therapy, the future trajectory of BP nanomaterials depends on perfecting liquid-phase exfoliation (LPE) methodologies to achieve consistent and reproducible production with high yields. The optimization of different parameters such as solvent selection, exfoliation techniques, and surface functionalization methods is critical to achieving BP flakes with uniform properties, which are essential in these fields. One area of exploration involves refining LPE methodologies to ensure consistent and replicable production of BP nanomaterials with high yields. This pursuit requires careful optimization of various factors, including solvent selection, exfoliation methodologies, and surface functionalization techniques. Researchers are trying to optimize these processes to obtain BP flakes with uniform properties including size, morphology, and surface chemistry, which are critical for biomedical applications.

Furthermore, there is a growing emphasis on developing scalable and economically viable production procedures for BP nanomaterials. By combining robust LPE methodologies with innovative synthesis and purification strategies, researchers aim to generate BP flakes in substantial quantities without compromising quality. Such scalability is essential for the transition of BP-based biomedical technologies from laboratories to clinical environments, where constant and reliable access to materials is paramount.

Additionally, advancements in surface functionalization techniques enable the customization of BP nanomaterials for specific biomedical applications. By modulating the surface chemistry of exfoliated BP flakes with biocompatible agents such as polymers or targeting ligands, researchers can fine-tune their properties to achieve desired functionalities. These functionalities may include extended circulation times, targeted delivery to specific tissues, or enhanced cellular uptake, thereby expanding the range of biomedical applications for BP nanomaterials.

In addition, the emerging field of therapeutics, which combines therapy with diagnostics, offers exciting prospects for BP nanomaterials. BP-based nanomaterials could be designed to simultaneously deliver therapeutic agents and enable real-time monitoring of treatment response through imaging modalities such as photoacoustic imaging or NIR fluorescence imaging. This integrated approach could lead to more personalized and effective cancer treatments. Furthermore, the development of combination therapies involving BP nanomaterials is very promising. By combining BP-mediated therapies with conventional ones such as chemotherapy or immunotherapy, synergistic effects can be achieved, improving overall treatment efficacy and overcoming mechanisms of drug resistance.

Overall, the future of BP in cancer therapy is bright, with ongoing research efforts focusing on exploiting its unique properties for targeted and multifaceted therapeutic approaches. As our understanding of BP's interactions with biological systems continues to deepen, we can expect to see increasingly innovative and effective applications in the fight against cancer.

Abbreviations

PEG	Polyethylene glycol
BP	Black phosphorus
BPQDs	Black phosphorus quantum dots
PLGA	Poly(lactic-*co*-glycolic acid)
PTT	Photothermal therapy
PDT	Photodynamic therapy
SDT	Sonodynamic therapy
DOX	Doxorubicin
MHT	Magnetic hyperthermia
LPE	Liquid phase exfoliation
NMP	*N*-Methyl-2-pyrrolidone
DMSO	Dimethyl sulfoxide
DMF	Dimethylformamide
ST	Solvothermal
GSH	Glutathione

Author contributions

The manuscript was written with contributions from all authors, who have all approved the final version.

Data availability

No primary research results, software, or code have been included and no new data were generated or analyzed as part of this review.

Conflicts of interest

The authors declare no conflict of interest.

Acknowledgements

This study was performed as part of the activities of the National Center for Gene Therapy and Drugs Based on RNA Technology, funded in the framework of the National Recovery and Resilience Plan (NRRP), Mission 4 ''Education and Research'', Component 2 ''From Research to Business'', Investment 1.4 ''Strengthening research structures for supporting the creation of National Centres, national R&D leaders on some Key Enabling Technologies'', funded by the European Union - Next Generation EU, Project CN00000041, CUP B83C22002860006, Spoke 2 ''Development of gene therapy and drugs with RNA technology''. The authors also thank the POR Campania FESR 2014-2020 (Campania imaging Infrastructure for Research in Oncology – C.I.R.O).

References

1 Y. Pang, Y. Fu, C. Li, Z. Wu, W. Cao, X. Hu, X. Sun, W. He, X. Cao, D. Ling, Q. Li, C. Fan, C. Yang, X. Kong and A. Qin, *Nano Lett.*, 2020, **20**, 829–840.
2 J. M. Keca, J. Chen, M. Overchuk, N. Muhanna, C. M. MacLaughlin, C. S. Jin, W. D. Foltz, J. C. Irish and G. Zheng, *Angew. Chem., Int. Ed.*, 2016, **55**, 6187–6191.
3 S. Son, J. H. Kim, X. Wang, C. Zhang, S. A. Yoon, J. Shin, A. Sharma, M. H. Lee, L. Cheng, J. Wu and J. S. Kim, *Chem. Soc. Rev.*, 2020, **49**, 3244–3261.
4 J. Yang, M. Hou, W. Sun, Q. Wu, J. Xu, L. Xiong, Y. Chai, Y. Liu, M. Yu, H. Wang, Z. P. Xu, X. Liang and C. Zhang, *Adv. Sci.*, 2020, **7**, 2001088.
5 F. P. Sellera, C. P. Sabino and M. R. Hamblin, *Photodyn. Ther. Vet. Med. From Basics to Clin. Pract.*, 2017, 1–10.
6 A. Farzin, S. A. Etesami, J. Quint, A. Memic and A. Tamayol, *Adv. Healthcare Mater.*, 2020, **9**, 1901058.
7 M. Xu, L. Zhou, L. Zheng, Q. Zhou, K. Liu, Y. Mao and S. Song, *Cancer Lett.*, 2021, **497**, 229–242.
8 S. Li, B. Gu, X. Li, S. Tang, L. Zheng, E. Ruiz-Hitzky, Z. Sun, C. Xu and X. Wang, *Adv. Healthcare Mater.*, 2022, **11**, 2102367.
9 A. Koyappayil, S. G. Chavan, Y. G. Roh and M. H. Lee, *Biosensors*, 2022, **12**, 454.

10 G. Zeng and Y. Chen, *Acta Biomater.*, 2020, **118**, 1–17.
11 A. Bigham, I. Fasolino, S. Borsacchi, C. Valente, L. Calucci, G. Turacchio, M. Pannico, M. Serrano-Ruiz, L. Ambrosio and M. G. Raucci, *Bioact. Mater.*, 2024, **35**, 99–121.
12 B. Yang, J. Yin, Y. Chen, S. Pan, H. Yao, Y. Gao and J. Shi, *Adv. Mater.*, 2018, **30**, 1705611.
13 M. G. Raucci, I. Fasolino, M. Caporali, M. Serrano-Ruiz, A. Soriente, M. Peruzzini and L. Ambrosio, *ACS Appl. Mater. Interfaces*, 2019, **11**, 9333–9342.
14 W. Zhou, T. Pan, H. Cui, Z. Zhao, P. K. Chu and X. F. Yu, *Angew. Chem., Int. Ed.*, 2019, **58**, 769–774.
15 N. Kong, X. Ji, J. Wang, X. Sun, G. Chen, T. Fan, W. Liang, H. Zhang, A. Xie, O. C. Farokhzad and W. Tao, *Nano Lett.*, 2020, **20**, 3943–3955.
16 Y. Zhang, C. Ma, J. Xie, H. Ågren and H. Zhang, *Adv. Mater.*, 2021, **33**, 2100113.
17 Z. Sun, H. Xie, S. Tang, X. F. Yu, Z. Guo, J. Shao, H. Zhang, H. Huang, H. Wang and P. K. Chu, *Angew. Chem., Int. Ed.*, 2015, **54**, 11526–11530.
18 X. Qian, Z. Gu and Y. Chen, *Mater. Horizons*, 2017, **4**, 800–816.
19 J. R. Choi, K. W. Yong, J. Y. Choi, A. Nilghaz, Y. Lin, J. Xu and X. Lu, *Theranostics*, 2018, **8**, 1005–1026.
20 X. Ge, Z. Xia and S. Guo, *Adv. Funct. Mater.*, 2019, **29**, 1900318.
21 M. Qiu, A. Singh, D. Wang, J. Qu, M. Swihart, H. Zhang and P. N. Prasad, *Nano Today*, 2019, **25**, 135–155.
22 M. Luo, T. Fan, Y. Zhou, H. Zhang and L. Mei, *Adv. Funct. Mater.*, 2019, **29**, 1808306.
23 L. Qin, S. Jiang, H. He, G. Ling and P. Zhang, *J. Control. Release*, 2020, **318**, 50–66.
24 H. Liu, Y. Mei, Q. Zhao, A. Zhang, L. Tang, H. Gao and W. Wang, *Pharmaceutics*, 2021, **13**, 1344.
25 W. Liu, A. Dong, B. Wang, H. Zhang, W. Liu, A. Dong, B. Wang and H. Zhang, *Adv. Sci.*, 2021, **8**, 2003033.
26 K. Hu, L. Xie, Y. Zhang, M. Hanyu, Z. Yang, K. Nagatsu, H. Suzuki, J. Ouyang, X. Ji, J. Wei, H. Xu, O. C. Farokhzad, S. H. Liang, L. Wang, W. Tao and M.-R. Zhang, *Nat. Commun.*, 2020, **11**, 2778.
27 T. Wu, Z. Ma, Y. He, X. Wu, B. Tang, Z. Yu, G. Wu, S. Chen and N. Bao, *Angew. Chem., Int. Ed.*, 2021, **60**, 10366–10374.
28 J. Chen, Y. Yang, S. Zhao, F. Bi, L. Song, N. Liu, J. Xu, Y. Wang and X. Zhang, *ACS Catal.*, 2022, **12**, 8069–8081.
29 H. Kim, S. Z. Uddin, D.-H. Lien, M. Yeh, N. S. Azar, S. Balendhran, T. Kim, N. Gupta, Y. Rho, C. P. Grigoropoulos, K. B. Crozier and A. Javey, *Nature*, 2021, **596**, 232–237.
30 F. Martini, S. Borsacchi, G. Barcaro, M. Caporali, M. Vanni, M. Serrano-Ruiz, M. Geppi, M. Peruzzini and L. Calucci, *J. Phys. Chem. Lett.*, 2019, **10**, 5122–5127.
31 S. Comber, M. Gardner, K. Georges, D. Blackwood and D. Gilmour, *Environ. Technol.*, 2013, **34**, 1349–1358.
32 G. Qu, T. Xia, W. Zhou, X. Zhang, H. Zhang, L. Hu, J. Shi, X. F. Yu and G. Jiang, *Chem. Rev.*, 2020, **120**, 2288–2346.
33 X. Liu, K. Chen, X. Li, Q. Xu, J. Weng and J. Xu, *Adv. Mater.*, 2021, **33**, 2005924.
34 P. W. Bridgman, *J. Am. Chem. Soc.*, 1914, **36**, 1344–1363.
35 H. Krebs, H. Weitz and K. H. Worms, *Z. Anorg. Allg. Chem.*, 1955, **280**, 119–133.
36 S. Lange, P. Schmidt and T. Nilges, *Inorg. Chem.*, 2007, **46**, 4028–4035.
37 M. Köpf, N. Eckstein, D. Pfister, C. Grotz, I. Krüger, M. Greiwe, T. Hansen, H. Kohlmann and T. Nilges, *J. Cryst. Growth*, 2014, **405**, 6–10.
38 M. Khurram, Z. Sun, Z. Zhang and Q. Yan, *Inorg. Chem. Front.*, 2020, **7**, 2867–2879.
39 Y. Wang, M. He, S. Ma, C. Yang, M. Yu, G. Yin and P. Zuo, *J. Phys. Chem. Lett.*, 2020, **11**, 2708–2716.
40 S. V. Pedersen, F. Muramutsa, J. D. Wood, C. Husko, D. Estrada and B. J. Jaques, *npj 2D Mater. Appl.*, 2020, **4**, 36.
41 H. Liu, A. T. Neal, Z. Zhu, Z. Luo, X. Xu, D. Tománek and P. D. Ye, *ACS Nano*, 2014, **8**, 4033–4041.
42 J. R. Brent, N. Savjani, E. A. Lewis, S. J. Haigh, D. J. Lewis and P. O'Brien, *Chem. Commun.*, 2014, **50**, 13338–13341.
43 W. Zhao, Z. Xue, J. Wang, J. Jiang, X. Zhao and T. Mu, *ACS Appl. Mater. Interfaces*, 2015, **7**, 27608–27612.
44 M. Serrano-Ruiz, M. Caporali, A. Ienco, V. Piazza, S. Heun and M. Peruzzini, *Adv. Mater. Interfaces*, 2016, **3**, 1500441.
45 M. B. Erande, M. S. Pawar and D. J. Late, *ACS Appl. Mater. Interfaces*, 2016, **8**, 11548–11556.
46 J. Li, C. Chen, S. Liu, J. Lu, W. P. Goh, H. Fang, Z. Qiu, B. Tian, Z. Chen, C. Yao, W. Liu, H. Yan, Y. Yu, D. Wang, Y. Wang, M. Lin, C. Su and J. Lu, *Chem. Mater.*, 2018, **30**, 2742–2749.
47 K. Du, W. Yang, S. Deng, X. Li and P. Yang, *Nanomaterials*, 2020, **10**(1), 139.
48 B. Tian, B. Tian, B. Smith, M. C. Scott, Q. Lei, R. Hua, Y. Tian and Y. Liu, *Proc. Natl. Acad. Sci. U. S. A.*, 2018, **115**, 4345–4350.
49 H. Xu, X. Han, Z. Li, W. Liu, X. Li, J. Wu, Z. Guo and H. Liu, *Adv. Mater. Interfaces*, 2018, **5**, 1801048.
50 Y. Xu, X. Shi, Y. Zhang, H. Zhang, Q. Zhang, Z. Huang, X. Xu, J. Guo, H. Zhang, L. Sun, Z. Zeng, A. Pan and K. Zhang, *Nat. Commun.*, 2020, **11**, 1330.
51 Z. Wu, Y. Lyu, Y. Zhang, R. Ding, B. Zheng, Z. Yang, S. P. Lau, X. H. Chen and J. Hao, *Nat. Mater.*, 2021, **20**, 1203–1209.
52 L. Li, Y. Yu, G. J. Ye, Q. Ge, X. Ou, H. Wu, D. Feng, X. H. Chen and Y. Zhang, *Nat. Nanotechnol.*, 2014, **9**, 372–377.
53 S. Lin, Y. Chui, Y. Li and S. P. Lau, *FlatChem*, 2017, **2**, 15–37.
54 L. Chen, G. Zhou, Z. Liu, X. Ma, J. Chen, Z. Zhang, X. Ma, F. Li, H.-M. Cheng and W. Ren, *Adv. Mater.*, 2016, **28**, 510–517.
55 J. Kang, S. A. Wells, J. D. Wood, J.-H. Lee, X. Liu, C. R. Ryder, J. Zhu, J. R. Guest, C. A. Husko and M. C. Hersam, *Proc. Natl. Acad. Sci. U. S. A.*, 2016, **113**, 11688–11693.
56 C. Hao, B. Yang, F. Wen, J. Xiang, L. Li, W. Wang, Z. Zeng, B. Xu, Z. Zhao, Z. Liu and Y. Tian, *Adv. Mater.*, 2016, **28**, 3194–3201.
57 P. Yasaei, B. Kumar, T. Foroozan, C. Wang, M. Asadi, D. Tuschel, J. E. Indacochea, R. F. Klie and A. Salehi-Khojin, *Adv. Mater.*, 2015, **27**, 1887–1892.

58 J. Kang, J. D. Wood, S. A. Wells, J.-H. Lee, X. Liu, K.-S. Chen and M. C. Hersam, *ACS Nano*, 2015, **9**, 3596–3604.
59 M. Bat-Erdene, M. Batmunkh, C. J. Shearer, S. A. Tawfik, M. J. Ford, L. Yu, A. J. Sibley, A. D. Slattery, J. S. Quinton, C. T. Gibson and J. G. Shapter, *Small Methods*, 2017, **1**, 1700260.
60 Z. Huang, H. Hou, Y. Zhang, C. Wang, X. Qiu and X. Ji, *Adv. Mater.*, 2017, **29**, 1702372.
61 S. Yang, K. Zhang, A. G. Ricciardulli, P. Zhang, Z. Liao, M. R. Lohe, E. Zschech, P. W. M. Blom, W. Pisula, K. Müllen and X. Feng, *Angew. Chem., Int. Ed.*, 2018, **57**, 4677–4681.
62 C. C. Mayorga-Martinez, N. Mohamad Latiff, A. Y. S. Eng, Z. Sofer and M. Pumera, *Anal. Chem.*, 2016, **88**, 10074–10079.
63 H. Fu, Z. Li, H. Xie, Z. Sun, B. Wang, H. Huang, G. Han, H. Wang, P. K. Chu and X. F. Yu, *RSC Adv.*, 2017, **7**, 14618–14624.
64 X. Zhang, H. Xie, Z. Liu, C. Tan, Z. Luo, H. Li, J. Lin, L. Sun, W. Chen, Z. Xu, L. Xie, W. Huang and H. Zhang, *Angew. Chem., Int. Ed.*, 2015, **54**, 3653–3657.
65 R. Gui, H. Jin, Z. Wang and J. Li, *Chem. Soc. Rev.*, 2018, **47**, 6795–6823.
66 W. Gu, X. Pei, Y. Cheng, C. Zhang, J. Zhang, Y. Yan, C. Ding and Y. Xian, *ACS Sensors*, 2017, **2**, 576–582.
67 Y. Miao, X. Wang, J. Sun and Z. Yan, *Nanoscale Adv.*, 2021, **3**, 1532–1550.
68 E. Kovalska, J. Luxa, T. Hartman, N. Antonatos, P. Shaban, E. Oparin, M. Zhukova and Z. Sofer, *Nanoscale*, 2020, **12**, 2638–2647.
69 W. Zheng, J. Lee, Z.-W. Gao, Y. Li, S. Lin, S. P. Lau and L. Y. S. Lee, *Adv. Energy Mater.*, 2020, **10**, 1903490.
70 Z. Sofer, D. Bouša, J. Luxa, V. Mazanek and M. Pumera, *Chem. Commun.*, 2016, **52**, 1563–1566.
71 S. Su, B. Xu, J. Ding and H. Yu, *New J. Chem.*, 2019, **43**, 19365–19371.
72 L. Lei, S. Zhang, W. Lou, X. Zhang, B. Qin, Q. Zhao and B. Xing, *Front. Environ. Sci.*, 2023, **11**, 1075842.
73 C.-H. Choi, Y.-J. Park, X. Wu and D.-P. Kim, *Chem. Eng. J.*, 2018, **333**, 336–342.
74 X. Mu, J. Y. Wang, X. Bai, F. Xu, H. Liu, J. Yang, Y. Jing, L. Liu, X. Xue, H. Dai, Q. Liu, Y. M. Sun, C. Liu and X. D. Zhang, *ACS Appl. Mater. Interfaces*, 2017, **9**, 20399–20409.
75 S. Liu, S. Lin, P. You, C. Surya, S. P. Lau and F. Yan, *Angew. Chem., Int. Ed.*, 2017, **56**, 13717–13721.
76 Z.-L. Xu, S. Lin, N. Onofrio, L. Zhou, F. Shi, W. Lu, K. Kang, Q. Zhang and S. P. Lau, *Nat. Commun.*, 2018, **9**, 4164.
77 D. Hanlon, C. Backes, E. Doherty, C. S. Cucinotta, N. C. Berner, C. Boland, K. Lee, A. Harvey, P. Lynch, Z. Gholamvand, S. Zhang, K. Wang, G. Moynihan, A. Pokle, Q. M. Ramasse, N. McEvoy, W. J. Blau, J. Wang, G. Abellan, F. Hauke, A. Hirsch, S. Sanvito, D. D. O'Regan, G. S. Duesberg, V. Nicolosi and J. N. Coleman, *Nat. Commun.*, 2015, **6**, 8563.
78 A. E. Del Rio Castillo, V. Pellegrini, H. Sun, J. Buha, D. A. Dinh, E. Lago, A. Ansaldo, A. Capasso, L. Manna and F. Bonaccorso, *Chem. Mater.*, 2018, **30**, 506–516.
79 Z. Sun, Y. Zhang, H. Yu, C. Yan, Y. Liu, S. Hong, H. Tao, A. W. Robertson, Z. Wang and A. A. H. Pádua, *Nanoscale*, 2018, **10**, 12543–12553.
80 J. R. Brent, A. K. Ganguli, V. Kumar, D. J. Lewis, P. D. McNaughter, P. O'Brien, P. Sabherwal and A. A. Tedstone, *RSC Adv.*, 2016, **6**, 86955–86958.
81 R. Jain, Y. Singh, S.-Y. Cho, S. P. Sasikala, S. H. Koo, R. Narayan, H.-T. Jung, Y. Jung and S. O. Kim, *Chem. Mater.*, 2019, **31**, 2786–2794.
82 M. Lee, A. K. Roy, S. Jo, Y. Choi, A. Chae, B. Kim, S. Y. Park and I. In, *Nanotechnology*, 2017, **28**, 125603.
83 C.-X. Hu, Q. Xiao, Y.-Y. Ren, M. Zhao, G.-H. Dun, H.-R. Wu, X.-Y. Li, Q.-Q. Yang, B. Sun, Y. Peng, F. Yan, Q. Wang and H.-L. Zhang, *Adv. Funct. Mater.*, 2018, **28**, 1805311.
84 P. D. Matthews, W. Hirunpinyopas, E. A. Lewis, J. R. Brent, P. D. McNaughter, N. Zeng, A. G. Thomas, P. O'Brien, B. Derby, M. A. Bissett, S. J. Haigh, R. A. W. Dryfe and D. J. Lewis, *Chem. Commun.*, 2018, **54**, 3831–3834.
85 Z. Guo, H. Zhang, S. Lu, Z. Wang, S. Tang, J. Shao, Z. Sun, H. Xie, H. Wang, X.-F. Yu and P. K. Chu, *Adv. Funct. Mater.*, 2015, **25**, 6996–7002.
86 S. Yan, H. Song, L. F. Wan, S. Lin, H. Wu, Y. Shi and J. Yao, *Nano Lett.*, 2020, **20**, 81–87.
87 Y. Xu, Z. Wang, Z. Guo, H. Huang, Q. Xiao, H. Zhang and X.-F. Yu, *Adv. Opt. Mater.*, 2016, **4**, 1223–1229.
88 C. P. Bartus, T. Hegedűs, G. Kozma, I. Szenti, R. Vajtai, Z. Kónya and Á. Kukovecz, *J. Mol. Struct.*, 2022, **1260**, 132862.
89 S. Seo, H. U. Lee, S. C. Lee, Y. Kim, H. Kim, J. Bang, J. Won, Y. Kim, B. Park and J. Lee, *Sci. Rep.*, 2016, **6**, 23736.
90 A. H. Woomer, T. W. Farnsworth, J. Hu, R. A. Wells, C. L. Donley and S. C. Warren, *ACS Nano*, 2015, **9**, 8869–8884.
91 Q.-Q. Guan, H.-J. Zhou, P. Ning, P.-C. Lian, B. Wang, L. He and X.-S. Chai, *Phys. B Condens. Matter*, 2018, **537**, 18–22.
92 H. Xiao, M. Zhao, J. Zhang, X. Ma, J. Zhang, T. Hu, T. Tang, J. Jia and H. Wu, *Electrochem. Commun.*, 2018, **89**, 10–13.
93 H. Liu, P. Lian, Q. Zhang, Y. Yang and Y. Mei, *Electrochem. Commun.*, 2019, **98**, 124–128.
94 F. Luo, D. Wang, J. Zhang, X. Li, D. Liu, H. Li, M. Lu, X. Xie, L. Huang and W. Huang, *ACS Appl. Nano Mater.*, 2019, **2**, 3793–3801.
95 M. Batmunkh, M. Myekhlai, A. S. R. Bati, S. Sahlos, A. D. Slattery, T. M. Benedetti, V. R. Gonçales, C. T. Gibson, J. J. Gooding, R. D. Tilley and J. G. Shapter, *J. Mater. Chem. A*, 2019, **7**, 12974–12978.
96 W. Wu, J. Xu, X. Tang, P. Xie, X. Liu, J. Xu, H. Zhou, D. Zhang and T. Fan, *Chem. Mater.*, 2018, **30**, 5932–5940.
97 Z. Yan, X. He, L. She, J. Sun, R. Jiang, H. Xu, F. Shi, Z. Lei and Z.-H. Liu, *J. Mater.*, 2018, **4**, 129–134.
98 Y. Zhang, H. Wang, Z. Luo, H. T. Tan, B. Li, S. Sun, Z. Li, Y. Zong, Z. J. Xu, Y. Yang, K. A. Khor and Q. Yan, *Adv. Energy Mater.*, 2016, **6**, 1600453.
99 Y. Xia, S. Wang, R. Huang, R. Su, W. Qi and Z. He, *Langmuir*, 2018, **34**, 8508–8515.
100 V. Mussi, I. Fasolino, D. Paria, S. De Simone, M. Caporali, M. Serrano-Ruiz, L. Ambrosio, I. Barman, M. G. Raucci and A. Convertino, *Nanomaterials*, 2022, **12**(12), 1994.

101 G. Tiouitchi, M. A. Ali, A. Benyoussef, M. Hamedoun, A. Lachgar, A. Kara, A. Ennaoui, A. Mahmoud, F. Boschini, H. Oughaddou, A. El Moutaouakil, A. El Kenz and O. Mounkachi, *R. Soc. Open Sci.*, 2020, **7**, 201210.
102 J. Shao, H. Xie, H. Huang, Z. Li, Z. Sun, Y. Xu, Q. Xiao, X. F. Yu, Y. Zhao, H. Zhang, H. Wang and P. K. Chu, *Nat. Commun.*, 2016, **7**, 1–13.
103 T. Bao, W. Yin, X. Zheng, X. Zhang, J. Yu, X. Dong, Y. Yong, F. Gao, L. Yan, Z. Gu and Y. Zhao, *Biomaterials*, 2016, **76**, 11–24.
104 J. Shao, C. Ruan, H. Xie, Z. Li, H. Wang, P. K. Chu, X.-F. Yu, J. Shao, C. Ruan, H. Xie, Z. Li, H. Wang, X. Yu and P. K. Chu, *Adv. Sci.*, 2018, **5**, 1700848.
105 X. Zhang, J. Tang, C. Li, Y. Lu, L. Cheng and J. Liu, *Bioact. Mater.*, 2021, **6**, 472–489.
106 W. Tao, X. Zhu, X. Yu, X. Zeng, Q. Xiao, X. Zhang, X. Ji, X. Wang, J. Shi, H. Zhang and L. Mei, *Adv. Mater.*, 2017, **29**, 1603276.
107 X. Zhang, Y. Dong, X. Zeng, X. Liang, X. Li, W. Tao, H. Chen, Y. Jiang, L. Mei and S.-S. Feng, *Biomaterials*, 2014, **35**, 1932–1943.
108 H. Wang, L. Zhong, Y. Liu, X. Xu, C. Xing, M. Wang, S.-M. Bai, C.-H. Lu and H.-H. Yang, *Chem. Commun.*, 2018, **54**, 3142–3145.
109 Y. Xiao, M. Xu, N. Lv, C. Cheng, P. Huang, J. Li, Y. Hu and M. Sun, *Acta Biomater.*, 2021, **122**, 291–305.
110 N. Gao, C. Xing, H. Wang, L. Feng, X. Zeng, L. Mei and Z. Peng, *Front. Pharmacol.*, 2019, **10**, 270.
111 Y. Su, X. Zhang, G. Ren, Z. Zhang, Y. Liang, S. Wu and J. Shen, *Chem. Eng. J.*, 2020, **400**, 125949.
112 N. Gao, J. Nie, H. Wang, C. Xing, L. Mei, W. Xiong, X. Zeng and Z. Peng, *J. Biomed. Nanotechnol.*, 2018, **14**, 1883–1897.
113 A. Bigham, A. O. M. Salehi, M. Rafienia, M. R. Salamat, S. Rahmati, M. G. Raucci and L. Ambrosio, *Mater. Sci. Eng. C*, 2021, **127**, 112242.
114 X.-W. Huang, J.-J. Wei, M.-Y. Zhang, X.-L. Zhang, X.-F. Yin, C.-H. Lu, J.-B. Song, S.-M. Bai and H.-H. Yang, *ACS Appl. Mater. Interfaces*, 2018, **10**, 35495–35502.
115 M. Qiu, D. Wang, W. Liang, L. Liu, Y. Zhang, X. Chen, D. K. Sang, C. Xing, Z. Li, B. Dong, F. Xing, D. Fan, S. Bao, H. Zhang and Y. Cao, *Proc. Natl. Acad. Sci. U. S. A.*, 2018, **115**, 501–506.
116 S. Thurakkal and X. Zhang, *Adv. Sci.*, 2020, **7**, 1902359.
117 L. Wu, J. Wang, J. Lu, D. Liu, N. Yang, H. Huang, P. K. Chu and X.-F. Yu, *Small*, 2018, **14**, 1801405.
118 X. Yang, D. Wang, Y. Shi, J. Zou, Q. Zhao, Q. Zhang, W. Huang, J. Shao, X. Xie and X. Dong, *ACS Appl. Mater. Interfaces*, 2018, **10**, 12431–12440.
119 C. Sun, L. Wen, J. Zeng, Y. Wang, Q. Sun, L. Deng, C. Zhao and Z. Li, *Biomaterials*, 2016, **91**, 81–89.
120 L. Chen, C. Chen, W. Chen, K. Li, X. Chen, X. Tang, G. Xie, X. Luo, X. Wang, H. Liang and S. Yu, *ACS Appl. Mater. Interfaces*, 2018, **10**, 21137–21148.
121 F. Wu, M. Zhang, X. Chu, Q. Zhang, Y. Su, B. Sun, T. Lu, N. Zhou, J. Zhang, J. Wang and X. Yi, *Chem. Eng. J.*, 2019, **370**, 387–399.
122 X. Yang, D. Wang, J. Zhu, L. Xue, C. Ou, W. Wang, M. Lu, X. Song and X. Dong, *Chem. Sci.*, 2019, **10**, 3779–3785.
123 J. Shao, H. Xie, H. Huang, Z. Li, Z. Sun, Y. Xu, Q. Xiao, X. F. Yu, Y. Zhao, H. Zhang, H. Wang and P. K. Chu, *Nat. Commun.*, 2016, **7**, 1–13.
124 X. Wang, J. Shao, M. Abd El Raouf, H. Xie, H. Huang, H. Wang, P. K. Chu, X. F. Yu, Y. Yang, A. B. M. AbdEl-Aal, N. H. M. Mekkawy, R. J. Miron and Y. Zhang, *Biomaterials*, 2018, **179**, 164–174.
125 S. Wang, J. Shao, Z. Li, Q. Ren, X.-F. Yu and S. Liu, *Nano Lett.*, 2019, **19**, 5587–5594.
126 Y. Wang, X. Hu, L. Zhang, C. Zhu, J. Wang, Y. Li, Y. Wang, C. Wang, Y. Zhang and Q. Yuan, *Nat. Commun.*, 2019, **10**, 1–10.
127 L. Qin, G. Ling, F. Peng, F. Zhang, S. Jiang, H. He, D. Yang and P. Zhang, *J. Colloid Interface Sci.*, 2019, **556**, 232–238.
128 F. Zhang, F. Peng, L. Qin, D. Yang, R. Li, S. Jiang, H. He and P. Zhang, *Colloids Surfaces B Biointerfaces*, 2019, **180**, 353–361.
129 X. Shao, Z. Ding, W. Zhou, Y. Li, Z. Li, H. Cui, X. Lin, G. Cao, B. Cheng, H. Sun, M. Li, K. Liu, D. Lu, S. Geng, W. Shi, G. Zhang, Q. Song, L. Chen, G. Wang, W. Su, L. Cai, L. Fang, D. T. Leong, Y. Li, X.-F. Yu and H. Li, *Nat. Nanotechnol.*, 2021, **16**, 1150–1160.
130 W. E. G. Müller, H. C. Schröder and X. Wang, *Chem. Rev.*, 2019, **119**, 12337–12374.
131 M. Biedulska, P. Jakóbczyk, M. Sosnowska, B. Dec, A. Muchlińska, A. J. Zaczek, D. Nidzworski and R. Bogdanowicz, *Sci. Rep.*, 2021, **11**, 1–17.
132 A. W. Shermoen and P. H. O'Farrell, *Cell*, 1991, **67**, 303–310.
133 H. Maiato and E. Logarinho, *Nat. Cell Biol.*, 2014, **16**, 386–394.
134 H. Sung, J. Ferlay, R. L. Siegel, M. Laversanne, I. Soerjomataram, A. Jemal and F. Bray, *CA. Cancer J. Clin.*, 2021, **71**, 209–249.
135 H. J. Burstein, G. Curigliano, B. Thürlimann, W. P. Weber, P. Poortmans, M. M. Regan, H. J. Senn, E. P. Winer, M. Gnant, S. Aebi, F. André, C. Barrios, J. Bergh, H. Bonnefoi, D. Bretel Morales, S. Brucker, H. Burstein, D. Cameron, F. Cardoso, L. Carey, B. Chua, E. Ciruelos, M. Colleoni, G. Curigliano, S. Delaloge, C. Denkert, P. Dubsky, B. Ejlertsen, F. Fitzal, P. Francis, V. Galimberti, H. Gamal El Din Mohamed Mahmoud, J. Garber, M. Gnant, W. Gradishar, B. Gulluoglu, N. Harbeck, C. S. Huang, J. Huober, A. Ilbawi, Z. Jiang, S. Johnston, E. S. Lee, S. Loibl, M. Morrow, A. Partridge, M. Piccart, P. Poortmans, A. Prat, M. Regan, I. Rubio, H. Rugo, E. Rutgers, F. Sedlmayer, V. Semiglazov, H. J. Senn, Z. Shao, T. Spanic, P. Tesarova, B. Thürlimann, S. Tjulandin, M. Toi, M. Trudeau, N. Turner, I. Vaz Luis, G. Viale, T. Watanabe, W. P. Weber, E. P. Winer and B. Xu, *Ann. Oncol.*, 2021, **32**, 1216–1235.
136 E. Ostańska, D. Aebisher and D. Bartusik-Aebisher, *Biomed. Pharmacother.*, 2021, **137**, 111302.
137 A. Burguin, C. Diorio and F. Durocher, *J. Pers. Med.*, 2021, **11**, 808.

138 M. Chen, Y. Miao, K. Qian, X. Zhou, L. Guo, Y. Qiu, R. Wang, Y. Gan and X. Zhang, *Nano Lett.*, 2021, **21**, 6031–6041.
139 P. J. Tanis, O. E. Nieweg, R. A. Valdés Olmos and B. B. R. Kroon, *J. Am. Coll. Surg.*, 2001, **192**, 399–409.
140 A. K. Bednarek, A. Sahin, A. J. Brenner, D. A. Johnston and C. M. Aldaz, *Clin. Cancer Res.*, 1997, **3**, 11–16.
141 R. Segal, W. Evans, D. Johnson, J. Smith, S. Colletta, J. Gayton, S. Woodard, G. Wells and R. Reid, *J. Clin. Oncol.*, 2001, **19**, 657–665.
142 M. S. Moran, S. J. Schnitt, A. E. Giuliano, J. R. Harris, S. A. Khan, J. Horton, S. Klimberg, M. Chavez-Macgregor, G. Freedman, N. Houssami, P. L. Johnson and M. Morrow, *Int. J. Radiat. Oncol.*, 2014, **88**, 553–564.
143 C. Jacquillat, M. Weil, F. Baillet, C. Borel, G. Auclerc, M. A. De Maublanc, M. Housset, G. Forget, L. Thill, C. Soubrane and D. Khayat, *Cancer*, 1990, **66**, 119–129.
144 H. B. Neuman, M. Morrogh, M. Gonen, K. J. Van Zee, M. Morrow and T. A. King, *Cancer*, 2010, **116**, 1226–1233.
145 X. Liu, B. Gaihre, M. N. George, Y. Li, M. Tilton, M. J. Yaszemski and L. Lu, *Biomater. Sci.*, 2021, **9**, 2768–2803.
146 H. Fu, Z. Li, H. Xie, Z. Sun, B. Wang, H. Huang, G. Han, H. Wang, P. K. Chu and X.-F. Yu, *RSC Adv.*, 2017, **7**, 14618–14624.
147 Y. Zhao, L. Tong, Z. Li, N. Yang, H. Fu, L. Wu, H. Cui, W. Zhou, J. Wang, H. Wang, P. K. Chu and X. F. Yu, *Chem. Mater.*, 2017, **29**, 7131–7139.
148 L. Deng, Y. Xu, C. Sun, B. Yun, Q. Sun, C. Zhao and Z. Li, *Sci. Bull.*, 2018, **63**, 917–924.
149 W. Pan, W. Chen, Y. Min, J. Wang, Z. Yang, T. Xu, F. Yu, G. Shen, Y. Hu and X. Ma, *ACS Omega*, 2021, **6**, 35505–35513.
150 J. Liu, S. Smith and C. Wang, *ACS Nano*, 2022, **16**, 3208–3220.
151 L. Sutrisno, H. Chen, Y. Chen, T. Yoshitomi, N. Kawazoe, Y. Yang and G. Chen, *Biomaterials*, 2021, **275**, 120923.
152 Y. Shang, Q. Wang, B. Wu, Q. Zhao, J. Li, X. Huang, W. Chen and R. Gui, *ACS Appl. Mater. Interfaces*, 2019, **11**, 28254–28266.
153 H. Yue, R. Huang, Y. Shan and D. Xing, *J. Mater. Chem. B*, 2020, **8**, 11096–11106.
154 H. Wang, X. Yang, W. Shao, S. Chen, J. Xie, X. Zhang, J. Wang and Y. Xie, *J. Am. Chem. Soc.*, 2015, **137**, 11376–11382.
155 Y. Liu, D. Zhu, X. Zhu, G. Cai, J. Wu, M. Chen, P. Du, Y. Chen, W. Liu and S. Yang, *Chem. Sci.*, 2020, **11**, 11435–11442.
156 Y. Liu, Z. Li, F. Fan, X. Zhu, L. Jia, M. Chen, P. Du, L. Yang and S. Yang, *Adv. Sci.*, 2021, **8**, 2102422.
157 B. K. Poudel, J. Hwang, S. K. Ku, J. O. Kim and J. H. Byeon, *NPG Asia Mater.*, 2018, **10**, 727–739.
158 A. Li, S. Wang, Z. Zhang, N. Xu, G. Ling and P. Zhang, *J. Mater. Chem. B*, 2022, **10**, 5191–5202.
159 H. Chen, Z. Liu, B. Wei, J. Huang, X. You, J. Zhang, Z. Yuan, Z. Tang, Z. Guo and J. Wu, *Bioact. Mater.*, 2021, **6**, 655–665.
160 X. Liang, X. Ye, C. Wang, C. Xing, Q. Miao, Z. Xie, X. Chen, X. Zhang, H. Zhang and L. Mei, *J. Control. Release*, 2019, **296**, 150–161.
161 H. Zhao, H. Chen, Z. Guo, W. Zhang, H. Yu, Z. Zhuang, H. Zhong and Z. Liu, *Chem. Eng. J.*, 2020, **394**, 124314.
162 S. Wan, B. Zhang, S. Li, B. He and Y. Pu, *J. Mater. Chem. B*, 2020, **8**, 2805–2813.
163 P. Zhao, Y. Xu, W. Ji, S. Zhou, L. Li, L. Qiu, Z. Qian, X. Wang and H. Zhang, *J. Nanobiotechnol.*, 2021, **19**, 181.
164 D. Huang, T. Wu, S. Lan, C. Liu, Z. Guo and W. Zhang, *Biomaterials*, 2022, **289**, 121808.
165 X. Shou, Y. Liu, D. Wu, H. Zhang, Y. Zhao, W. Sun and X. Shen, *Chem. Eng. J.*, 2021, **408**, 127349.
166 Z. Li, Y. Hu, Q. Fu, Y. Liu, J. Wang, J. Song, H. Yang, Z. Li, Y. Hu, Q. Fu, Y. Liu, J. Wang, J. Song and H. Yang, *Adv. Funct. Mater.*, 2020, **30**, 1905758.
167 F. Zeng, H. Qin, L. Liu, H. Chang, Q. Chen, L. Wu, L. Zhang, Z. Wu and D. Xing, *Nano Res.*, 2020, **13**, 3403–3415.
168 Y. Li, P. Feng, C. Wang, W. Miao and H. Huang, *Chem. Eng. J.*, 2020, **400**, 125851.
169 W. Chen, J. Wang, W. Du, J. Wang, L. Cheng, Z. Ge, S. Qiu, W. Pan, L. Song, X. Ma and Y. Hu, *ACS Appl. Nano Mater.*, 2021, **4**, 7963–7973.
170 Y. Zhu, Y. Liu, Z. Xie, T. He, L. Su, F. Guo, G. Arkin, X. Lai, J. Xu and H. Zhang, *Nanophotonics*, 2021, **10**, 3339–3358.
171 W. Chen, J. Ouyang, H. Liu, M. Chen, K. Zeng, J. Sheng, Z. Liu, Y. Han, L. Wang, J. Li, L. Deng, Y.-N. Liu, S. Guo, W. Chen, Y.-N. Liu, J. Ouyang, M. Chen, K. Zeng, J. Sheng, Z. Liu, Y. Han, L. Wang, J. Li, L. Deng, H. Liu and S. Guo, *Adv. Mater.*, 2017, **29**, 1603864.
172 Y. Li, J. Xiong, W. Guo, Y. Jin, W. Miao, C. Wang, H. Zhang, Y. Hu and H. Huang, *J. Control. Release*, 2021, **335**, 59–74.
173 C. Zhao, X. Han, S. Wang, Z. Y. Pan, X. Tang and Z. Jiang, *Adv. Healthcare Mater.*, 2023, **12**, 2201995.
174 A. Bigham, V. Rahimkhoei, P. Abasian, M. Delfi, J. Naderi, M. Ghomi, F. Dabbagh Moghaddam, T. Waqar, Y. Nuri Ertas, S. Sharifi, N. Rabiee, S. Ersoy, A. Maleki, E. Nazarzadeh Zare, E. Sharifi, E. Jabbari, P. Makvandi and A. Akbari, *Chem. Eng. J*, 2021, 134146.
175 M. Chang, Z. Hou, M. Wang, C. Li and J. Lin, *Adv. Mater.*, 2021, **33**, 2004788.
176 C. Wang, J. Wang, X. Zhang, S. Yu, D. Wen, Q. Hu, Y. Ye, H. Bomba, X. Hu, Z. Liu, G. Dotti and Z. Gu, *Sci. Transl. Med.*, 2018, **10**, eaan3682.
177 X. Li, B. Cho, R. Martin, M. Seu, C. Zhang, Z. Zhou, J. S. Choi, X. Jiang, L. Chen, G. Walia, J. Yan, M. Callanan, H. Liu, K. Colbert, J. Morrissette-McAlmon, W. Grayson, S. Reddy, J. M. Sacks and H. Q. Mao, *Sci. Transl. Med.*, 2019, **11**, eaau6210.
178 M. Montaño-Samaniego, D. M. Bravo-Estupiñan, O. Méndez-Guerrero, E. Alarcón-Hernández and M. Ibáñez-Hernández, *Front. Oncol.*, 2020, **10**, 605380.
179 R. J. Youle and A. Strasser, *Nat. Rev. Mol. Cell Biol.*, 2008, **9**, 47–59.
180 H. Bian, D. Ma, X. Zhang, K. Xin, Y. Yang, X. Peng and Y. Xiao, *Small*, 2021, **17**, 2100398.
181 X. Wang, X. Zhong, Z. Liu and L. Cheng, *Nano Today*, 2020, **35**, 100946.

182 C. Wang, S. Ding, S. Wang, Z. Shi, N. K. Pandey, L. Chudal, L. Wang, Z. Zhang, Y. Wen, H. Yao, L. Lin, W. Chen and L. Xiong, *Coord. Chem. Rev.*, 2021, **426**, 213529.
183 J. Noh, B. Kwon, E. Han, M. Park, W. Yang, W. Cho, W. Yoo, G. Khang and D. Lee, *Nat. Commun.*, 2015, **6**, 6907.
184 J. Wang, W. Chen, W. Du, H. Zhang, M. Ilmer, L. Song, Y. Hu and X. Ma, *Int. J. Nanomedicine*, 2023, **18**, 2389–2409.
185 H. Lin, Y. Chen and J. Shi, *Chem. Soc. Rev.*, 2018, **47**, 1938–1958.
186 A. D. Dey, A. Bigham, Y. Esmaeili, M. Ashrafizadeh, F. D. Moghaddam, S. C. Tan, S. Yousefiasl, S. Sharma, A. Maleki, N. Rabiee, A. P. Kumar, V. K. Thakur, G. Orive, E. Sharifi, A. Kumar and P. Makvandi, *Semin. Cancer Biol.*, 2022, **86**(Part 2), 396–419.
187 M. Yan, Y. Liu, X. Zhu, X. Wang, L. Liu, H. Sun, C. Wang, D. Kong and G. Ma, *ACS Appl. Mater. Interfaces*, 2019, **11**, 1876–1885.
188 Y. Liu, P. Bhattarai, Z. Dai and X. Chen, *Chem. Soc. Rev.*, 2019, **48**, 2053–2108.
189 W. Tang, Z. Yang, S. Wang, Z. Wang, J. Song, G. Yu, W. Fan, Y. Dai, J. Wang, L. Shan, G. Niu, Q. Fan and X. Chen, *ACS Nano*, 2018, **12**, 2610–2622.
190 F. Zhou, S. Wu, Y. Yuan, W. R. Chen and D. Xing, *Small*, 2012, **8**, 1543–1550.
191 R. Vankayala and K. C. Hwang, *Adv. Mater.*, 2018, **30**, 1706320.
192 R. Di Corato, G. Béalle, J. Kolosnjaj-Tabi, A. Espinosa, O. Clément, A. K. A. Silva, C. Ménager and C. Wilhelm, *ACS Nano*, 2015, **9**, 2904–2916.
193 M. Rafienia, A. Bigham and S. A. Hassanzadeh-Tabrizi, *J. Med. Signals Sens.*, 2018, **8**(2), 108–118.
194 Y. Su, T. Wang, Y. Su, M. Li, J. Zhou, W. Zhang and W. Wang, *Mater. Horizons*, 2020, **7**, 574–585.
195 Y. Cao, L. Tang, C. Fu, Y. Yin, H. Liu, J. Feng, J. Gao, W. Shu, Z. Li, Y. Zhu and W. Wang, *Nano Lett.*, 2024, **24**, 6767–6777.
196 R. Guo, Y. Tian, Y. Wang and W. Yang, *Adv. Funct. Mater.*, 2017, **27**, 1606398.
197 H. Wang, H. Wang, J. Liang, Y. Jiang, Q. Guo, H. Peng, Q. Xu and Y. Huang, *Mol. Pharm.*, 2014, **11**, 3352–3360.
198 Y. Mei, L. Tang, L. Zhang, J. Hu, Z. Zhang, S. He, J. Zang and W. Wang, *Mater. Today*, 2022, **60**, 52–68.
199 W. Hittorf, *Ann. Phys.*, 1865, **202**, 193–228.
200 L. Zhang, H. Huang, B. Zhang, M. Gu, D. Zhao, X. Zhao, L. Li, J. Zhou, K. Wu, Y. Cheng and J. Zhang, *Angew. Chem., Int. Ed.*, 2020, **59**, 1074–1080.
201 B. Zhang, L. Zhang, Z. Wang, Y. Li, Y. Cheng, L. Ma and J. Zhang, *J. Mater. Chem. A*, 2021, **9**, 13855–13860.
202 A. G. Ricciardulli, Y. Wang, S. Yang and P. Samorì, *J. Am. Chem. Soc.*, 2022, **144**, 3660–3666.
203 R. Zhao, S. Liu, X. Zhao, M. Gu, Y. Zhang, M. Jin, Y. Wang, Y. Cheng and J. Zhang, *J. Mater. Chem. A*, 2022, **10**, 245–250.
204 M. Qi, X. Zhao, X. Zhao, H. Zhang, Z. Li, X. Zhang, R. Fan, Q. Li, J. Zhang and D. Xu, *Chem. Eng. J.*, 2023, **475**, 145884.
205 Q. Shen, Z. Li, H. Bai, M. Gu, J. Kang, R. Jia, J. Zhang and A. Dong, *J. Mater. Chem. B*, 2024, **12**, 3392–3403.
206 Q. Wu, T. Deng, J. Cheng, Y. Yang, Y. Wang, Y. Xiao and Y. Zhang, *ACS Nano*, 2024, **18**, 11988–12009.
207 Z. Zhang, Z. Hao, R. Shan, M. W. Tasleem, J. Wang, J. Zhou and H. Zhang, *Food Chem. X*, 2023, **20**, 100990.
208 B. Yang, Y. Chen and J. Shi, *Adv. Mater.*, 2019, **31**, 1901778.
209 L. Raj, T. Ide, A. U. Gurkar, M. Foley, M. Schenone, X. Li, N. J. Tolliday, T. R. Golub, S. A. Carr, A. F. Shamji, A. M. Stern, A. Mandinova, S. L. Schreiber and S. W. Lee, *Nature*, 2011, **475**, 231–234.
210 J. Ouyang, A. Xie, J. Zhou, R. Liu, L. Wang, H. Liu, N. Kong and W. Tao, *Chem. Soc. Rev.*, 2022, **51**, 4996–5041.
211 H. Zhang, Y. Zhang, Y. Zhang, H. Li, M. Ou, Y. Yu, F. Zhang, H. Yin, Z. Mao and L. Mei, *Nat. Commun.*, 2024, **15**, 6783.
212 K. Urbanska, J. Sokolowska, M. Szmidt and P. Sysa, *Contemp. Oncol.*, 2014, **18**, 307.
213 P. MacMahon, C. M. Labak, S. E. Martin-Bach, A. Issawi, K. Velpula and A. J. Tsung, *CNS Oncol.*, 2018, **7**, CNS25.
214 L. Jin, P. Hu, Y. Wang, L. Wu, K. Qin, H. Cheng, S. Wang, B. Pan, H. Xin, W. Zhang, X. Wang, L. Jin, H. Cheng, S. Wang, X. Wang, Y. Wang, L. Wu, K. Qin, H. Xin, P. Hu, B. Pan and W. Zhang, *Adv. Mater.*, 2020, **32**, 1906050.
215 S. Xiong, Z. Li, Y. Liu, Q. Wang, J. Luo, X. Chen, Z. Xie, Y. Zhang, H. Zhang and T. Chen, *Biomaterials*, 2020, **260**, 120339.
216 Y. Li, Z. Du, X. Liu, M. Ma, D. Yu, Y. Lu, J. Ren, X. Qu, Y. Li, Z. Du, X. Liu, M. Ma, D. Yu, J. Ren, X. Qu and Y. Lu, *Small*, 2019, **15**, 1901116.
217 M. Luo, Y. Zhou, N. Gao, W. Cheng, X. Wang, J. Cao, X. Zeng, G. Liu and L. Mei, *Chem. Eng. J.*, 2020, **385**, 123942.
218 H. H. Wu, Y. Zhou, Y. Tabata and J. Q. Gao, *J. Control. Release*, 2019, **294**, 102–113.
219 W. Wang, Q. Zhang, M. Zhang, X. Lv, Z. Li, M. Mohammadniaei, N. Zhou and Y. Sun, *Carbohydr. Polym.*, 2021, **265**, 118065.
220 X. Huang, K. Ren, Z. Chang, Y. Ye, D. Huang, W. Zhao, L. Yang, Y. Dong, Z. Cao and H. Qiao, *Chem. Eng. J.*, 2022, **430**, 132898.
221 Z. Li, C. Zhao, Q. Fu, J. Ye, L. Su, X. Ge, L. Chen, J. Song and H. Yang, *Small*, 2022, **18**, 2105160.
222 H. Wang, Y. Ma, S. Zhao, Y. Li, L. Wu, H. Qin and D. Xing, *Appl. Phys. Lett.*, 2021, **119**, 143701.
223 X. Chen, S. Zhang, J. Liu, M. Ren, D. Xing and H. Qin, *Biomaterials*, 2022, **287**, 121662.
224 H. Schmidberger, M. Rapp, A. Ebersberger, S. Hey-Koch, C. Loquai, S. Grabbe and A. Mayer, *Strahlentherapie und Onkol.*, 2018, **194**, 1144–1151.
225 A. Arheden, J. Skalenius, S. Bjursten, U. Stierner, L. Ny, M. Levin and H. Jespersen, *Acta Oncol.*, 2019, **58**, 962–966.
226 V. W. Rebecca, R. Somasundaram and M. Herlyn, *Nat. Commun.*, 2020, **11**, 1–9.
227 M. Shakiba, M. Sheikhi, Z. Pahnavar, A. Tajiki, A. Bigham, A. Foroozandeh, S. Darvishan, M. Pourmadadi, H. Emadi, J. Rezatabar, H. Abdouss and M. Abdouss, *Int. J. Pharm.*, 2023, **642**, 123207.
228 M. Shakiba, P. Jahangiri, E. Rahmani, S. M. Hosseini, A. Bigham, A. Foroozandeh, A. Tajiki, M. Pourmadadi,

S. Nasiri, S. Jouybar and M. Abdouss, *ACS Appl. Polym. Mater.*, 2023, **5**, 5662–5675.
229 L. Chan, P. Gao, W. Zhou, C. Mei, Y. Huang, X. F. Yu, P. K. Chu and T. Chen, *ACS Nano*, 2018, **12**, 12401–12415.
230 H. Huang, L. He, W. Zhou, G. Qu, J. Wang, N. Yang, J. Gao, T. Chen, P. K. Chu and X. F. Yu, *Biomaterials*, 2018, **171**, 12–22.
231 S. J. Song, I. S. Raja, Y. Bin Lee, M. S. Kang, H. J. Seo, H. U. Lee and D. W. Han, *Biomater. Res.*, 2019, **23**, 1–7.
232 L. Sutrisno, H. Chen, T. Yoshitomi, N. Kawazoe, Y. Yang and G. Chen, *J. Mater. Chem. B*, 2022, **10**, 204–213.
233 C. Xue, L. Sutrisno, M. Li, W. Zhu, Y. Fei, C. Liu, X. Wang, K. Cai, Y. Hu and Z. Luo, *Biomaterials*, 2021, **269**, 120623.
234 H. Ding, D. Wang, H. Huang, X. Chen, J. Wang, J. Sun, J. Zhang, L. Lu, B. Miao, Y. Cai, K. Fan, Y. Lu, H. Dong, X. Yan, G. Nie and M. Liang, *Nano Res.*, 2021, **15**, 1554–1563.
235 G. Song, C. Ji, C. Liang, X. Song, X. Yi, Z. Dong, K. Yang and Z. Liu, *Biomaterials*, 2017, **112**, 257–263.
236 Y. Yang, Q. Xie, Z. Zhao, L. He, L. Chan, Y. Liu, Y. Chen, M. Bai, T. Pan, Y. Qu, L. Ling and T. Chen, *ACS Appl. Mater. Interfaces*, 2017, **9**, 25857–25869.
237 J. Wu, X. Wang, Q. Wang, Z. Lou, S. Li, Y. Zhu, L. Qin and H. Wei, *Chem. Soc. Rev.*, 2019, **48**, 1004–1076.
238 X. Huang, Y. Zhong, Y. Li, X. Zhou, L. Yang, B. Zhao, J. Zhou, H. Qiao, D. Huang, H. Qian and W. Chen, *ACS Appl. Mater. Interfaces*, 2022, **14**, 37466–37477.
239 R. L. Siegel, K. D. Miller, H. E. Fuchs and A. Jemal, *CA. Cancer J. Clin.*, 2022, **72**, 7–33.
240 N. Mottet, R. C. N. van den Bergh, E. Briers, T. Van den Broeck, M. G. Cumberbatch, M. De Santis, S. Fanti, N. Fossati, G. Gandaglia, S. Gillessen, N. Grivas, J. Grummet, A. M. Henry, T. H. van der Kwast, T. B. Lam, M. Lardas, M. Liew, M. D. Mason, L. Moris, D. E. Oprea-Lager, H. G. van der Poel, O. Rouvière, I. G. Schoots, D. Tilki, T. Wiegel, P. P. M. Willemse and P. Cornford, *Eur. Urol.*, 2021, **79**, 243–262.
241 A. Olivas and R. S. Price, *Nutr. Cancer*, 2020, **73**, 2232–2248.
242 D. Raghavan, K. Cox, B. S. Pearson, G. J. Coorey, J. Rogers, W. H. Watt, A. S. Coates, E. Mcneil and J. J. Grygiel, *Br. J. Urol.*, 1993, **72**, 625–628.
243 D. P. Petrylak, C. M. Tangen, M. H. A. Hussain, P. N. J. Lara, J. A. Jones, M. E. Taplin, P. A. Burch, D. Berry, C. Moinpour, M. Kohli, M. C. Benson, E. J. Small, D. Raghavan and E. D. Crawford, *N. Engl. J. Med.*, 2004, **351**, 1513–1520.
244 N. G. Zaorsky, B. J. Davis, P. L. Nguyen, T. N. Showalter, P. J. Hoskin, Y. Yoshioka, G. C. Morton and E. M. Horwitz, *Nat. Rev. Urol.*, 2017, **14**, 415–439.
245 J. Zhao, C. Zhang, W. Wang, C. Li, X. Mu and K. Hu, *Biomed. Pharmacother.*, 2022, **155**, 113714.
246 M. Fojtů, J. Balvan, M. Raudenská, T. Vičar, D. Bouša, Z. Sofer, M. Masařík and M. Pumera, *Chem. – A Eur. J.*, 2019, **25**, 349–360.
247 S. L. Kelleher, N. H. McCormick, V. Velasquez and V. Lopez, *Adv. Nutr.*, 2011, **2**, 101–111.
248 X. Chen, X. Che, J. Wang, F. Chen, X. Wang, Z. Zhang, B. Fan, D. Yang and X. Song, *Acta Biochim. Biophys. Sin.*, 2012, **45**, 353–358.
249 M. Yan, K. Hardin and E. Ho, *J. Nutr. Biochem.*, 2010, **21**, 687–694.
250 L. Gao, R. Teng, S. Zhang, Y. Zhou, M. Luo, Y. Fang, L. Lei and B. Ge, *Front. Bioeng. Biotechnol.*, 2020, **8**, 769.
251 L. Li, B. Zhou, H. Xu, H. Shi, L. Gao and B. Ge, *Front. Endocrinol.*, 2022, **13**, 505.
252 I. Fasolino, A. Soriente, M. Caporali, M. Serrano-Ruiz, M. Peruzzini, L. Ambrosio and M. G. Raucci, *Sci. Reports*, 2021, **11**, 1–13.
253 E. B. Kurutas, *Nutr. J.*, 2016, **15**, 1–22.
254 F. Borrelli, I. Fasolino, B. Romano, R. Capasso, F. Maiello, D. Coppola, P. Orlando, G. Battista, E. Pagano, V. Di Marzo and A. A. Izzo, *Biochem. Pharmacol.*, 2013, **85**, 1306–1316.
255 F. Yang, J. Lu, Q. Ke, X. Peng, Y. Guo and X. Xie, *Sci. Rep.*, 2018, **8**, 7345.
256 J. Liao, R. Han, Y. Wu and Z. Qian, *Bone Res.*, 2021, **9**, 18.
257 H. Ma, T. Li, Z. Huan, M. Zhang, Z. Yang, J. Wang, J. Chang and C. Wu, *NPG Asia Mater.*, 2018, **10**, 31–44.
258 C. Wang, X. Ye, Y. Zhao, L. Bai, Z. He, Q. Tong, X. Xie, H. Zhu, D. Cai, Y. Zhou, B. Lu, Y. Wei, L. Mei, D. Xie and M. Wang, *Biofabrication*, 2020, **12**, 035004.
259 M. G. Raucci, U. D'Amora, A. Ronca and L. Ambrosio, *Adv. Healthcare Mater.*, 2020, **9**, 2000349.
260 S. Li, Y. Qing, Y. Lou, R. Li, H. Wang, X. Wang, B. Ying, X. Tang and Y. Qin, *Int. J. Biol. Macromol.*, 2023, **239**, 124209.
261 Y. Zhao, X. Peng, X. Xu, M. Wu, F. Sun, Q. Xin, H. Zhang, L. Zuo, Y. Cao, Y. Xia, J. Luo, C. Ding and J. Li, *Carbohydr. Polym.*, 2023, **300**, 120264.
262 W. Ou, J. H. Byeon, R. K. Thapa, S. K. Ku, C. S. Yong and J. O. Kim, *ACS Nano*, 2018, **12**, 10061–10074.
263 W. Ou, J. H. Byeon, Z. C. Soe, B. K. Kim, R. K. Thapa, B. Gupta, B. K. Poudel, S. K. Ku, C. S. Yong and J. O. Kim, *Theranostics*, 2019, **9**, 6780.
264 Y. Fang, Z. Zhang, Y. Liu, T. Gao, S. Liang, Q. Chu, L. Guan, W. Mu, S. Fu, H. Yang, N. Zhang and Y. Liu, *ACS Appl. Mater. Interfaces*, 2022, **14**(18), 20628–20640.
265 J. Wang, H. Zhang, X. Xiao, D. Liang, X. Liang, L. Mi, J. Wang and J. Liu, *Acta Biomater.*, 2020, **107**, 260–271.
266 F. Ruan, R. Liu, K. Wang, J. Zeng and Z. Zuo, *J. Hazard. Mater.*, 2021, **402**, 122875.
267 Z. Lin, Q. Deng, Q. Fang, X. Li, X. Liu, J. Wang, S. Chen, X. Huang, L. Yang, Y. Miao and X. Y. Yu, *J. Drug Targeting*, 2022, **30**, 614–622.
268 J. Liu, K. Yi, Q. Zhang, H. Xu, X. Zhang, D. He, F. Wang, X. Xiao, J. Liu, Q. Zhang, H. Xu, D. He, X. Xiao, K. Yi, F. Wang and X. Zhang, *Small*, 2021, **17**, 2104585.
269 Y. Wu, Z. Chen, Z. Yao, K. Zhao, F. Shao, J. Su and S. Liu, *Adv. Funct. Mater.*, 2021, **31**, 2104643.
270 M. Fojtů, X. Chia, Z. Sofer, M. Masařík, M. Pumera, M. Fojtů, X. Chia, M. Pumera, Z. Sofer and M. Masařík, *Adv. Funct. Mater.*, 2017, **27**, 1701955.

271 F. Yin, K. Hu, S. Chen, D. Wang, J. Zhang, M. Xie, D. Yang, M. Qiu, H. Zhang and Z. G. Li, *J. Mater. Chem. B*, 2017, **5**, 5433–5440.
272 J. Liu, P. Du, H. Mao, L. Zhang, H. Ju and J. Lei, *Biomaterials*, 2018, **172**, 83–91.
273 J. Shao, C. Ruan, H. Xie, Z. Li, H. Wang, P. K. Chu, X.-F. Yu, J. Shao, C. Ruan, H. Xie, Z. Li, H. Wang, X. Yu and P. K. Chu, *Adv. Sci.*, 2018, **5**, 1700848.
274 Z. Li, Q. Liu, Y. Zhang, Y. Yang, X. Zhou, W. Peng, Z. Liang, X. Zeng, Q. Wang and N. Gao, *Drug Deliv.*, 2021, **28**, 700–708.
275 J. Jie Zeng, Z. Gui Tang, J. Zou and J. Gang Yu, *Trans. Nonferrous Met. Soc. China*, 2021, **31**, 2812–2822.
276 N. Krasteva and M. Georgieva, *Pharmaceutics*, 2022, **14**, 1213.
277 P. Ji, J. Chen, H. Wang, L. Shi, X. Tang and Y. Duo, *Biomater. Sci.*, 2023, **11**, 4727.
278 F. Bray, J. Ferlay, I. Soerjomataram, R. L. Siegel, L. A. Torre and A. Jemal, *CA. Cancer J. Clin.*, 2018, **68**, 394–424.
279 M. Ramezani Farani, M. Azarian, H. Heydari Sheikh Hossein, Z. Abdolvahabi, Z. Mohammadi Abgarmi, A. Moradi, S. M. Mousavi, M. Ashrafizadeh, P. Makvandi, M. R. Saeb and N. Rabiee, *ACS Appl. Bio Mater.*, 2022, **5**, 1305–1318.
280 S. Marcazzan, E. M. Varoni, E. Blanco, G. Lodi and M. Ferrari, *Oral Oncol.*, 2018, **76**, 1–7.
281 E. Izumchenko, R. Hasina, A. K. Hariharan, A. Shanmugam, S. Irusappan, S. Maji, U. Bahadur, V. Veeramachaneni, R. Bettadapura, A. Ravichandran, R. Hariharan, V. Gupta, V. U. S. Rao, R. K. Bagadia, N. M. L. Manjunath, M. W. Lingen and N. Agrawal, *J. Clin. Oncol.*, 2020, **38**, 6562.
282 J. Ma, D. Xue, T. Xu, G. Wei, C. Gu, Y. Zhang and T. Jiang, *Colloids Surfaces B Biointerfaces*, 2023, **227**, 113338.
283 W. Kim, N. K. Ly, Y. He, Y. Li, Z. Yuan and Y. Yeo, *Adv. Drug Deliv. Rev.*, 2023, **192**, 114635.
284 A. Bigham, M. G. Raucci, K. Zheng, A. R. Boccaccini and L. Ambrosio, *Adv. Mater.*, 2023, 2302858.
285 R. L. Pinals, L. Chio, F. Ledesma and M. P. Landry, *Analyst*, 2020, **145**, 5090–5112.
286 U. Sakulkhu, L. Maurizi, M. Mahmoudi, M. Motazacker, M. Vries, A. Gramoun, M. G. Ollivier Beuzelin, J. P. Vallée, F. Rezaee and H. Hofmann, *Nanoscale*, 2014, **6**, 11439–11450.
287 J. Mo, Q. Xie, W. Wei and J. Zhao, *Nat. Commun.*, 2018, **9**, 2480.
288 J. Mo, Y. Xu, X. Wang, W. Wei and J. Zhao, *Nanoscale*, 2020, **12**, 1742–1748.
289 Q. Xiao, X. Tu, H. Cao, H. Luo, B. Li, J. Liu, Y. Liu and S. Huang, *J. Mol. Struct.*, 2023, **1276**, 134725.
290 G. Qu, W. Liu, Y. Zhao, J. Gao, T. Xia, J. Shi, L. Hu, W. Zhou, J. Gao, H. Wang, Q. Luo, Q. Zhou, S. Liu, X. F. Yu and G. Jiang, *Angew. Chem., Int. Ed.*, 2017, **56**, 14488–14493.
291 Y. Zhong, Y. Lin, Y. Chen, G. Chen, J. Zhang, L. Li, A. Huang, L. Zhang, Y. Ma, Z. Y. Xie and Q. Liao, *ACS Appl. Bio Mater.*, 2021, **4**, 1704–1719.
292 N. M. Latiff, W. Z. Teo, Z. Sofer, A. C. Fisher and M. Pumera, *Chem. – A Eur. J.*, 2015, **21**, 13991–13995.
293 X. Zhang, Z. Zhang, S. Zhang, D. Li, W. Ma, C. Ma, F. Wu, Q. Zhao, Q. Yan and B. Xing, *Small*, 2017, **13**, 1701210.
294 O. Bawadkji, M. Cherri, A. Schäfer, S. Herziger, P. Nickl, K. Achazi, I. S. Donskyi, M. Adeli, R. Haag, O. Bawadkji, M. Cherri, A. Schäfer, P. Nickl, K. Achazi, I. S. Donskyi, R. Haag, S. Herziger and M. Adeli, *Adv. Mater. Interfaces*, 2022, **9**, 2201245.
295 I. S. Donskyi, X. Huang, N. Wichmann, O. Bawadkji, R. Ahmed, P. Nickl, S. Herziger, J. Radnik, K. Achazi, H. Qiao and M. Adeli, *ACS Appl. Nano Mater.*, 2022, **5**, 13417–13424.
296 N. Mohamad Latiff, C. C. Mayorga-Martinez, Z. Sofer, A. C. Fisher and M. Pumera, *Appl. Mater. Today*, 2018, **13**, 310–319.
297 D. Peer, J. M. Karp, S. Hong, O. C. Farokhzad, R. Margalit and R. Langer, *Nat. Nanotechnol.*, 2007, **2**, 751–760.
298 J. Hou, H. Wang, Z. Ge, T. Zuo, Q. Chen, X. Liu, S. Mou, C. Fan, Y. Xie and L. Wang, *Nano Lett.*, 2020, **20**, 1447–1454.
299 S. Geng, T. Pan, W. Zhou, H. Cui, L. Wu, Z. Li, P. K. Chu and X. F. Yu, *Theranostics*, 2020, **10**, 4720–4736.
300 C. Sun, Y. Xu, L. Deng, H. Zhang, Q. Sun, C. Zhao and Z. Li, *ACS Appl. Bio Mater.*, 2018, **1**, 673–682.
301 T. Guo, Y. Wu, Y. Lin, X. Xu, H. Lian, G. Huang, J. Z. Liu, X. Wu and H. H. Yang, *Small*, 2018, **14**, 1702815.
302 S. Geng, X. Zhang, T. Luo, M. Jiang, C. Chu, L. Wu, P. Gong and W. Zhou, *J. Control. Release*, 2023, **354**, 889–901.
303 L. Chan, X. Chen, P. Gao, J. Xie, Z. Zhang, J. Zhao and T. Chen, *ACS Nano*, 2021, **15**, 3047–3060.
304 C. He, F. Ruan, S. Jiang, J. Zeng, H. Yin, R. Liu, Y. Zhang, L. Huang, C. Wang, S. Ma and Z. Zuo, *Small*, 2020, **16**, 2001371.
305 L. Peng, N. Abbasi, Y. Xiao and Z. Xie, *Adv. Mater. Interfaces*, 2020, **7**, 2001538.
306 H. Xie, Z. Chen, N. Zhang, F. Wu, H. Su, Y. Liu, D. Xie and Y. Mei, *J. Mater. Sci.*, 2024, **59**, 12129–12153.
307 X. Su, Y. Chi, T. Liu, H. Xun, Y. Wu, X. Liu, J. Zheng, F. Hu, S. Han, H. Duan and J. Chai, *ACS Appl. Mater. Interfaces*, 2024, **16**, 43892–43906.
308 X. Zhang, I. S. Donskyi, W. Tang, S. Deng, D. Liu, S. Zhang, Q. Zhao and B. Xing, *Angew. Chem., Int. Ed.*, 2023, **62**, e202213336.
309 H. Qin, J. Chen, Y. Li, L. Gao, J. Wang, G. Qu, M. Yang, X. Zhou and Z. Sun, *Sci. Total Environ.*, 2021, **782**, 146860.